IMPERIAL COLLEGE LONDON

APPLICATIONS OF GUIDED WAVE PROPAGATION ON WAVEGUIDES WITH IRREGULAR CROSS-SECTION

by

Zheng Fan

A thesis submitted to the Imperial College London for the degree of

Doctor of Philosophy

Department of Mechanical Engineering

Imperial College London

London SW7 2AZ

June 2010

Abstract

Guided waves are interesting for Non-destructive Testing (NDT) since they offer the potential for rapid inspections of a large variety of structures. Analytical methods are well known for predicting properties of guided waves such as mode shapes and dispersion curves on regular geometries, e.g. plain plates or cylindrical structures. However these methods cannot be used to study guided wave propagation in waveguides having irregular cross-sectional geometries, such as railway lines, T-shape beams or stiffened plates. This thesis applies and develops a Semi-Analytical Finite Element (SAFE) method, which uses finite elements to represent the cross-section of the waveguide and a harmonic description along the propagation direction, to investigate the modal properties of structures with irregular cross-section. Two attractive applications have been investigated with the SAFE method, and the results are encouraging.

The first application relates to fluid characterization. Guided torsional waves in a bar with a non-circular cross-section have been exploited by previous researchers to measure the density of fluids. However, due to the complexity of the wave behavior in the non-circular cross-sectional shape, the previous theory can only provide an approximate prediction; thus the accuracy of the measurement has been compromised. The SAFE method is developed to model accurately the propagation velocity and leakage of guided waves along an immersed waveguide with arbitrary non-circular cross-section. An accurate inverse model is then provided to measure the density of the fluid by measuring the change of the torsional wave speed. The model also enables the optimization of the dipstick sensor by changing the material of the dipstick and the geometry of the cross-section. Experimental results obtained with a rectangular bar in a range of fluids show very good agreement with the theoretical predictions.

The second application relates to the inspection of large areas of complex structures. An experimental observation on a large welded plate found that the weld can concentrate and guide the energy of a guided wave traveling along the direc-

tion of the weld. This is attractive for NDE since it offers the potential to quickly inspect for defects such as cracking or corrosion along long lengths of welds. The SAFE method is applied to provide a modal study of the elastic waves which are guided by the welded joint in a plate. This brings understanding to the compression wave which was previously observed in the experiment. However, during the study, a shear weld-guided mode, which is non-leaky and almost non-dispersive has also been discovered. Its characteristics are particularly attractive for NDT, so this is a significant new finding. The properties for both the compression and the shear mode are discussed and compared, and the physical reason for the energy trapping phenomena is explained. Experiments have been undertaken to validate the existence of the shear weld-guided mode and the accuracy of the FE model, showing very good results. The sensitivity of compression and shear weld-guided modes to different types of defects close to the weld is investigated, by both finite element simulations and experiments. Due to similar reasons for energy trapping, the feature guiding phenomena also exists in a wide range of geometries. This thesis finally discusses feature guided waves on lap joints, stiffened plates and interconnected heat exchanger tube plates, and their potential applications.

Acknowledgements

I would like to express my deepest gratitude to my supervisor Professor Mike Lowe for his excellent guidance throughout this work. I would also like to thank Professor Peter Cawley for all the invaluable discussions, and for offering me a Ph.D position in the well organized Non-destructive Testing Lab.

I want to appreciate the co-operation with Professor Michel Castaings and Professor Christophe Bacon from Université de Bordeaux during the stage of setting up the the model. Many thanks for their input and insightful discussions. I also want to acknowledge Dr. Norrie McPherson from BVT Surface Fleet Ltd for supporting us with experimental pieces.

A special thanks to Dr. MA Jian for introducing me to the NDT lab, and also giving me very valuable advice during my Ph.D. I would also like to extend my thanks to all my current and former colleagues in the NDT group, for their help and for creating a such friendly working environment, especially Dr. Prabhu Rajagopal, Dr. Frederic Cegla, Dr. Daniel Hesse and Dr. Bubyoung Kang.

Further more, I must acknowledge the Engineering and Physical Sciences Research Council (EPSRC), which has primarily funded this work, and the sponsorship of the two industrial partners: Shell and National Nuclear Laboratory (NNL).

Finally, I am forever indebted to my family: my father FAN Gang, my mother XU Nianci and my wife ZHANG Xin for their understanding, endless patience and encouragement. To them I dedicate this thesis.

Contents

1 Introduction **20**

1.1 Motivation 20

1.2 Outline of Thesis 25

2 Guided Waves **27**

2.1 Background 27

2.2 Wave Propagation in Bulk Media 28

2.3 Guided Waves Propagation in Waveguides with Regular Cross-sections 29

2.3.1 Guided waves 29

2.3.2 Dispersion curves 31

2.3.3 Mode shapes 34

2.3.4 Leaky guided waves 35

2.4 Semi Analytical Finite Element (SAFE) method 38

2.4.1 Literature review 39

2.4.2 SAFE method in solids 41

2.4.3 SAFE method in perfect fluids 42

2.4.4 SAFE method in viscous fluids 43

2.4.5 Absorbing region 45

2.5 SAFE Method Validation 46

2.5.1 Solid waveguide immersed in a perfect fluid 46

2.5.2 Solid waveguide immersed in a viscous fluid 50

2.6 Summary 53

3 Dipstick for Ultrasonic Density Measurements 54

3.1 Background 54

3.2 Previous Theory of Torsional Dipstick 58

3.3 Modal Study of Rectangular Bar Immersed in a Perfect Fluid 60

3.3.1 Model description 60

3.3.2 Fundamental modes at single frequency 62

3.3.3 Dispersion curve of the torsional mode 62

3.3.4 Inverse model for density prediction 64

3.4 Experiment 66

3.4.1 Experimental setup 66

3.4.2 Results 69

3.4.3 Error analysis 70

3.5 Potential for Sensor Optimization 72

3.6 Summary 76

4 Investigation on feature guided waves **78**

4.1 Discovery of the Feature Guided Wave 78

4.2 Time Step Finite Element Simulations 81

4.3 SAFE Modelling 83

4.3.1 Model description 83

4.3.2 Mode shapes at single frequencies 85

4.3.3 Dispersion curve 87

4.4 Discovery of Shear Feature Guided Wave 89

4.4.1 Mode shapes of the shear mode at single frequencies 90

4.4.2 Dispersion curve of the shear weld guided mode 93

4.5 Energy Trapping Effect 94

4.6 Experiment on the Shear Guided Mode 98

4.6.1 Experimental setup 98

4.6.2 Validation of group velocity and attenuation 100

4.6.3 Validation of energy concentration effect 100

4.7 Summary 101

5 Scattering of Weld Guided Modes from Defects Located Around the Weld **104**

5.1 Background 104

5.2 Experiment 106

5.2.1 Experiment preparation 106

5.2.2 Experimental setup 107

5.2.3 Typical results 108

5.2.4 Calibration experiment 109

5.3 Finite Element Modelling 111

5.3.1 SAFE modelling 111

5.3.2 Time step finite element simulation 115

5.4 Interaction of Shear Weld Guided Mode with Defects Around the Weld 119

5.4.1 Cracks parallel to the weld 119

5.4.2 Cracks normal to the weld 122

5.4.3 Flat-bottom holes 124

5.5 Interaction of Compression Weld Guided Mode with Defects Around the Weld 126

5.6 Summary 128

6 Feature Guided Waves on Other Geometries 130

6.1 Lap Joints 131

6.1.1 Introduction 131

6.1.2 Geometry and model description 131

6.1.3 Results and discussion 133

6.2 Plate with Stiffener 138

6.2.1 Introduction and model description 138

6.2.2 Results and discussion 139

6.3 Interconnected Heat Exchanger Tube (Tube plate) 145

6.3.1 Introduction 145

6.3.2 SAFE modelling and discussion 147

6.4 Summary 151

7 Conclusions **152**

7.1 Thesis Review 152

7.2 Summary of Findings 153

7.2.1 Extension of Semi-Analytical Finite Element Method 153

7.2.2 Dipstick for ultrasonic density measurements 154

7.2.3 Feature guided waves 155

7.3 Future Work 158

A Laser Interferometric Measurement **160**

References **171**

List of Publications **172**

List of Figures

1.1 *Schematic of a torsional "dipstick" sensor.* 22

1.2 *Schematic of the propagation of a feature-guided wave on a welded plate from a pulse excitation.* 24

2.1 *Phase velocity (a) and group velocity (b) dispersion curves for a steel plate in vacuum. Longitudinal modes are plotted in solid lines (—), flexural modes in dashed lines (- - -), and shear horizontal modes in dotted lines (· · ·).* 32

2.2 *5 cycle Hanning windowed toneburst signal at excitation(a) and a prediction by the DISPERSE software of the signal after 0.5 m propagation distance as S0 mode (b) and SH0 mode (c) on a 1mm thick steel plate.* 33

2.3 *Displacement mode shapes of the (a) S0 mode, (b) SH0 mode, (c) A0 mode at frequency thickness 0.2 MHz mm in a steel plate, and (d) shows the coordinate system.* 34

2.4 *Schematic showing a leaky waveguide, which leaks bulk waves at an angle θ.* 35

2.5 *Phase velocity dispersion curves for a 1mm radius steel bar immersed in water. Longitudinal modes are plotted in solid lines (—), flexural modes in dashed lines (- - -), and torsional modes in dotted lines (· · ·).* 36

2.6 *Attenuation dispersion curves for a 1mm radius steel bar immersed in water. Only fundamental longitudinal modes (—), flexural modes (- - -), and torsional modes (···) are plotted.* 37

2.7 *Displacement mode shapes of the (a) L(0,1) mode at frequency radius 0.2 MHz mm, (b) L(0,1) mode at 1 MHz mm, (c) T(0,1) mode at 0.2 MHz mm and (d) F(1,1) mode at 0.2 MHz mm.* 38

2.8 *Schematic of the SAFE method (a) and periodic finite element method (b).* 39

2.9 *Schematic of the FE model used for a circular bar immersed in a fluid.* 45

2.10 *Cross-section distribution of normal stress in solid and pressure in fluid at 500 kHz for example modal results: (a) L(0,1) mode (b) T(0,1) mode and (c) F(1,1) mode; (d) mode resonating in the absorbing region.* 48

2.11 *Dispersion curves of phase velocity (a), wavenumber (b), group velocity (c) and attenuation (d) of 1mm radius circular steel cylinder bar immersed in water, predicted by the SAFE method (∘) and DISPERSE (—).* 49

2.12 *Dispersion curves of phase velocity (a) and attenuation (b) of 1mm radius circular steel cylinder bar immersed in glycerol, predicted by the SAFE method (∘) and DISPERSE (—).* 52

3.1 *(a) Dipstick for fluid viscosity measurement [56], (b) dipstick for fluid bulk velocity measurement [57]* 56

3.2 *Dipstick sensor designed for fluid density measurements.* 57

3.3 *Schematic of the FE model used for the rectangular aluminium bar immersed in alcohol* 61

3.4 *Theoretical prediction of mode shape of four fundamental modes of aluminium bar with rectangular cross-section (*$1.1mm \times 2.2mm$*) immersed in alcohol, at* 70 *kHz: (a) Longitudinal mode (b) Torsional mode, (c) flexural mode 1 and (d) flexural mode 2. The radial (with respect to the center of the bar) stress in solid and pressure in fluid is displayed in a grey scale* 63

3.5 *A zoomed picture of torsional mode of aluminium bar with rectangular cross-section (*$1.1mm \times 2.2mm$*) immersed in alcohol at* 70 *kHz. The radial (with respect to the center of the bar) stress in solid and pressure in fluid is displayed in a grey scale. Arrows indicate displacements in cross-section of fluid and the bar* 64

3.6 *Phase velocity dispersion curves of aluminium bar with rectangular cross-section (*$1.1mm \times 2.2mm$*) immersed in alcohol (circles) and in vacuum (line) predicted by the SAFE method* 65

3.7 *Inverse Model relating the group velocity of the torsional wave of the immersed rectangular bar and the density of the fluids* 66

3.8 *Experimental setup* 67

3.9 *Time trace at 70 kHz with aluminum rectangular bar immersed in alcohol at 170mm (a) and in air (b)* 68

3.10 *Measured (stars) and theoretically predicted (line) group velocity of aluminium bar with rectangular cross-section immersed in alcohol* . . . 70

3.11 *Measured (stars) and theoretically predicted (line) group velocity of aluminium bar with rectangular cross-section immersed in different fluids compared with previous theory prediction (dashed line)* 71

3.12 *Torsional mode on bars with different cross section immersed in alcohol: (a) square shape, (b) diamond shape, (c) elliptical shape and (d) hollow rectangular shape. The radial (with respect to the center of the bar) stress in solid and pressure in fluid is displayed in a grey scale* 73

3.13 *(a) Measurement sensitivity comparison for aluminum rectangular bars with aspect ratio from 1:1 to 1:4. (b)Dispersion comparison for aluminum rectangular bars with aspect ratio from 1:1 to 1:4* 74

3.14 *Measurement sensitivity comparison for aluminum bars of rectangular, elliptical, diamond-shaped and hollow rectangular cross-sections with aspect ratio of 1:3* 74

3.15 *Measurement sensitivity comparison for bars which are made of copper, steel, aluminum and magnesium of diamond-shaped cross-sections with aspect ratio of 1:3.* 75

4.1 *Experimental discovery of feature guided wave.* 79

4.2 *Illustration of the trapped wave due to different propagation velocities in the weld compared with the plate* 80

4.3 *Schematic of time-step finite element modelling of guided wave propagation on an idealized welded plate [23]* 81

4.4 *Snapshot of propagation of the weld-guided waves at 100 kHz (a) and 500 kHz(b) [23].* 82

4.5 *The schematic of the two dimensional SAFE model of a welded plate.* 84

4.6 *Compression weld guided mode at 100 kHz: (a) snapshot of the axial component of energy-flow (white=high energy-flow, black=low energy-flow), (b) the mode shape in the center of the weld along x_2 (u_1, u_2, u_3 represent displacements of x_1, x_2 and x_3 respectively) (c) the axial displacement in the center of the plate along x_1.* 87

4.7 *Energy flow snapshots for the compression weld guided mode from frequency 50 kHz to 300 kHz.* 88

4.8 *Phase velocity (a) and attenuation (b) dispersion curve of compression weld guided mode predicted by SAFE method.* 89

4.9 *Schematic of the shear weld guided mode.* 90

4.10 *Mode shape of shear weld guided mode at 100 kHz: (a) snapshot of the axial component of energy-flow (white=high energy-flow, black=low energy-flow), (b) the mode shape in the center of the weld along x_2 (u_1, u_2, u_3 represent displacements of x_1, x_2 and x_3 respectively) (c) the horizontal displacement in the center of the plate along x_1* 91

4.11 *Energy flow snapshots for the shear weld guided mode from frequency 50 kHz to 300 kHz.* 92

4.12 *Phase velocity dispersion curve of shear weld guided mode predicted by SAFE method.* 93

4.13 *Mode shapes of four fundamental propagation modes of the weld at 100 kHz. Arrows indicate displacements in the cross section.* 95

4.14 *Phase velocity dispersion curves of the fundamental propagation modes in the steel weld and in the 6-mm-thick steel plate.* 96

4.15 *The FWHM of the shear weld guided mode at 100 kHz.* 97

4.16 *The energy distribution (FWHM) with different height (a) and width (b) of the weld.* 98

4.17 *Experimental setup. (a) plan view, (b) side view* 99

4.18 *Measured (stars) and theoretically predicted (line) group velocity dispersion curve of the shear weld-guided mode.* 101

4.19 *Normalized displacement amplitude measured at different locations along monitor line one (stars) and comparison with the beam spreading wave from a point source on a plate (dashed line).* 102

4.20 *Measured (stars) and theoretically predicted (solid line) normalized amplitude of displacement monitored along monitor line two, 300 mm from the source, and comparison with the beam spreading wave from a point source on a plate (dashed line). The width of the bar is also shown.* 103

5.1 *Experimental setup* 107

5.2 *Time trace of the shear weld guided mode monitored at 300 mm away from the source at 100 kHz (a) and 60 kHz (b)* 109

5.3 *Experimental results of the reflection ratio spectrum of the shear weld guided mode obtained from 30 mm slit parallel to the edge of the weld.* 110

5.4 *Calibration experiment setup (a) and the results of group velocity dispersion curve (b), attenuation (c) and displacement mode shapes (d).* 111

5.5 *Schematic of the calibration modelling using the SAFE method* 112

5.6 *Mode shapes in terms of displacement monitored in a line across the center of the weld for different geometries, predicted from the SAFE method (lines) and measured from the experiment (stars).* 113

5.7 *(a) SAFE predictions (−) of the group velocity dispersion curve of shear weld guided mode on the geometry with* $h1 = 2.5mm, h2 = 2.5mm$ *and compares with experimental results (∗); (b) SAFE predictions (−) of the attenuation velocity dispersion curve.* 114

5.8 *The spectrum of the FWHM from 50 kHz to 150 kHz.* 114

5.9 *Schematic of the three-dimensional time step simulation.* 116

5.10 *Time snapshots of the shear weld guided mode propagation along the weld: (a) and (b) show the incident wave; (c) and (d) show the reflected wave.* 117

5.11 *(a) Time trace of a 3 cycle toneburst signal monitored at 100 mm and 400 mm away from the source. (b) Zoomed picture of the reflected waves.* 118

5.12 *Reflection coefficient spectrum with cracks of different lengths (solid line 30 mm, dashed line 24 mm and dotted line 16 mm) parallel to the edge of the weld: (a) FE results (b) experimental results* 120

5.13 *Variation of reflection coefficient with location of the cracks parallel to the weld.* 122

5.14 *Reflection coefficient spectrum for cracks normal to the edge of the weld: (a) FE predictions (b) experimental results.* 123

5.15 *Reflection coefficient spectrum for flat-bottom holes with different depths: (a) FE predictions (b) experimental results.* 125

5.16 *Time snapshots of the compression weld guided mode propagation along the weld (a), and scattering from a crack parallel to the edge of the weld (b), a crack normal to the edge of the weld (c) and a flat-bottom hole in the heat affected zone (d).* 127

6.1 *Schematic of a lap joint showing the possible defects (a) and the SAFE modelling of this geometry (b)* 132

6.2 *Cross-section distribution of axial energy flow for several eigen solutions obtained for the lap joints at 100 kHz. The solid lines show two feature guided modes, while the dashed lines show unwanted plate resonance solutions. The grey zone indicates the joint area.* 134

6.3 *(a) Energy flow snapshot for the feature guided mode 1 at 100 kHz, with arrows indicating displacements of the cross-section, (b) the mode shape of displacement through the thickness of the plate, (c) the dispersion curve of phase velocity from 30 kHz to 100 kHz, (d) the dispersion curve of attenuation from 30 kHz to 100 kHz* 135

6.4 *(a) Energy flow snapshot for feature guided mode 2 at 100 kHz, with arrows indicating displacements of the cross-section, (b) the mode shape of displacement through the thickness of the plate, (c) the dispersion curve of phase velocity from 30 kHz to 150 kHz, (d) the dispersion curve of attenuation from 30 kHz to 150 kHz* 136

6.5 *(a) Phase velocity dispersion curves of the propagation modes in the joint geometry and in the 1.6-mm-thick aluminium plate, (b) mode shapes of four propagation modes of the joint geometry at 100 kHz. Arrows indicate displacements in the cross section* 137

6.6 *Schematic of 2D model of a aluminium stiffener bonded on a aluminium plate.* 138

6.7 *Cross-section distribution of axial energy flow for one eigen solution selected corresponding to a wave mode propagating along the stiffener-bond-plate region and radiating energy in the aluminium plate, at 100 kHz. The grey zone indicates the stiffened region.* 140

6.8 *The energy flow snapshot for the three feature guided modes at 40 kHz, with arrows indicating displacements of the cross-section.* 141

6.9 *Phase velocity dispersion curves of the central geometry with the aluminium stiffener, adhesive and aluminium plate with the same width as the stiffener, from 10 kHz to 70 kHz, are shown in solid lines. Phase velocity dispersion curves of a 3-mm thick aluminium plate are shown in dash-dot lines.* 142

6.10 *Energy flow snapshots for the three guided modes which can form the feature guided modes at 40 kHz, with their displacement mode shapes on the border of the plate along the thickness presented in the right column.* 143

6.11 *Energy flow snapshot for the four feature guided modes at 60 kHz, with arrows indicating displacements of the cross-section.* 144

6.12 *The energy flow snapshot for mode 4, 1 and 7 in the central structure including the stiffener at 60 kHz, and their displacement mode shapes along the thickness of the plate are presented in the right column.* . . 145

6.13 *(a) Picture of a heat exchange tube plate and (b) 2D cross-section of 1 period of the geometry.* 146

6.14 *Phase velocity dispersion curves of 7 mm thick steel pipe with 24 mm inner radius.* 147

6.15 *The energy flow snapshot for all the guided modes in the heat exchanger tube at 30 kHz, with arrows indicating displacements of the cross-section.* 148

6.16 *Phase velocity dispersion curves of the heat exchanger tube from 10 kHz to 60 kHz, without showing higher order modes.* 150

7.1 *Schematic of feature guided wave inspection with absorbers to attenuate guided waves in plates.* 159

A.1 *Schematic of a laser interferometer* 161

A.2 *Schematic of the measurement of out-of-plane (a) and in-plane (b) vibration* 162

List of Tables

2.1 Comparison of SAFE solution and DISPERSE prediction of the guided modes on a 1mm radius steel cylinder immersed in glycerol. 52

3.1 Mechanical properties for materials used in the SAFE modelling. . . . 61

6.1 Mechanical properties for materials used in the SAFE modelling. . . . 132

Chapter 1

Introduction

1.1 Motivation

Conventional Non-Destructive Testing (NDT) techniques such as ultrasonics [1–3] and eddy current [4, 5] are mainly based on point-by-point inspection systems, thus are time-consuming and tedious. Ultrasonic guided wave testing is an attractive alternative for large-area inspection since it offers the potential for rapid screening from a single transducer position and remote inspection of physically inaccessible areas of the structure. Compared to bulk waves, guided waves exist only in waveguides, such as plates and pipes, in which they continually interact with the boundaries of the material, therefore they are confined and allowed to propagate over long distance. However, guided wave inspection is complex because there are many modes in plates and pipes and they are in general dispersive (their velocity is a function of frequency). Therefore understanding the properties of guided waves, such as the dispersion curves, through-thickness mode shapes and attenuation, is essential for choosing proper modes and frequencies for inspection.

For waveguides defined by simple geometries (flat plates or cylindrical structures), analytical methods are used to determine the solutions of dispersion equation. For a multi-layered structure, more general solutions can be obtained using methods based on the superposition of bulk waves, including, for example, the transfer ma-

trix method [6], the global matrix method [7] or the surface impedance matrix method [8]. A software package named DISPERSE [9] was developed in the NDT laboratory at Imperial College, which provides a tool to quickly evaluate the properties of guided waves. It applies the global matrix method to model regular structures such as plates or cylinders made of homogeneous or multilayered, isotropic or transversely isotropic materials, immersed in a fluid or embedded in a solid. Based on the analytical solutions for guided waves, screening systems for pipeline inspection have been commercialized and applied in industry [10–13]. Developments for using guided waves to inspect plate structures are also advanced [14].

However guided waves propagation on irregular cross-sectional geometries, such as railway lines or T-shaped beams cannot be solved by analytical methods. For such cases the Semi-Analytical Finite Element (SAFE) method has been developed, which is also called the "spectral element", "strip element", or "waveguide finite element" method. This uses a finite element representation of the cross section of the waveguide, thereby enabling arbitrary definitions of shapes, together with a harmonic description along the propagation direction. Thus only a two-dimensional discretization of the cross-section is needed, with considerable computation saving compared to a three-dimensional discretization of the waveguide. Research on the SAFE method has been undertaken for many years to investigate guided wave propagation on thin walled shells [15], rails [16, 17], wedges [18] and bars with complex shape [19]. However most of the work in literature requires specific programming inside a Finite Element (FE) code. In addition, little study has been done to address problems where some of the energy leaks from the waveguide into the surrounding fluid or solid medium of infinite extent, because the guided waves then attenuate, needing a complex description of their propagation. Such cases are important, particularly for two practical problems which have motivated this thesis.

The first motivation is related to fluid density measurement. Conventional ultrasonic measurements of density use the time of flight and reflection coefficient methods, however for these methods the liquid compressibility has to be known and measurements have to be carried out in a test cell. An ultrasonic "dipstick" sensor is an

attractive alternative without the need for accurately machined test cells. The idea is that an ultrasonic wave which propagates in a solid waveguide structure can sense the presence and nature of the adjacent fluids. As it is shown in Fig. 1.1, when a torsional wave pulse propagates along a waveguide submerged in a fluid, it interacts at the boundary with surrounding fluid. As a result, the boundary layer of the fluid is alternately accelerated and decelerated. If the waveguide has a non-circular cross section, normal forces are exerted on the surrounding fluid, and fluid will have to be displaced as the cross section rotates back and forth. This mechanism effectively adds some of the mass of the fluid to the waveguide and changes its inertia. The change in inertia is reflected in a change in torsional wave velocity of the wave in the waveguide. Hence by measuring the speed of propagation of the torsional wave, the density of the fluid can be estimated. Bau [20] suggested an approximate theory to relate the speed of the torsional wave to the density of the surrounding fluid, with a calculation of a two-dimensional, inviscid flow field of the fluid. However, the accuracy of the approximate inversion of the measurements to infer the density of the fluids has been compromised due to the complexity of the wave behaviour in the noncircular cross-sectional shape.

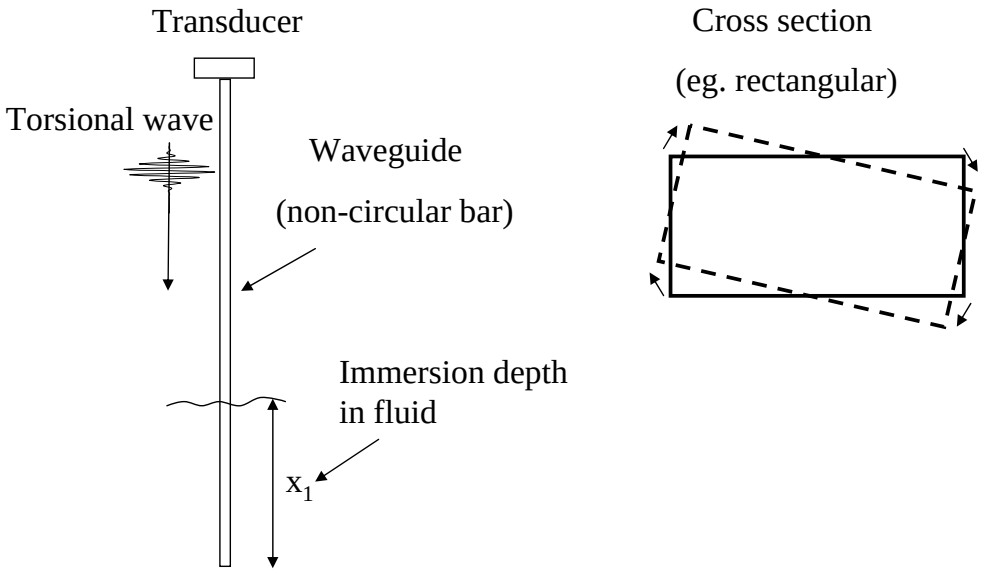

Figure 1.1: *Schematic of a torsional "dipstick" sensor.*

The second motivation is related to large area inspection of plates with features. An experimental study [21] was undertaken by Dr Jeff Sargent of BAe Systems, working at Imperial College, on the detection of defects in a welded plate, which revealed a strong received signal at positions close to the weld when the transmitting transducer was placed with appropriate orientation upstream and close to the weld. This implies that there existed 'weld-guided' modes which can propagate along the weld and concentrate the energy in and around the weld. Similar trapped modes have also been demonstrated subsequently by Postnova and Craster [22] from an analytical calculation on a welded plate structure based on the long-wave theory. Fig. 1.2 schematically shows the propagation of a feature-guided wave on a welded plate from a pulse excitation, which excites an in-plane displacement parallel to the weld. As can be seen from the figure, due to the geometry change, part of the energy is trapped in and around the weld and propagates along the weld. This is very attractive for NDE as we know defects frequently occur preferentially in or near the weld, and the same is true for other geometric features, such as joints and stiffeners. Therefore, instead of seeing the features as a problem, it may be possible to exploit them as waveguides to focus the energy of the guided wave, which offers the potential to quickly inspect for defects such as corrosion along long lengths of features on plate-like structures.

In order to exploit this feature-guided wave, it is necessary to understand its nature and propagation characteristics. Juluri *et al.* [23] performed a three dimensional time step finite element simulation on an idealized welded plate geometry, and demonstrated the existence of the compression weld-guided mode (similar to the Lamb S0 mode in the plate), which had been experimentally detected [21]. However these simulations are very time consuming, and can only model the chosen frequency and wave mode, thus they are not sufficient to investigate the guided wave properties over ranges of parameters and feature geometries. In order to further understand how the guiding is affected by the geometry and frequency, it is therefore necessary to perform a modal study of the welded-plate, in order to fully predict the properties of the waves which are guided by the features. Such a model may then also create the possibility of finding other feature-guided modes which could be candidates for

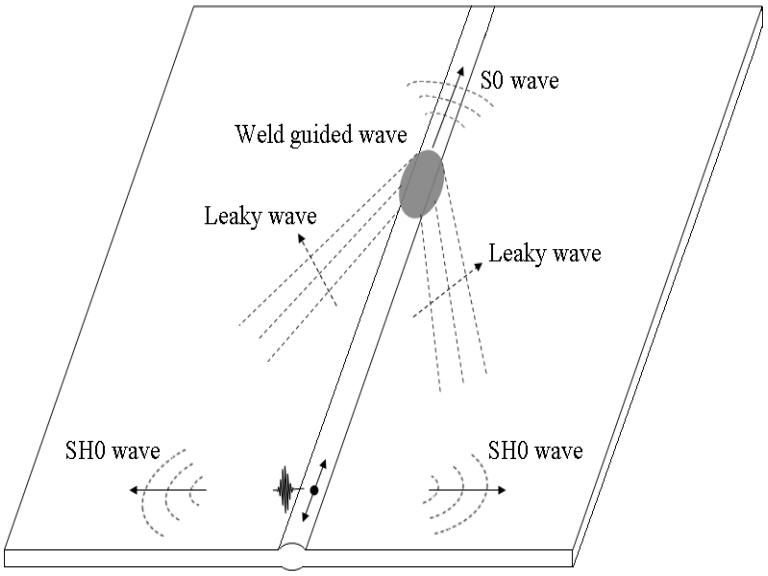

Figure 1.2: *Schematic of the propagation of a feature-guided wave on a welded plate from a pulse excitation.*

inspection but have not yet been discovered.

It can be seen that both problems require models which can address cases of leaky guided waves from an arbitrary cross-sectional geometry. This thesis aims to provide a generic tool to predict the properties of guided waves propagating along waveguide structures of arbitrary cross-section, including the possibility of energy partially leaking into the attached adjacent material. It will be useable on all such kinds of wave guides including welds, bends, stiffeners and other attached features, lap joints, tubeplates, railway lines, beams, and immersed or embedded waveguides. The model will predict the dispersion curves (frequency-velocity relationships for the possible guided wave modes), the rate of attenuation by leakage of energy into the adjacent material, and the mode shapes (distributions of stress and displacement across the section of the waveguide).

1.2 Outline of Thesis

The thesis can be generally divided into three parts. Chapter 2 describes the theory and development of the Semi-Analytical Finite Element (SAFE) method, which will be used throughout the thesis to modally investigate the guided wave modal properties in structures with irregular cross-sections. Two applications based on the method are presented in the following parts of the thesis. Chapter 3 presents the study on the torsional dipstick, while chapters 4-6 describe the application to feature guided waves. Specifically, subsequent to the introductory remarks in this chapter, the thesis is structured in the following way.

Chapter 2 first reviews the background of the guided waves and their properties on simple geometries such as plates and cylinders based on analytical solutions. Since this is well documented in literature, it will be restricted to explanations which are essential for the comparison with the FE modelling. Then the SAFE method is described for the prediction of wave properties on irregular cross-sectional shapes. The model is validated by comparing the results with the analytical model on two cases of a solid bar immersed in a perfect and a viscous fluid respectively.

Chapter 3 applies the SAFE method to model accurately the propagation velocity and leakage of guided waves along an immersed waveguide with arbitrary non-circular cross-section. An accurate inverse model is provided to measure the density of the fluid by measuring the change of the torsional wave speed. Experimental results obtained with a rectangular bar in a range of fluids show very good agreement with the theoretical predictions. The potential to use the model for sensor optimization is also discussed in this chapter.

In Chapter 4, the SAFE model is applied on a geometry of a real welded plate and provides modal investigation on the properties of feature guided waves and the physical reason for the energy trapping effect. Significantly, during the modal study, another interesting shear mode, which is similar to the SH0 mode in the plate, has been discovered. The particle displacement of this mode is perpendicular to the plane of propagation and therefore it is expected to be more sensitive than the

compression mode to the fatigue cracks that are typically aligned along the weld in the heat affected zone. In addition this shear mode has no leakage to the side plates and is almost non-dispersive, thus it is very interesting as a candidate mode for industrial inspection. Experiments have been set up to demonstrate the existence of this shear weld guided mode and the accuracy of the SAFE model, showing very good agreement.

Chapter 5 presents the study on the interaction of weld-guided modes with different type of defects, including cracks perpendicular or parallel to the weld and circular holes, in the heat affected zone next to the weld. The results are obtained from both Finite Element simulations and experimental measurements, showing good agreement. The sensitivity of the two welded-guided modes to different defects has been discussed and suitable choices of frequency to detect these defects for each mode have been suggested.

Chapter 6 applies the SAFE method on three geometries: lap joints, stiffened plates and heat exchanging tubes, in which similar feature guided waves are discovered. The properties of the discovered modes and potential applications of detecting defects on these geometries are discussed.

Chapter 7 summarizes the findings in the thesis and discusses the potential for future work.

Chapter 2

Guided Waves

2.1 Background

This chapter introduces the fundamental concept of ultrasonic waves propagation in unbounded media and guided ultrasonic waves propagation in waveguides with both regular(eg. plate, cylindrical structure) and irregular geometries.

In unbounded, infinite, elastic media, only two types of waves can exist, the longitudinal (also named as compression) waves and shear (also named as transverse) waves, their velocity being constant with frequency. However in bounded media such as plates, rods and pipes, different modes of guided waves can propagate which is the result of the interaction of compression and shear waves at the boundary. For the waveguides with regular geometries analytical methods have been well developed to predict the properties of guided waves, while for waveguides with irregular cross-sectional geometry finite element methods seem necessary. The following characteristics of guided waves such as their dispersion properties which describe the relation between velocity and frequency, and the mode shapes which are the distribution of field variables over the cross-section of the wave guide, will be discussed in this chapter.

2.2 Wave Propagation in Bulk Media

As the theory of elastic waves propagation in unbounded media is well documented in many text books [24–27], only the principal equations are outlined in this section.

Combining Euler's equation of motion and Hooke's law yields Navier's differential equation of motion for an isotropic elastic medium:

$$\mu\nabla^2\mathbf{u} + (\lambda+\mu)\nabla\nabla\cdot\mathbf{u} = \rho\frac{\partial^2\mathbf{u}}{\partial t^2}, \tag{2.1}$$

where $\mathbf{u}$ is the particle displacement vector, ρ is the material density, λ and μ are the Lamé constants and the ∇^2 is the three dimensional differential operator. Eq. 2.1 is a compact expression which can be expanded in its three spatial components x,y,z:

$$\begin{aligned}
\mu(\frac{\partial^2}{\partial x^2}+\frac{\partial^2}{\partial y^2}+\frac{\partial^2}{\partial z^2})u_x + (\lambda+\mu)\frac{\partial}{\partial x}(\frac{\partial u_x}{\partial x}+\frac{\partial u_y}{\partial y}+\frac{\partial u_z}{\partial z}) &= \rho\frac{\partial^2 u_x}{\partial t^2} \\
\mu(\frac{\partial^2}{\partial x^2}+\frac{\partial^2}{\partial y^2}+\frac{\partial^2}{\partial z^2})u_y + (\lambda+\mu)\frac{\partial}{\partial x}(\frac{\partial u_x}{\partial x}+\frac{\partial u_y}{\partial y}+\frac{\partial u_z}{\partial z}) &= \rho\frac{\partial^2 u_y}{\partial t^2} \\
\mu(\frac{\partial^2}{\partial x^2}+\frac{\partial^2}{\partial y^2}+\frac{\partial^2}{\partial z^2})u_z + (\lambda+\mu)\frac{\partial}{\partial x}(\frac{\partial u_x}{\partial x}+\frac{\partial u_y}{\partial y}+\frac{\partial u_z}{\partial z}) &= \rho\frac{\partial^2 u_z}{\partial t^2},
\end{aligned} \tag{2.2}$$

By means of the Helmholtz decomposition, $\mathbf{u}$ can be expressed as a sum of the gradient of a compressional scalar potential $\nabla\phi$ and the curl of an equivoluminal vector potential $\mathbf{H}$:

$$\mathbf{u} = \nabla\phi + \nabla\times\mathbf{H}, \tag{2.3}$$

where $\mathbf{H}$ has zero divergence:

$$\nabla\cdot\mathbf{H} = 0, \tag{2.4}$$

By substituting these potential functions in the Navier's equation 2.1, the equation of motion can be separated into two independent equations for two potentials

$$\frac{\partial^2\phi}{\partial t^2} = c_l^2\nabla^2\phi, \tag{2.5}$$

$$\frac{\partial^2 \mathbf{H}}{\partial t^2} = c_s^2 \nabla^2 \mathbf{H}, \tag{2.6}$$

where c_l and c_s are the velocities of longitudinal and shear waves in the infinite isotropic medium which can be expressed as

$$c_l = \sqrt{\frac{\lambda + 2\mu}{\rho}}, \tag{2.7}$$

$$c_s = \sqrt{\frac{\mu}{\rho}}. \tag{2.8}$$

A general solution to Eq. (2.5) and (2.6) is

$$\phi = \phi_0 e^{i(k_l z - \omega t)}, \tag{2.9}$$

$$\mathbf{H} = \mathbf{H}_0 e^{i(k_s z - \omega t)}, \tag{2.10}$$

where ϕ_0 and $\mathbf{H}_0$ are arbitrary initial constants, z is the spatial coordinate of the wave propagation direction, t is the time variable, $\omega = 2\pi f$ is the angular frequency and $k_{l,s}$ are the longitudinal and shear wavenumbers from which it follows that

$$k_{l,s}^2 = \frac{\omega^2}{c_{l,s}^2} \tag{2.11}$$

2.3 Guided Waves Propagation in Waveguides with Regular Cross-sections

2.3.1 Guided waves

An ultrasonic guided wave is a wave whose energy is concentrated between the boundaries, and is guided along a structure (waveguide), similarly as light in an optical fibre. It can be thought as a superposition of bulk waves that propagate in a structure and get reflected back and forth between the boundaries. The amplitudes, directions and phases of the partial waves must be determined such that the boundary conditions at the boundaries of the waveguide are satisfied.

In general, guided waves can be described by expressions for the field variables such as stress and displacement. For example, in a flat plate structure, the displacement

field can be written as

$$u(x, y, z, t) = u(y)e^{i(kz-\omega t)}, \tag{2.12}$$

where $u(y)$ is a displacement distribution function, k is the wavenumber of the guided wave mode, z the propagation direction, y the direction normal to the propagation direction, $\omega = 2\pi f$ the angular frequency and t the time variable. In a cylindrical system, the displacement field can be expressed as:

$$u(r, \theta, z, t) = u(r)e^{i\nu\theta}e^{i(kz-\omega t)}, \tag{2.13}$$

where ν is the angular wavenumber, $u(r, \theta, z, t)$ is a radial distribution function of the displacement in r, θ and z directions, respectively. Since only propagation in the direction of the axis of the cylinder is considered, and the field variables such as displacements and stresses must be continuous in the angular direction, ν must be a whole number. It is commonly referred to as the circumferential order.

The wavenumber k can be complex if the waveguide is embedded or immersed in another medium, which extends infinitely, the partial waves may be transmitted across the interface, thus bulk waves may be excited in the embedding or immersing medium, leaking away from the waveguide.

The waveguide can also consist of a number of layers itself. In order to determine the guided waves in arbitrary multilayered system, a general purpose software package DISPERSE was developed in the laboratory by Lowe [7] and Pavlakovic [9,28]. This is based on the 'global matrix method' proposed by Knopoff [29], later refined by Schmidt and Jensen [30]. The global matrix method involves the construction of a single matrix equation, which describes the displacement and stress fields associated with a harmonic wave propagating along the whole multilayered structure. The size of the matrix is determined by the number of layers and the number of partial waves needed within each layer.

Initially, the magnitudes and phases of the partial waves are not known, and they have to be found by considering the boundary conditions. A set of fields for the whole collection of layers requires the stress and displacement to be consistent at

all of the interfaces between the layers, and appropriate boundary conditions must also be satisfied at the extreme surfaces of the structure. For example, in the simple case of a hollow pipe, the normal stresses at the inner and outside surfaces of the pipe must be zero. It follows that all the partial bulk waves are totally reflected within the waveguide. The calculations then consist of searches to find solutions when all of these boundary conditions can be satisfied simultaneously. The set of boundary conditions is expressed in a global matrix [G], which relates the partial wave amplitudes to the physical constraints of the whole system and solves

$$[G]\{A\} = 0 \tag{2.14}$$

where $\{A\}$ is a vector of the partial wave magnitudes and phases. The above equation is satisfied when the determinant of the global matrix vanishes, and solutions are sought in the wavenumber-frequency space. For a particular structure, there is an infinite number of solutions to satisfy the above equation, which makes it possible for many guided wave modes to coexist. Each mode has its own phase velocity-frequency relation (dispersion) and a corresponding mode shape, which can be calculated by the algorithms described by Lowe [7].

2.3.2 Dispersion curves

The phase velocity is the rate at which the phase of the wave propagates in space. It is given in terms of the wavelength λ and frequency f:

$$c_p = \lambda f \tag{2.15}$$

Or, equivalently, in terms of the wave's angular frequency ω and wavenumber k by

$$c_p = \frac{\omega}{k} \tag{2.16}$$

Another commonly used concept is the group velocity which describes the speed at which a wave packet (or envelope) travels. This rate is determined by how quickly the energy of the wave will propagate down the structure and will always be smaller than the fastest bulk wave present in the system. The group velocity is related

to the phase velocity through the following equation (see [24] and [27] for more details)

$$c_g = \frac{d\omega}{dk} = c_p + k\frac{dc_p}{dk} \tag{2.17}$$

Guided waves are generally dispersive, which means their phase velocity, group velocity and attenuation varies with frequency. The dispersion of guided modes results in the distortion of the shape of a multi frequency wave packet that propagates for long distances. In order to select the suitable guided modes and frequency for inspection, it is therefore important to understand the dispersion curves of guided modes.

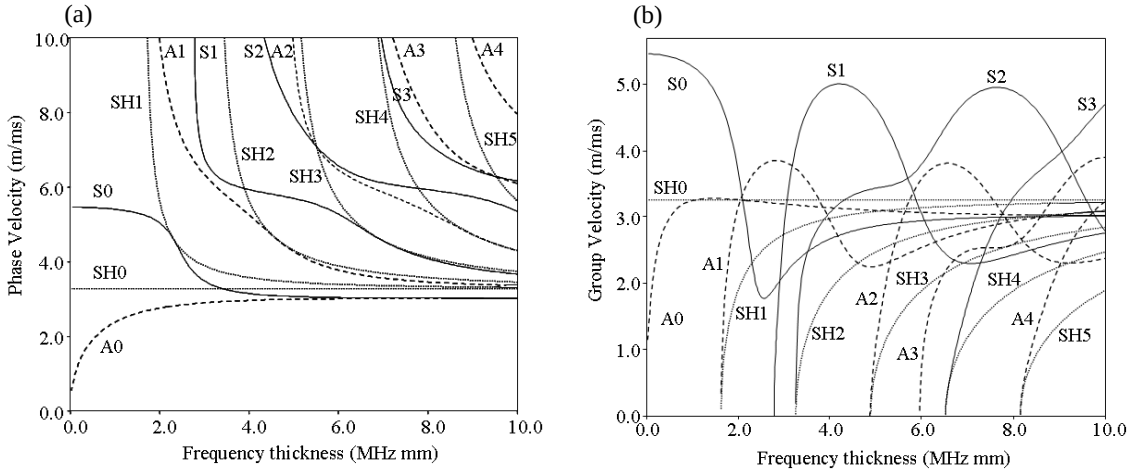

Figure 2.1: *Phase velocity (a) and group velocity (b) dispersion curves for a steel plate in vacuum. Longitudinal modes are plotted in solid lines (—), flexural modes in dashed lines (- - -), and shear horizontal modes in dotted lines (· · ·).*

Typical dispersion curves of a steel plate are shown in Fig. 2.1 for phase velocity and group velocity respectively, which are generated by DISPERSE. Since the frequency axis may be scaled with the plate thickness, the scale is plotted as frequency-thickness for generality. There are three families of guided modes: longitudinal, flexural and shear horizontal modes. Each family comprises an infinite number of modes. In a plate system they can also be labeled conventionally as S mode (symmetric), A mode (antisymmetric) and SH modes respectively, the numbers following indicating their harmonic order. As it can be seen from the figure, more modes exist

at higher frequency. Except the SH0 mode, which is completely nondispersive, all the other guided wave modes have different characteristics at different frequencies.

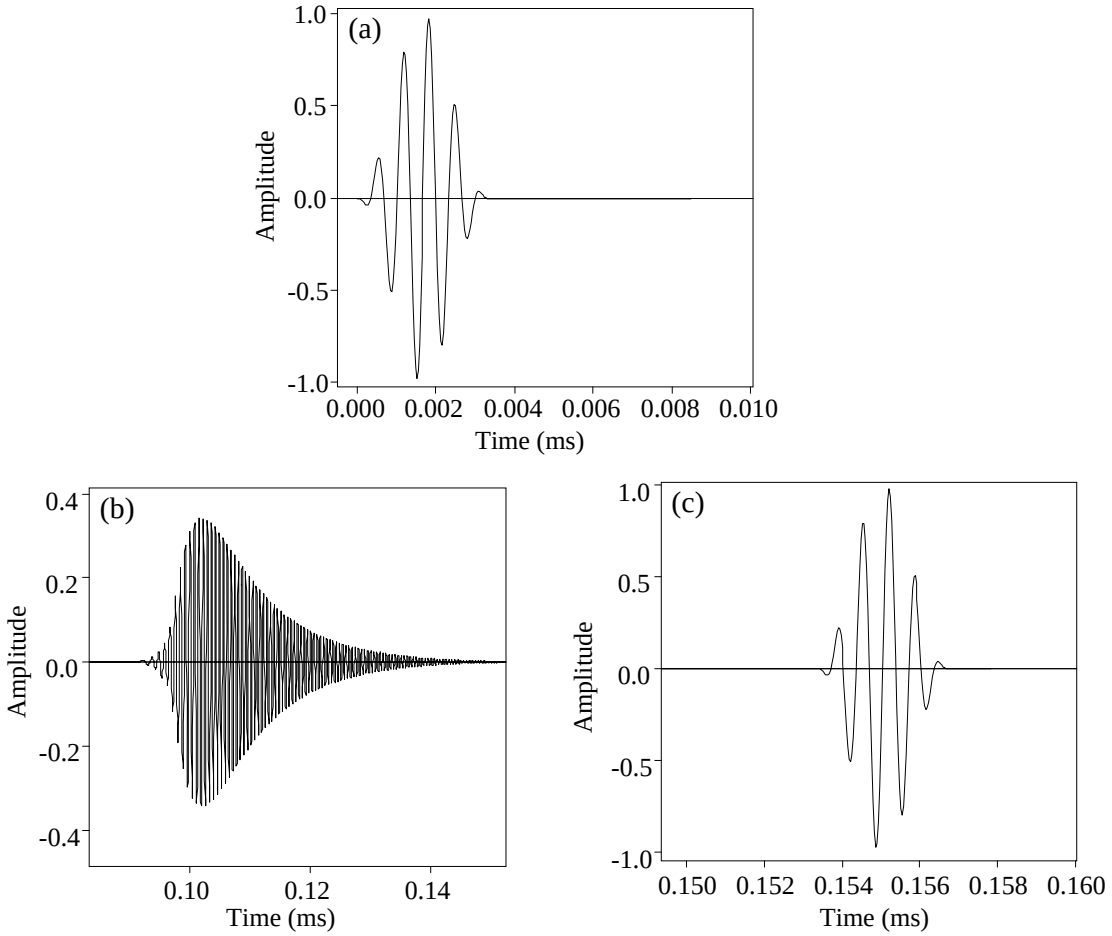

Figure 2.2: *5 cycle Hanning windowed toneburst signal at excitation(a) and a prediction by the DISPERSE software of the signal after 0.5 m propagation distance as S0 mode (b) and SH0 mode (c) on a 1mm thick steel plate.*

To illustrate the dispersion effect, Fig. 2.2 compares (calculated by DISPERSE) a 5 cycle Hanning windowed toneburst signal of the S0 and SH0 mode propagation with center frequency of 2 MHz monitored after 0.5 m. It can be seen that the S0 mode at this frequency suffers from strong dispersion: the wave-packet becomes distorted and the amplitude decreases. The further it propagates, the more it will disperse out. On the other hand, the SH0 mode has no dispersion, and thus the signal remains the same shape as the excitation. Practically it is more convenient to work with modes that have no or very little dispersion for long range testing,

although compensation methods [31, 32] can be applied if a dispersive mode has to be used.

2.3.3 Mode shapes

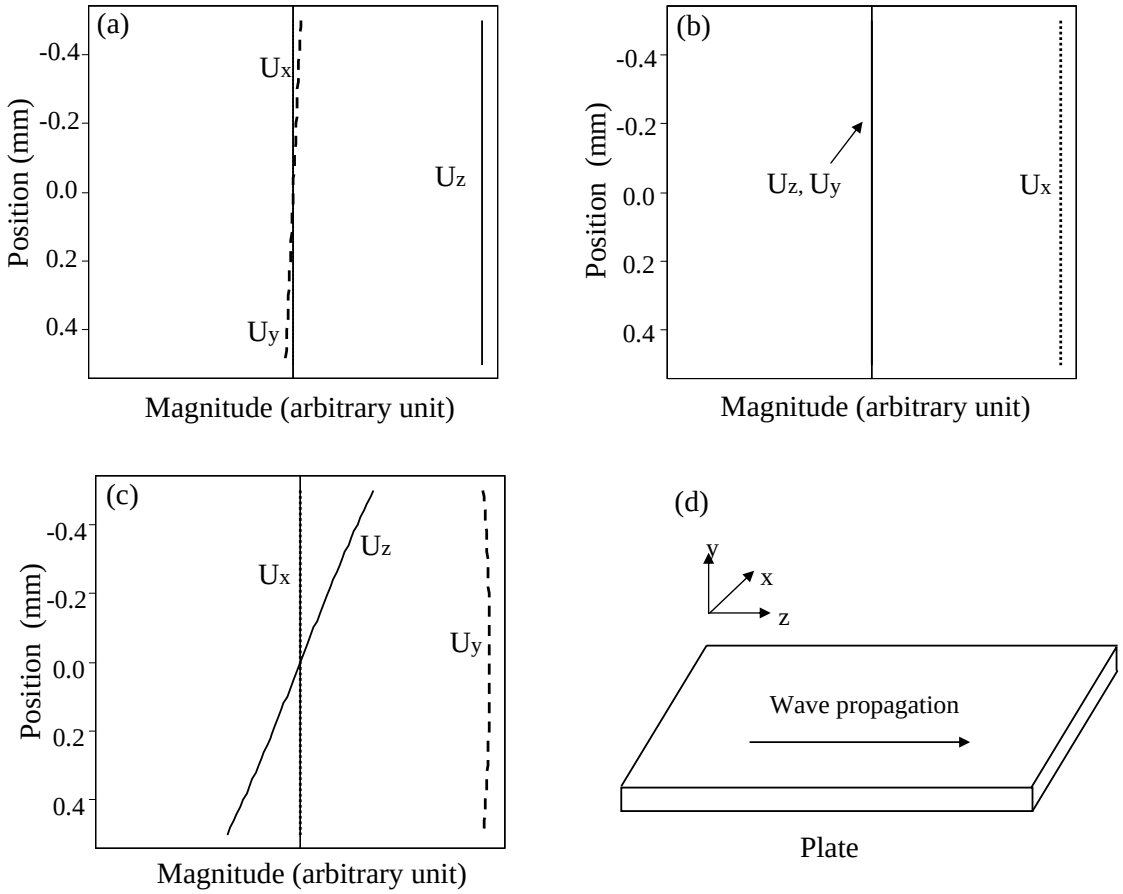

Figure 2.3: *Displacement mode shapes of the (a) S0 mode, (b) SH0 mode, (c) A0 mode at frequency thickness 0.2 MHz mm in a steel plate, and (d) shows the coordinate system.*

The mode shapes of the mode are the distribution of the field quantities (displacements, stresses, power flow etc.) across the cross section of the waveguide. The different mode families are best distinguished by considering the components of their displacement mode shapes. Fig. 2.3 (a-c) show as an example, the displacement mode shapes of the three fundamental plate modes at a frequency-thickness product of 0.2 MHz mm, and Fig. 2.3 (d) shows the coordinate system. It can be seen that the mode shape of the S0 mode at this frequency-thickness product

is dominated by the in-plane displacement u_z; there is only little displacement in the y direction and no displacement in the x direction. The mode shape of the SH0 mode has in-plane displacement u_x only, and propagates at the bulk shear velocity of the waveguide. The A0 mode is dominated by the out-of-plane displacement u_y, and also has a linear variation of the less strong in-plane displacement u_z across the thickness.

2.3.4 Leaky guided waves

If the wave guide is surrounded by an infinite medium, the energy from the guided waves may be transmitted across the interface. Thus bulk waves are excited in the surrounding medium, radiating away from the waveguide. Thereby, the guided wave which is propagating along the axial direction has attenuation due to the energy leaking out from the waveguide. Fig. 2.4 shows a schematic of the leaky guided wave. The leakage angle θ is determined by the Snell's law [33], via the relationship

$$\sin\theta = \frac{c_1}{c_p}, \tag{2.18}$$

where c_1 is the bulk velocity of the surrounding medium and c_p is the phase velocity of the guided mode. The rate of the leakage depends on both the material properties of the waveguide and the surrounding medium. Generally, the smaller the difference in the acoustic impedance of the materials, the higher is the attenuation due to the large transmission coefficient of the bulk waves across the interface.

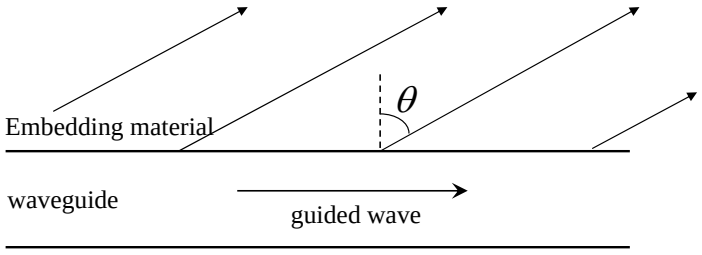

Figure 2.4: *Schematic showing a leaky waveguide, which leaks bulk waves at an angle θ.*

Eq. (2.18) is not valid if the phase velocity of the guide mode is smaller than the

bulk velocity of the surrounding medium. In these cases, the bulk waves propagate parallel to the interface, causing the energy being trapped to the waveguide surface. Therefore, these guided modes are non-leaky, for example the Scholte wave [27, 34].

An example calculation of the leaky guided wave has been carried out on a cylindrical system, in which a 1 mm radius steel bar is immersed in water. The dispersion curves of the phase velocity are traced using the DISPERSE software, which are shown in Fig. 2.5. The notation of a cylindrical system has been adopted after Silk and Bainton [35]. Letters L, T, F stand for longitudinal, torsional and flexural wave respectively. The first number in the bracket indicates the circumferential order, being zero for both longitudinal and torsional modes as they are both axial-symmetric, whereas the second number in the bracket is a counter in order to distinguish between the modes of one family. There are an infinite number of circumferential orders and an infinite number of modes for each of these circumferential orders. In the figure we present dispersion curves for the longitudinal, torsional and flexural modes up to the 3rd order.

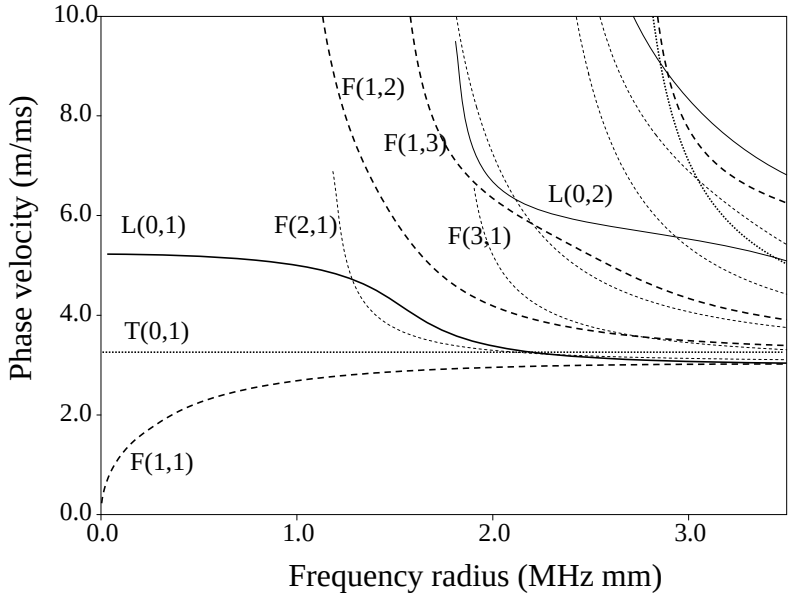

Figure 2.5: *Phase velocity dispersion curves for a 1mm radius steel bar immersed in water. Longitudinal modes are plotted in solid lines (—), flexural modes in dashed lines (- - -), and torsional modes in dotted lines (· · ·).*

Fig. 2.6 shows the attenuation dispersion curve for the three fundamental modes

L(0,1), T(0,1) and F(1,1). The attenuation of these guided modes is caused by the energy leaking away into the water while the guided wave is propagating along the bar. It can be seen from the figure that the attenuation of the L(0,1) mode is very small at low frequencies and increases at higher frequency. The T(0,1) mode has no attenuation at all. The F(1,1) mode does not attenuate at low frequencies, and then its attenuation increases with the increasing of frequency.

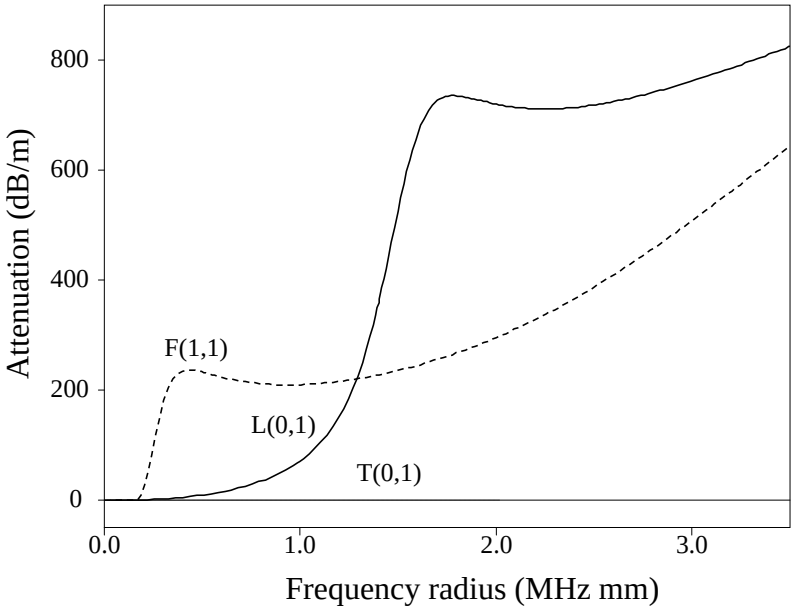

Figure 2.6: *Attenuation dispersion curves for a 1mm radius steel bar immersed in water. Only fundamental longitudinal modes (—), flexural modes (- - -), and torsional modes (· · ·) are plotted.*

These phenomena can be explained by their mode shapes. The L(0,1) mode has attenuation since it has surface displacement in the radial direction (out of plane displacement). As the frequency increases, the radial displacement of the longitudinal mode increases with respect to the axial displacement, so that more energy couples to the water, thus the attenuation increases. For the T(0,1) mode, the displacements are entirely in the angular direction, which are in-plane displacement at the surface. Since only compression bulk waves can propagate in water, the in-plane displacement on the surface of the circular bar does not couple into the water, thus there is no leakage. For the F(1,1) mode, it has no attenuation at low frequency since the phase velocity is lower than the bulk velocity in water. Thus there is no energy

leaking according to the Snell's law. The attenuation increases with the increasing of frequency due to the increasing of the proportion of the radial displacement.

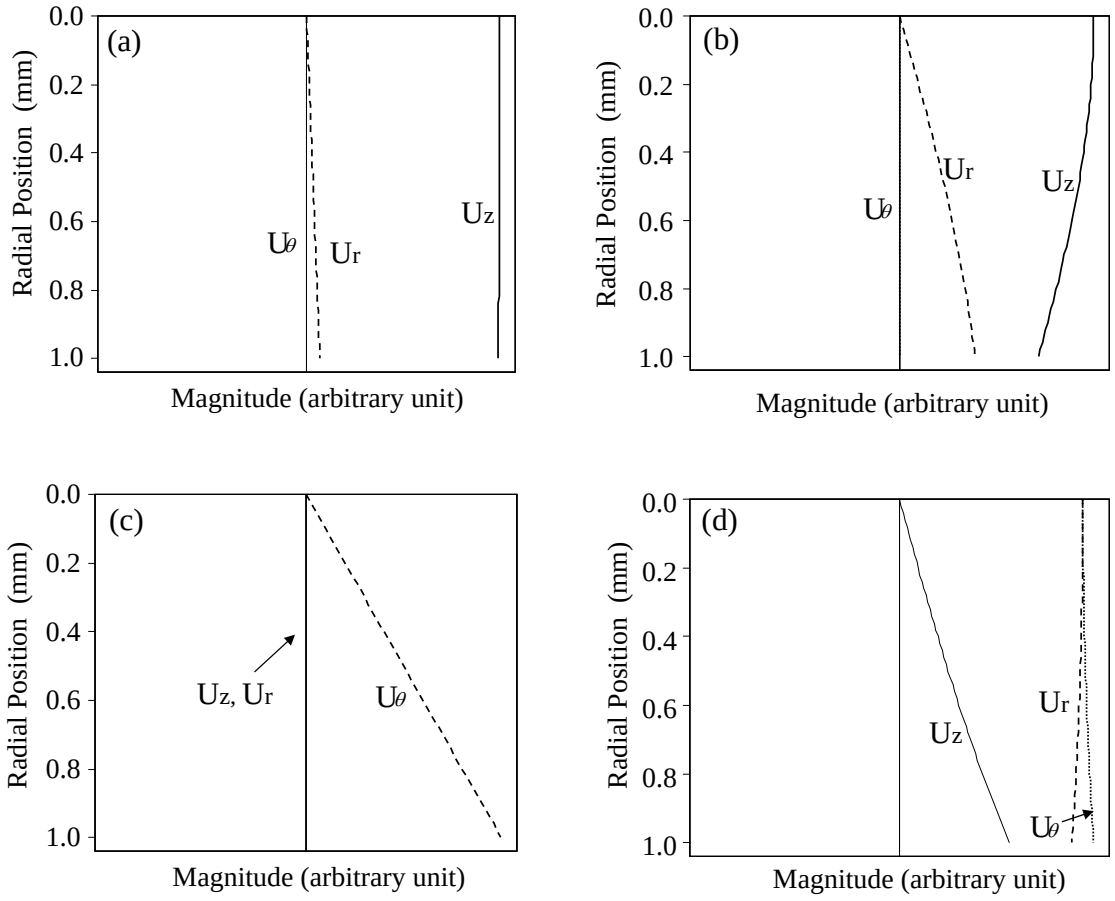

Figure 2.7: *Displacement mode shapes of the (a) L(0,1) mode at frequency radius 0.2 MHz mm, (b) L(0,1) mode at 1 MHz mm, (c) T(0,1) mode at 0.2 MHz mm and (d) F(1,1) mode at 0.2 MHz mm.*

2.4 Semi Analytical Finite Element (SAFE) method

In the above sections, we have revisited analytical solutions to the bulk wave propagation in unbounded media and the guided wave propagation in regular shaped structures such as plates and cylinders. In irregular geometries, such as railway lines or T-shaped beams, guided waves also exist due to partial waves reverberating between boundaries of the structures, however analytical methods are not able to

solve these problems. For such cases, it becomes necessary to introduce another approach, such as the finite element method, to predict the guided wave propagation on a geometry with irregular cross-section.

2.4.1 Literature review

There are two commonly-taken finite element approaches. One is named the Semi-Analytical Finite Element (SAFE) method, which is also called the spectral element, strip element, or waveguide finite element method. This is the method to study uniform waveguides of arbitrary cross sections. Fig. 2.8(a) shows the schematic of the SAFE method. In the SAFE method, only the cross-section, which is normal to the direction of wave propagation, needs to be meshed by finite elements. The waves are assumed to propagate harmonically. The other approach is called the periodic finite element method, whose schematic is shown in Fig. 2.8(b). In this method, the waveguide is assumed to be a periodic chain of the given guide section over one element depth, repeating this cell along the guide using periodicity conditions. A review of this method can be found in Ref. [36]. Based on a general theory presented by Mead [37] some periodic FE approaches and procedures have then been developed−see, for instance, Refs. [38–41]. However, in the applications discussed in this thesis, the cross-section will always be constant, therefore only the SAFE method will be investigated.

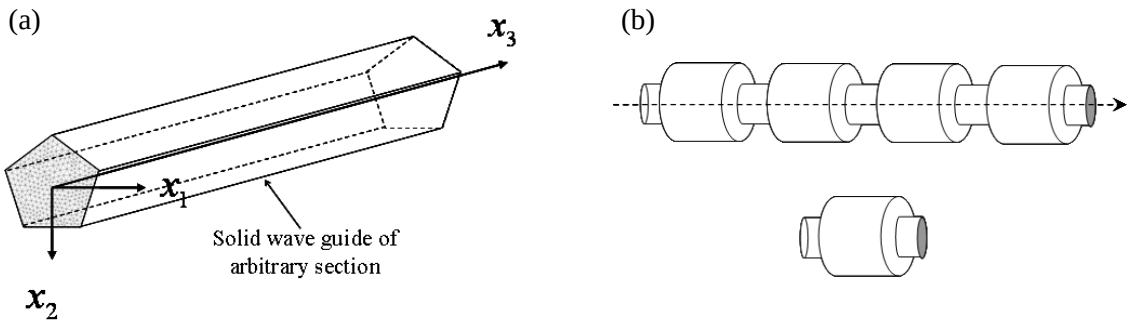

Figure 2.8: *Schematic of the SAFE method (a) and periodic finite element method (b).*

The SAFE method was first demonstrated in 1972 for dispersion solutions of solid

waveguides of arbitrary geometries [42]. Later, Damljanovic and Weaver [43] have developed the model to calculate both propagative modes and nonpropagative, evanescent modes (complex wavenumbers) for anisotropic cylinders. More recently, SAFE methods confined to obtaining the propagative solutions were applied to thin-walled waveguides [15], rails [16, 17], wedges [18], nonhomogeneous anisotropic beams [44] and rods [17]. Bartoli *et al* [45] extended the SAFE model to allow for viscoelastic material damping, so that the solutions are necessarily complex, the damping of the guided waves being represented by the imaginary part of the wavenumber.

A drawback of these models is that they all need to be developed in specific FE codes. Wilcox *et al* [46] have implemented an approximation of the SAFE method in a standard finite element package (in this case FINEL/FE77 [47]) by imposing a cyclic axial symmetry condition. It works by defining an axially-symmetric model with a very large radius compared to the dimensions of the cross section. For a specific cyclic order, the finite element eigensolver generates a chosen number of eigenfrequencies and eigenvectors, i.e. the vibration solutions of standing waves in the ring. The cyclic order of the standing wave corresponds to the number of wavelengths of a guided wave mode around the axisymmetric body, with the eigenvector being its displacement distribution or mode shape at the corresponding eigen frequency. However, this model can only describe the waveguide with stress-free exterior boundaries.

Predoi *et al* [48] have implemented the SAFE method in a commercial finite element package (COMSOL [49]) by reorganizing the SAFE equations in a standard Finite Element eigenvalue formalism which can be solved by commercial software. He also introduced the periodic boundary conditions in the SAFE method, which allow the modelling of infinitely wide guides with periodic changes in geometry or material properties along the width. Castaings and Lowe [50] have developed this model to address the leaky wave problem in which guided waves propagate along an elastic waveguide with arbitrary cross-section and radiate into a solid of infinite extent. This has been achieved by using an absorbing region to absorb the leaking waves

thus simulating an infinite extent of the solid medium. In our work, we have done a further development of the modelling capability, addressing the problem of leaky waves propagating along solid waveguides immersed in fluids, which will be described in the following sections.

2.4.2 SAFE method in solids

The mathematical model of the SAFE method in solids is based on the three dimensional elasticity approach. The differential equations of motion in an elastic domain of mass density ρ and elastic constants C_{ijkl} are

$$\sum_{j,k,l=1}^{3} [C_{ikjl} \frac{\partial^2 U_j}{\partial x_k \partial x_l}] + \rho\omega^2 U_i = 0; i = 1, 2, 3 \tag{2.19}$$

In the SAFE modelling, the displacement along the wave propagation direction (x_3 in Fig. 2.8(a)) are assumed to be harmonic, which can be written as:

$$u_i(x_1, x_2, x_3, t) = U_i(x_1, x_2) e^{I(kx_3 - \omega t)}, I = \sqrt{-1} \tag{2.20}$$

in which k is the wavenumber, $\omega = 2\pi f$ is the angular frequency, f being the frequency, t is the time variable and the subscript $i = 1, 2, 3$. Consequently, the wave modes are considered to be 'prismatic' in that the cross sectional distribution propagates according to a complex exponential function. This allows the equilibrium equation to be expressed in a two-dimensional eigenvalue problem that could be solved for wavenumber k in the propagation direction. After some intermediary transformations, Eq. 2.19 can be written in the following form:

$$C_{ikjl} \frac{\partial^2 U_j}{\partial x_k \partial x_l} + I(C_{i3jk} + C_{ikj3}) \frac{\partial (kU_j)}{\partial x_k} - kC_{i3j3}(kU_j) + \rho\omega^2 \delta_{ij} U_j = 0 \tag{2.21}$$

with summation over the indices $j = 1, 2, 3$ and $k, l = 1, 2$. The coefficients C_{ijkl} are the stiffness moduli and δ_{ij} is the Kronecker symbol. In the commercial FEM

code [49] used in this study, the formalism for eigenvalue problems has the general expression:

$$\nabla \cdot (c\nabla U + \alpha U - \gamma) - \beta \nabla U - aU + \lambda d_a U - \lambda^2 e_a U = 0 \tag{2.22}$$

in which all matrix coefficients are given by Predoi *et al* [48].

The nature of the solution is thus to find eigenvalues of complex wavenumber k for chosen values of angular frequency ω. Each solution at a chosen frequency will reveal the wavenumbers of all of the possible modes at that frequency. The full dispersion curve spectrum can be found by repeating the eigenvalue solutions over the desired range of frequencies, and combining modes with the most similar mode shapes after each frequency step. The SAFE method is able to calculate guided wave modes in both isotropic and anisotropic materials, however, in this thesis only isotropic materials are considered.

2.4.3 SAFE method in perfect fluids

The equation of dynamic equilibrium in a perfect fluid can be written:

$$\nabla \cdot (K_f \nabla P) + \rho \omega^2 p = 0 \tag{2.23}$$

in which p is the pressure of the fluid, and K_f is the compressibility coefficient of the fluid.

When the surface of the fluid is in contact with a deformable solid, we have the boundary equation at the interface:

$$\vec{n} \cdot (K_f \nabla p) = \rho \omega^2 K_f \vec{n} \cdot \vec{u}^{(solid)} \tag{2.24}$$

where $\vec{n}$ is the outward unit vector of the fluid domain on the interface and $\vec{u}^{(solid)}$ is the displacement of the interface calculated in the solid domain. For the solid

waveguide, the boundary condition involves the pressure p in the fluid by writing that the stress vector is $-p\vec{n}$, $\vec{n}$ being the outward unit vector of the solid.

For wave propagation along the Ox_3 direction, the pressure of the fluid can be written as:

$$p(x_1, x_2, x_3, t) = p(x_1, x_2)e^{I(kx_3-\omega t)}, I = \sqrt{-1} \tag{2.25}$$

By combining Eq. (2.23) and Eq. (2.24) and comparing with Eq. (2.22), the pressure can be chosen as the finite element variable and the coefficients become:

$$c = K_f, a = -\rho\omega^2, d_a = \alpha = \beta = \gamma = 0, e_a = K_f \tag{2.26}$$

2.4.4 SAFE method in viscous fluids

A viscous fluid can be modeled as a hypothetical solid [51–53] with appropriate bulk longitudinal velocity, shear velocity and attenuation. The elastic modulus of the solid-like material can be related to the properties of the viscous fluid by the following equations:

$$\begin{aligned} c_{11} = c_{22} = c_{33} &= \frac{3K_f + 4i\omega\eta}{3} \\ c_{12} = c_{13} = c_{23} &= \frac{3K_f - 2i\omega\eta}{3} \\ c_{44} = c_{55} = c_{66} &= i\omega\eta, \end{aligned} \tag{2.27}$$

where $c_{ij}, (1 \leq i, j \leq 6)$ are the elastic stiffness constants from the stress-strain law (Hooke's Law) [26], K_f is the compressibility coefficient of the fluid, η is the shear viscosity, $\omega = 2\pi f$ is the circular frequency. The shear velocity of the viscous liquid can be expressed:

$$c_s = \sqrt{\frac{2\eta\omega}{\rho}}, \tag{2.28}$$

and the shear attenuation can be calculated as:

$$\alpha_s = \sqrt{\frac{\omega\rho}{2\eta}}. \tag{2.29}$$

The longitudinal velocity of the viscous fluid is expressed in the same way as for the non-viscous fluid:

$$c_l = \sqrt{\frac{K_f}{\rho}}, \tag{2.30}$$

The longitudinal attenuation is assumed to arise entirely from the shear viscosity and can be derived as:

$$\alpha_l \approx \frac{2\omega^2\eta}{3c_l^3\rho}, \tag{2.31}$$

The SAFE model can therefore be considered to be the same as that for a solid waveguide which has been investigated previously [48, 50].

It has been discussed that the group velocity is calculated by $c_{gr} = d\omega/dk$ (where ω is the angular frequency and k is the wave number in the propagation direction). It will only be valid if the k is real, which stands for the non-attenuating waves [54]. Therefore when the fluid has viscosity, strictly the group velocity calculation is not valid. However it is reasonably accurate if the attenuation is small and only the real part of the wavenumber is used for calculation. When the attenuation is large, the group velocity calculation may yield non-physical solutions, in this case an accurate alternative is to calculated the energy velocity. It is the velocity at which the wave carries its potential and kinetic energy along the structure. The energy velocity can be calculated by the following equation:

$$V_e = \int_S (P_z/(E_c + E_p)) \tag{2.32}$$

in which S is the cross section of the whole geometry; P_z is the power flow density (Poynting vector) in the propagation direction; E_c and E_p are the kinetic and strain energy density respectively. The details of their expressions can be found in [26] and [55].

2.4.5 Absorbing region

In order to solve the problem of a solid waveguide immersed in an infinite fluid, an exterior absorbing region is needed to model the surrounding medium [50]. This region, shown in Fig. 2.9, has the same mass density as the fluid but has damping properties which increase with the distance away from the central axis of the system. To achieve this, the imaginary part of its compressibility coefficient gradually increases according to the following law:

$$K_{fa} = K_f[1 + I\alpha_1(\frac{|r - r_a|}{L_a})^3], I = \sqrt{-1} \tag{2.33}$$

where K_f represents the compressibility of the liquid, r_a is the inner radius of the absorbing region, L_a is its radial length, and r is the radial position in this absorbing region. α_1 is a coefficient that defines the proportion of the damping at the outer limit of the absorbing region.

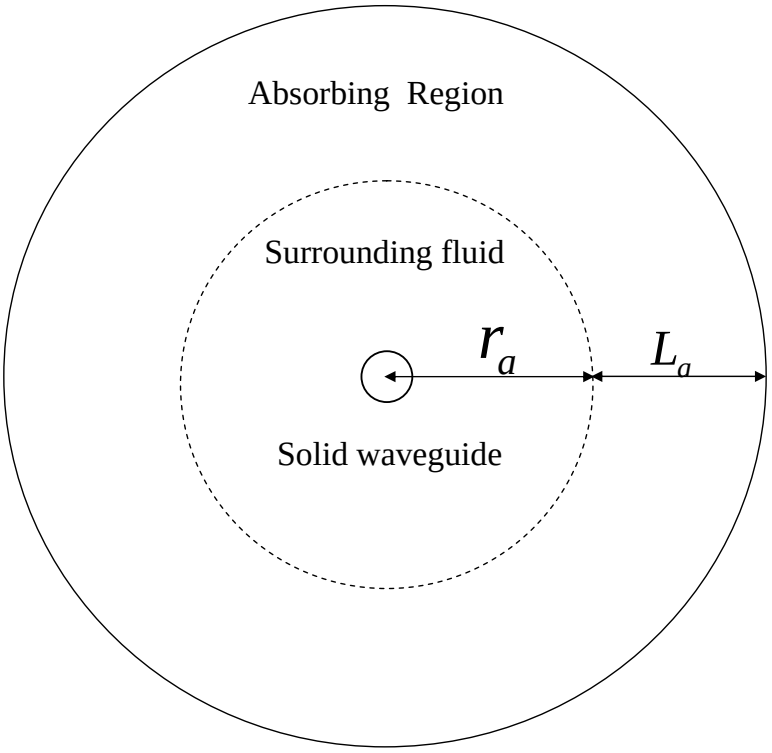

Figure 2.9: *Schematic of the FE model used for a circular bar immersed in a fluid.*

By introducing the imaginary part of the compressibility, the propagation wave

numbers, which are eigen solutions of the system, become complex ($k = k' + Ik''$). The imaginary parts (k'') represent the attenuation due to leakage from the bar to the infinite fluid. In the previous studies of a leaky waveguide surrounded by a solid of infinite extent [50], the length of the absorbing region was recommended to be 2 to 3 times the biggest wavelength of any radiated wave in the whole frequency range. However, according to our numerical testing results here, we found that if the surrounding material is fluid, the length of the absorbing region can be much shorter. The reason is because the leaking energy carried in the fluid is much smaller than the energy carried in the solid waveguide. Therefore the relative amount of fluid-borne energy that is reflected back to the waveguide is very small, which can be further reduced by a short absorbing region, and won't affect the eigen solutions of the system. In our numerical testing, the length of the absorbing region was proved to be efficient by a convergence check. When the length was increased we still obtained the same solutions for the propagating modes in the waveguide.

2.5 SAFE Method Validation

2.5.1 Solid waveguide immersed in a perfect fluid

This study is to validate the SAFE method for waveguides immersed in perfect fluids. A 1mm radius steel cylinder bar immersed in water is used, the results of which have already been studied by DISPERSE and shown in Sec. 2.3.4. The geometry of the system is shown in Fig. 2.9. The steel bar is 2mm in diameter and the surrounding water is modeled by a 4mm thick ring having an inner diameter of 2mm. The absorbing region is modeled by a 5mm thick ring having an inner diameter of 10mm. The material properties are chosen to be the same as they were used in DISPERSE. The whole geometry is meshed by 7563 triangular elements of 1st order (each element has 3 nodes), which are automatically generated by the software used [49]. The number of degrees of freedom is 14912. A typical calculation of one SAFE model presented here takes approximately half a minute on a Pentium

4 PC with 1 Gbyte memory.

The system is solved using the SAFE method to find values of the wavenumber k at different frequencies. For each frequency, several solutions are obtained. For each solution, the amplitude of normal stress in the radial direction T_{rr} is calculated at each nodal position in the solid domain and the pressure p is calculated at each nodal position in the fluid domain and in the absorbing region. These quantities are equal at the border between the solid and fluid according to the imposed boundary condition. Solutions which have higher values of T_{rr} in the solid domain than $-p$ in the fluid domain generally represent modes guided along the bar and radiating in the water, while other solutions represent resonances of the whole system and are unwanted.

Fig. 2.10 shows SAFE solutions at 500 kHz. There are three propagating modes existing at this frequency: the L(0,1) mode which is shown in Fig. 2.10(a), the T(0,1) mode which is shown in Fig. 2.10(b), and the F(1,1) mode which is shown in Fig. 2.10(c). Fig. 2.10(d) shows an unwanted solution that corresponds to a resonance of the absorbing region. From the figure, it can be seen in the longitudinal mode that the radial normal stress is concentrated in the center of the bar and some energy is radiating to the water; in the torsional mode the radial normal stress is almost zero (theoretically it should be zero, but there is a very small value due to the numerical approximation); in the flexural mode the radial normal stress is symmetric with respect to a diameter of the bar and energy is radiating to the water. It can be seen that the mode shapes of three fundamental modes agree with the DISPERSE prediction shown in Fig. 2.7.

In order to compare the dispersion curves over a range of frequencies, the system is then solved for 71 frequencies from 100 kHz to 1500 kHz, and solutions which represent the propagating modes are sought according to the above rule. The mode shape information (displacements in each direction) is recorded at each nodal position for each sought eigensolution. By comparing these mode shapes, all the solutions can be classified into the different modes. Fig. 2.11 presents the dispersion curves of wave modes propagating along the steel bar and eventually radiating energy in the

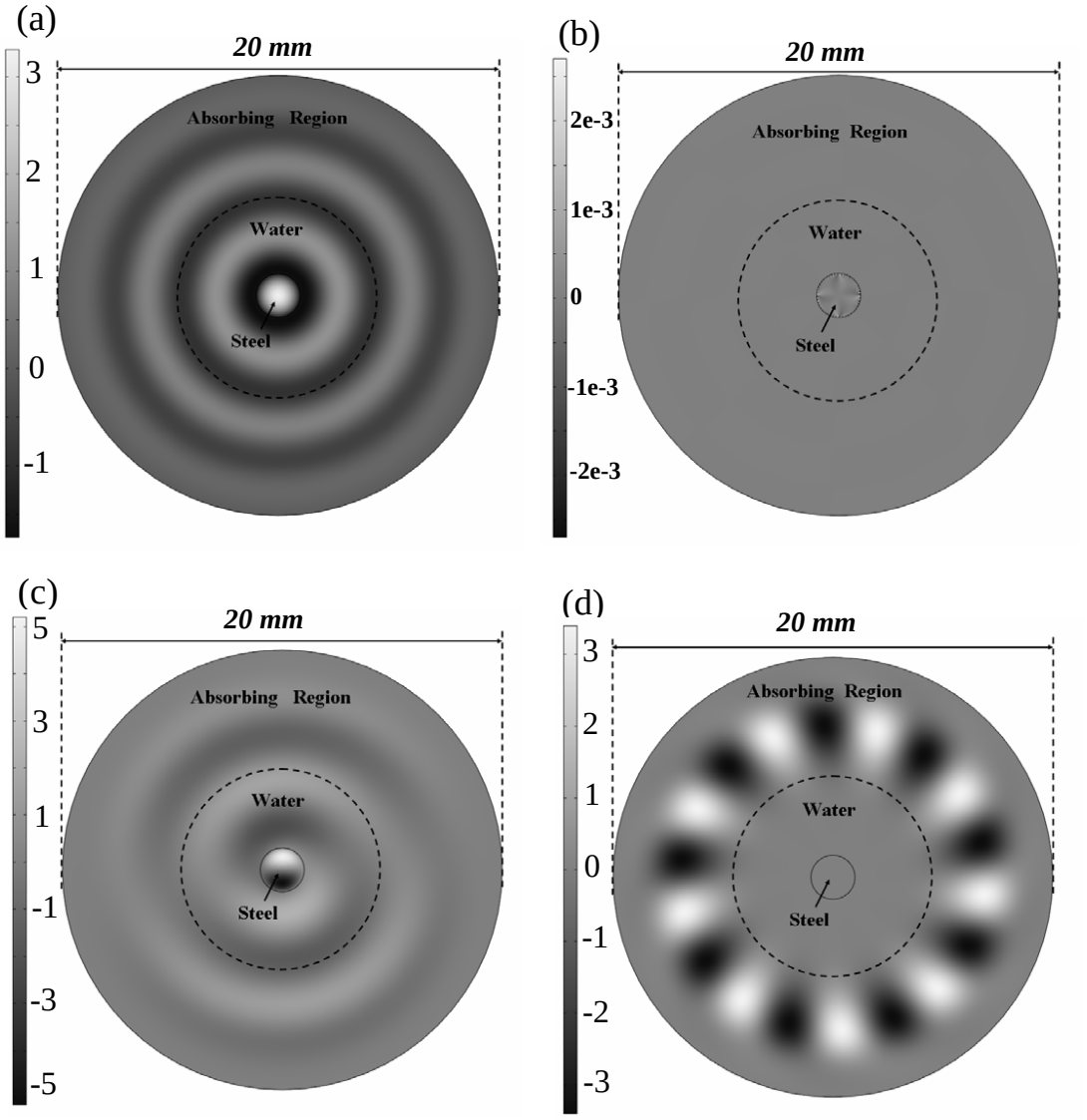

Figure 2.10: *Cross-section distribution of normal stress in solid and pressure in fluid at 500 kHz for example modal results: (a) L(0,1) mode (b) T(0,1) mode and (c) F(1,1) mode; (d) mode resonating in the absorbing region.*

infinite water from 100 to 1500 kHz, showing the phase velocity, real wave number, group velocity and attenuation. The real wave number and the attenuation can be obtained from the eigensolutions directly, while the phase velocity can be calculated by $C_{ph} = \omega/k'$ and the group velocity is obtained by doing a numerical derivation $C_{gr} = d\omega/dk'$. Plain lines are predictions made with the DISPERSE software, while circles represent the SAFE solutions obtained with the model.

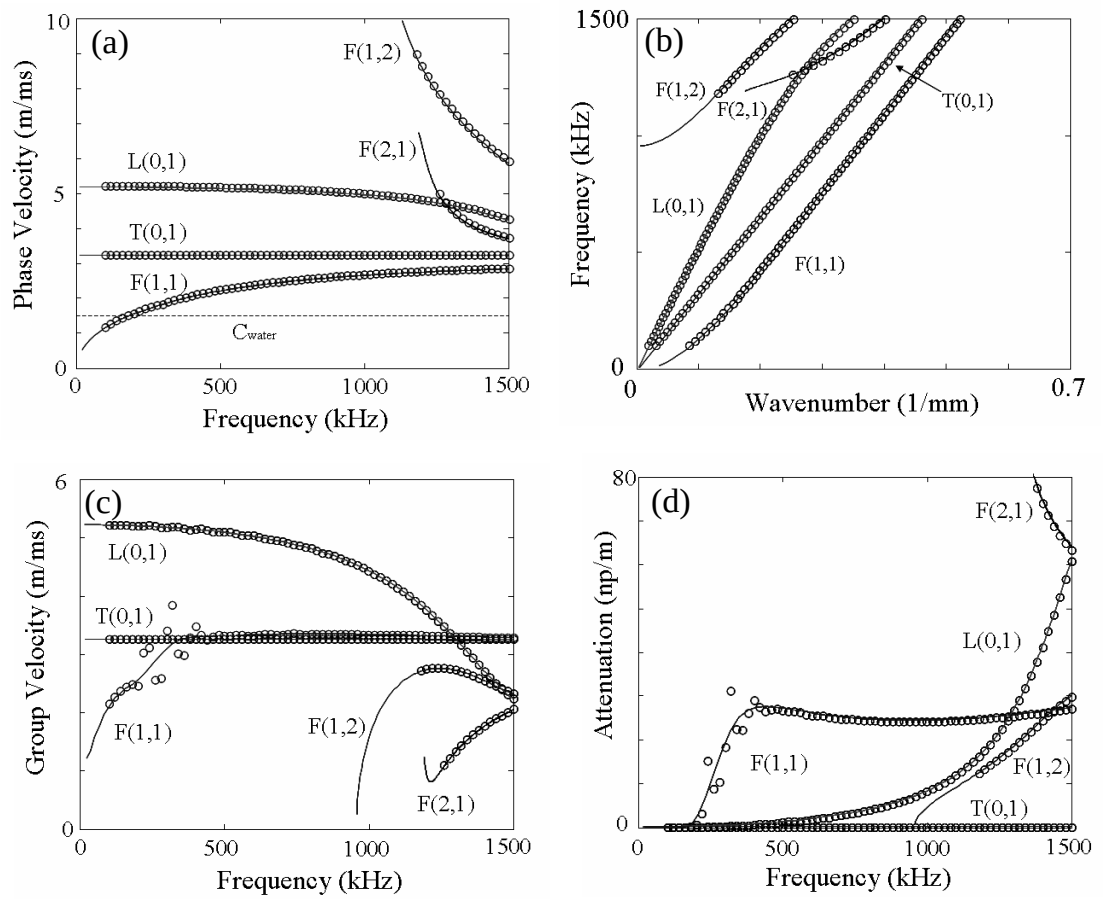

Figure 2.11: *Dispersion curves of phase velocity (a), wavenumber (b), group velocity (c) and attenuation (d) of 1mm radius circular steel cylinder bar immersed in water, predicted by the SAFE method (∘) and DISPERSE (—).*

From the figure it can be seen that the SAFE predictions have good agreement with DISPERSE results at most of the frequencies. The only disagreement appears at 250 kHz - 400 kHz of the F(1,1) mode on the group velocity and attenuation curves, which is a result of inefficiency of the absorbing region at these frequencies. As it has been introduced in Sec. 2.4.5, an efficient length of the absorbing region is dependent on the longest wavelength projecting to the radial direction. In water, only the bulk wave can be radiated, thus only the angle of the radiation decides the

maximum radiated wavelength in the radial direction. This can be derived using:

$$\lambda_{rad} = \frac{\lambda_{water}}{cos\theta} \tag{2.34}$$

Where λ_{water} is the radiation wavelength in water and λ_{rad} is its projection in the radial direction. θ is the radiation angle illustrated in Fig. 2.4 which has been decided by Eq. (2.18). If the phase velocity of the guided mode is lower than the bulk velocity of water, there will be no radiation.

From Fig. 2.11(a), it can be seen that the phase velocity of the F(1,1) mode at 250 kHz to 400 kHz is just above the bulk velocity of water, therefore leaky waves have large angles of radiation θ, so that λ_{rad} is very large, thus the absorbing region does not perform well in such cases according to the previous studies [50]. By increasing the length of the absorbing region, the inaccurate frequency range can be reduced, however it will be much more time consuming to solve the model.

2.5.2 Solid waveguide immersed in a viscous fluid

The second validation model is a solid waveguide immersed in a viscous fluid. A 1mm radius steel cylinder bar is chosen, and the fluid used in the model is glycerol, whose density is ($1258kg/m^3$) and dynamic viscosity is assumed to be 1 Pa s. (The dynamic viscosity is sensitive to the temperature, and is around 1.2 Pa s at $20°C$.)

Since the fluid has shear viscosity, the geometry of the model as well as the mesh has to be chosen carefully. The size of the model needs to consider the possible radiation from the longitudinal waves in the viscous fluid, and the wavelengths and the angles of radiation will condition the size of the absorbing region. Meanwhile, since the shear waves in the viscous fluid have extremely small wavelengths, thus very fine meshing will be required in the region of the viscous fluid. However the fine mesh could not be applied over the whole geometry, as it would exceed the modelling capacity of the software. A special meshing technique which only used fine mesh at the boundary between the solid and the liquid but regular mesh at

other part of the geometry, was carried out and it will be described in the following paragraph.

The surrounding glycerol is modeled by a 1 mm thick ring having an inner diameter of 2 mm. The absorbing region is modeled by a 13 mm thick ring having an inner diameter of 4 mm. Quadratic elements, which contains 6 nodes, are used in the model. The geometry was first meshed automatically over the whole region, which produces small elements in the center around the solid bar and elements with gradually increased size towards the border of the geometry. The length of absorbing region has been decided after some trials, in order to model properly the leakage and its absorption at infinity. Then the mesh along the boundary between the bar and the glycerol is refined in order to accurately present the shear viscosity of the fluid. The resulting maximum size of element is about 0.4 mm within the fluid and about 0.03 mm along the bar-fluid border. The mesh consists of 15666 elements, and the number of degrees of freedom is around 189000, which makes it a quite large model but still solvable. The FE model took around an hour to solve at one single frequency on a more powerful computer (2× Dual-Core 2.6GHz AMD Opterons workstation, with 16 GB memory) than previously used.

The model was first run at a single frequency. Wave modes which have higher energy (power flow) in the bar than in the fluid were picked up, as they correspond to the modes that propagate along the bar and radiate into the fluid. Three modes were found at 1200 kHz in the calculation, and the solutions (wavenumber) of the propagation modes are listed in Tab. 2.1. The real part of the wavenumber relates to the phase velocity of the mode while the imaginary part describes the attenuation. Meanwhile, this model can also be solved by DISPERSE. The results from DISPERSE are also listed in the table, which show good agreement with the SAFE prediction.

Then the system is solved for 11 frequencies over the range from 500 kHz to 1500 kHz, and solutions which represent the propagating modes are sought according to the above criterion. As for the method introduced previously, by comparing the mode shapes between two neighbouring frequencies, it is possible to get the dispersion

Table 2.1: Comparison of SAFE solution and DISPERSE prediction of the guided modes on a 1mm radius steel cylinder immersed in glycerol.

	Real wavenumber (rad/m)			Attenuation (Np/m)		
	SAFE	DISPERSE	error	SAFE	DISPERSE	error
L(0,1) mode	1561	1560	0.06%	29.446	29.8	1.18%
T(0,1) mode	2318	2316	0.08%	5.261	5.3	0.73%
F(1,1) mode	2720	2722	0.07%	45.367	45.3	0.14%

curve for different modes existing in the frequency range. The whole process took over 14 hours to complete on the workstation introduced above. Fig. 2.12 presents the phase velocity and attenuation dispersion curves of wave modes propagating along the steel bar and eventually radiating energy in the glycerol, from 500 to 1500 kHz. Circles present the SAFE results, while plain lines are predictions made with the DISPERSE software. The figure shows good agreement between SAFE predictions and results from DISPERSE in the frequency range. Comparing with Fig. 2.6, it can also be noted that the attenuation of the waves in the bar immersed in viscous fluid is much higher than for the one in perfect fluid, and the T(0,1) mode starts to have attenuation.

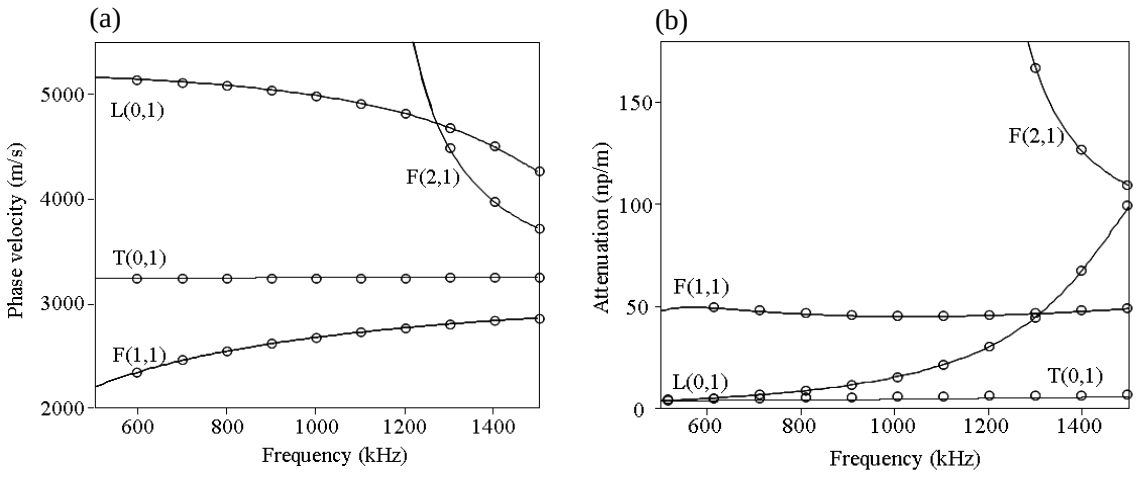

Figure 2.12: *Dispersion curves of phase velocity (a) and attenuation (b) of 1mm radius circular steel cylinder bar immersed in glycerol, predicted by the SAFE method (∘) and DISPERSE (—).*

2.6 Summary

In this chapter, the fundamental concepts of bulk ultrasonic waves propagating in infinite media and guided waves propagating in waveguides with regular geometry have been revisited. In an unbounded elastic medium, there are two modes of propagation: longitudinal and shear modes, and the velocity of these waves is constant with frequency. In waveguides, partial bulk waves continuously interacting with the boundaries of the waveguide superpose to form a guided wave propagating along the structure. The properties of guided waves are usually dispersive, i.e., velocities depends on frequency; and mode shapes also vary with frequency.

For waveguides with regular geometry such as plates or pipes, analytical methods such as the global matrix method reviewed in this chapter can be applied to study the properties of guided waves propagating in these structures. The dispersion curves and mode shapes of guided waves on a plate system have been analyzed. When a waveguide is immersed or embedded in another medium, the guided wave may be attenuated, with the energy leaking away from the waveguide while propagating. An example of a cylindrical bar immersed in water has been presented and discussed in the chapter.

For waveguides with irregular cross-sectional shapes, the Semi-Analytical Finite Element method has been introduced, which uses a finite element representation of the cross section, together with a harmonic description along the propagation direction. In this chapter, the work on the SAFE method has been recalled and then extended for a solid waveguide immersed in fluids. This extension enables the SAFE method to address the problem of leaky guided waves in fluids. Two validation cases have been carried out, which have studied the problems of solid cylindrical waveguides immersed in non-viscous and viscous fluids. The solution from the SAFE method as well as the analytical method have been obtained and compared, showing good agreement.

Chapter 3

Dipstick for Ultrasonic Density Measurements

3.1 Background

This chapter presents an application of guided wave propagation on a waveguide with irregular cross section in measuring the density of a fluid in which the waveguide is immersed. The density is an important bulk property of any material and its measurement is very important in many disciplines such as material characterization, quality or process control. Ultrasonic density measurement is an attractive idea for the rapid non-destructive evaluation of a material's density.

Conventional ultrasonic density measurements can be carried out by determining the time of flight of an ultrasonic wave between an emitting and a receiving transducer; this is a measure of the speed of sound in the material. Since the speed of sound in any medium is dependent on the bulk modulus (compressibility) and the density of the medium only, the density of the medium can be determined if the bulk modulus is known and the speed of sound is measured:

$$\rho = \frac{K}{c^2} \tag{3.1}$$

where c is the speed of sound in the material, K is the bulk modulus and ρ is the density of the material.

Graff [24] gives a good account of waves in infinite media and their properties. A further approach to measure ultrasonic density can be by means of the amplitude of the reflection of an ultrasonic wave by an interface between a known material and an unknown material (also described by Graff). The reflection coefficient (ratio of the amplitude of the reflected wave over the amplitude of the incident wave) depends on the ratio of acoustic impedances of the known and unknown materials. The acoustic impedance is defined by: $Z = \rho c$, where Z is the acoustic impedance, ρ is the density of the material and c is the speed of sound in the material. The reflection coefficient for normally incident waves (travelling at 90 degrees to the plane of the interface) is given by the equation:

$$RC = \frac{Z_1 - Z_2}{Z_1 + Z_2}, \tag{3.2}$$

where Z_1 is the impedance of material 1 that the wave is travelling in and Z_2 is the impedance of material 2 that forms the interface with material 1 from which the wave is to be reflected. This shows that if the reflection coefficient is used to deduce the density of the material that the wave is reflected from, some further information has to be known about material 2, namely its speed of sound.

A disadvantage of the ultrasonic determination of density using the time of flight and the reflection coefficient methods is the need to know the compressibility of the medium in order to calculate the density from the measurement results. A further disadvantage is the need for accurate positioning of sending and receiving transducers relative to the sample. Especially for fluid samples this means that the measurement has to take place in a carefully designed test cell of tightly controlled

dimensions. For accurate measurements it is also important to ensure that transducers are mounted with parallel surfaces. This can be impractical if measurements have to be carried out in the field.

Recently several ultrasonic "dipstick" techniques have been developed in order to measure fluid properties ultrasonically. The idea is that an ultrasonic wave which propagates in a solid structure can sense the presence and nature of the adjacent fluids. For example, Fig. 3.1 shows two dipsticks which were developed by Vogt *et al* [56] to measure fluid viscosity and by Cegla *et al* [57] for fluid bulk velocity measurements.

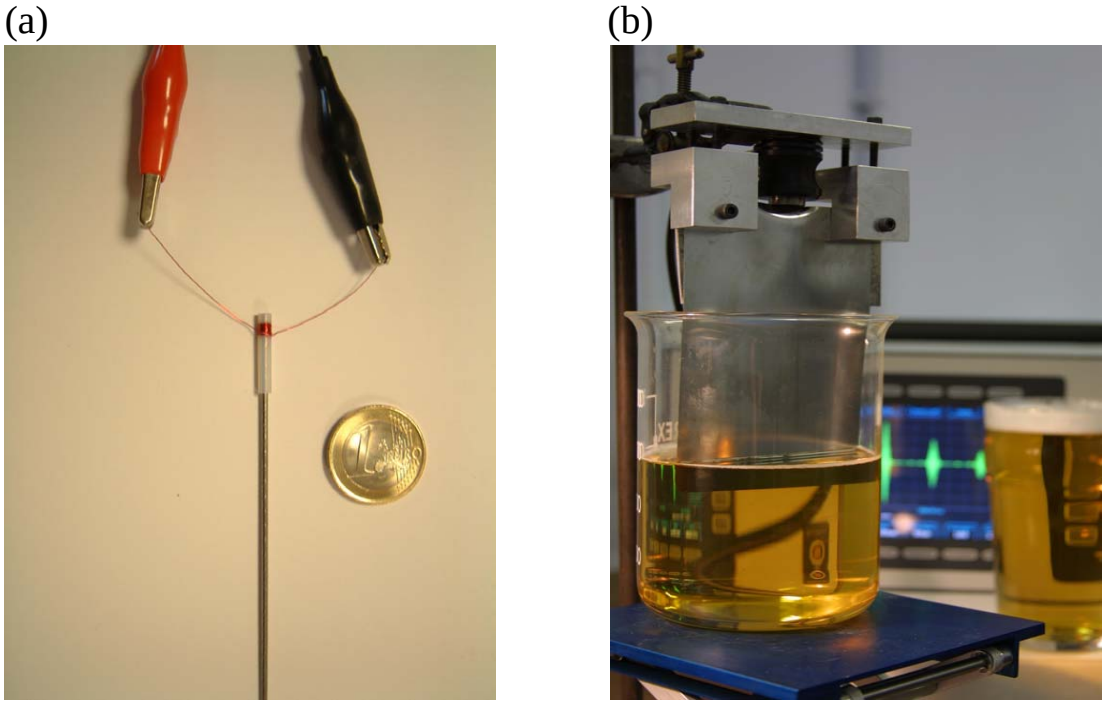

Figure 3.1: *(a) Dipstick for fluid viscosity measurement [56], (b) dipstick for fluid bulk velocity measurement [57] .*

Fig. 3.2 shows the dipstick sensor designed by the author to measure fluid density, which contains a rectangular bar and two shear transducers at one end. When a torsional wave pulse propagates along the bar submerged in a fluid, it interacts at the boundary with the surrounding fluid. As a result, the boundary layer of the fluid is alternately accelerated and decelerated. As the waveguide has a non-circular cross-section, normal forces are exerted on the surrounding fluid, thus some fluid will

be trapped at the corners of the cross-section and will affect the propagation of the torsional wave. This mechanism can be attributed to the inertia of the surrounding fluid and is characterized by the density of the fluid [20,58]. Hence by measuring the speed of propagation of the torsional wave, the density of the fluid can be estimated.

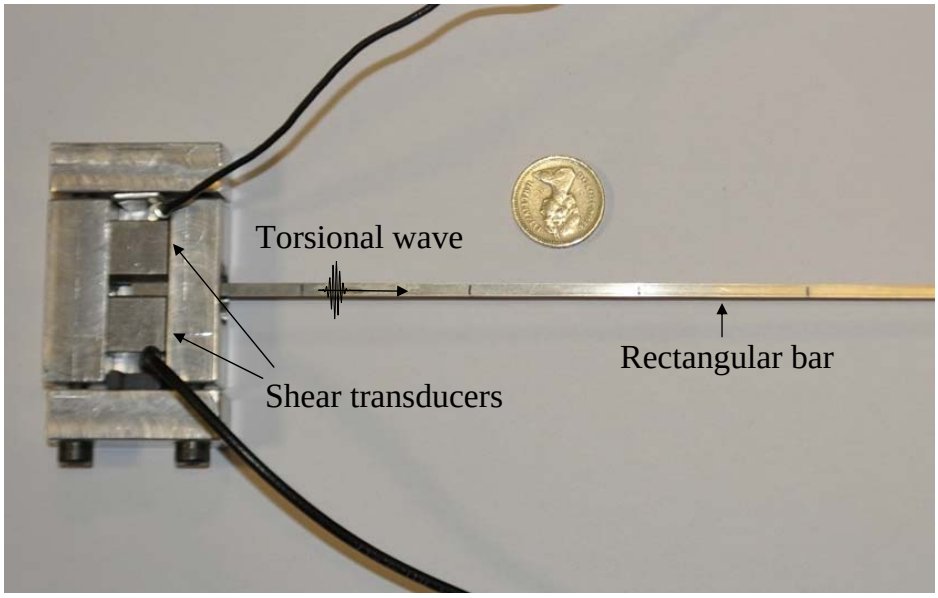

Figure 3.2: *Dipstick sensor designed for fluid density measurements. .*

Lynnworth [59] made the first application of such a torsional wave sensor to measure fluid densities. Later, Bau [20] presented a simple quantitative theory to relate the speed of the torsional wave to the density of the surrounding fluid, with a calculation of a two-dimensional, inviscid flow field of the fluid. Based on this theory, various researchers made further applications [58,60,61]. Kim and Bau [58] analyzed waveguides with various types of cross-sections in order to optimize the performance of the sensor. Shepard *et al* [60] measured the density and viscosity in a variety of fluids, including fluids with high concentration of suspended solids. Smit *et al* [61] made use of a continuous excited torsional wave to allow large cross-sectional dimensions for density measurements. However, due to the complexity of the wave behavior in the non-circular cross-sectional shape, the accuracy of the inversion of the measurements to infer the density of the fluids has been compromised. These authors [20, 60, 61] have reported deviations of the measured velocity of torsional waves and theoretical predictions of over 20%. Therefore better theoretical predic-

tions are required to improve the accuracy of the sensors. In this chapter, the SAFE model is applied to predict accurately the wave propagation along a solid bar with a non-circular cross-section immersed in a fluid. Then a more precise inverse model relating the group velocity of the torsional wave and the density of the surrounding fluid can be provided.

This chapter starts with a review of the approximate theory [20]. The SAFE method is then applied to model a torsional wave propagated along a waveguide with a rectangular cross-section that is immersed in a fluid. The velocity change of the torsional wave can be obtained as a function of the density of the fluid, and therefore an accurate inverse model for the density measurements can be provided. In Sec. 3.4 experiments are designed to validate the inverse model, showing excellent agreement. General discussions on the optimization of the sensor are presented finally in Sec. 3.5.

3.2 Previous Theory of Torsional Dipstick

Bau's approximate theory suggests that the speed of propagation of torsional waves in a solid, elastic waveguide with a non-circular cross section is inversely proportional to the density of the fluid adjacent to the waveguide [20]. However in this theory, two assumptions have to be made to achieve the conclusion. The first one is the first-order approximation to the two-dimensional flow field calculation, with which the torsional wave speed c in a solid waveguide can be presented as [20]:

$$\frac{C}{C_0} = (1 + \frac{\rho_f I_f}{\rho_s I_s})^{-1/2} \tag{3.3}$$

where I_s and I_f are the polar moment of inertia [62] of the solid waveguide and the adjacent liquid respectively, which need to be overcome by the torsional pulse, $C_0 = K(G/\rho_s)^{1/2}$ is the torsional wave speed for a waveguide in vacuum, G is the shear modulus of the solid, $K = (D/I_s)^{1/2}$ is a "shape" factor, D is the torsional rigidity of the cross section, and ρ_s and ρ_f are the densities of the solid and adjacent fluid respectively.

Kim and Bau [58] have obtained the values of I_f/I_s and K from finite element computation of the flow field around a non-circular cross-section. Then a second assumption, $(\rho_f I_f)/(\rho_s I_s) \ll 1$, has been made to get the linear relationship:

$$\frac{C}{C_0} \approx 1 - \frac{\rho_f I_f}{2\rho_s I_s} \tag{3.4}$$

Thus the density of the fluid ρ_f can be calculated from Eq. (3.4). However, when I_f/I_s is large or when the density of the solid is close to the density of the fluid, the calculation becomes inaccurate. This can be seen easily, for example, in the case of an aluminum bar with a diamond-shaped cross-section which has an aspect ratio 1:3 immersed in alcohol. In this case $I_f/I_s \approx 3$, which can be obtained from Kim's calculation [58]. Thus $(\rho_f I_f)/(\rho_s Is) \approx 1$, and this makes the second assumption invalid.

In addition, any dispersion characteristics of the waves are excluded from this theory, but torsional waves in a geometry with a non-circular cross section are always slightly dispersive, which make the group velocity measured from a pulse-echo experiment slightly different from the phase velocity of the theoretical prediction. This can also lead to deviation between the theory and the experimental measurements [20,60,61].

In the following sections of this chapter, an accurate semi-analytical finite element model of waves propagating along a non-circular bar immersed in a fluid will be provided, and the dispersion curve (relating frequency and group velocity) of the torsional mode in a certain fluid can be obtained from the model. Therefore, more explicit correlation between the group velocity of the torsional mode at certain frequency and the density of the fluid can be established.

3.3 Modal Study of Rectangular Bar Immersed in a Perfect Fluid

3.3.1 Model description

As was shown in Chapter 2, by the SAFE method one can accurately predict the propagation and leakage of guided waves along an immersed waveguide. Therefore, by performing accurate predictions, such as are undertaken here, it should be possible to construct an inverse relationship so that measurements of the torsional wave could be used to infer the density of the fluid.

The schematic of a model is shown in Fig. 3.3 using the example of a rectangular aluminium bar immersed in a alcohol. A rectangular bar of $1.1mm \times 2.2mm$ was modeled, corresponding to the measured dimensions of a real bar which was used for experiments. The material properties are shown in Tab. 3.1. In order to suppress the reflections from the outer border of the alcohol region, an absorbing region was modeled. This had the same density as the alcohol but increased damping with distance away from the center. The length of the absorbing region was chosen to be 10 mm, which was proved to be efficient by a convergence check. When the length was increased in a trial the same solutions were still obtained. The geometry was meshed by 8376 triangular elements of 1st order. These elements are automatically generated by the software used [49],and are finer in the bar than in the adjacent fluid. The number of degrees of freedom was 17282.

The model system was solved using the SAFE method to find values of the wave number k at different frequencies. For each frequency, several solutions were obtained. For each solution, the amplitude of normal stress in the radial direction Trr was calculated at each nodal position in the solid domain and the pressure p was calculated at each nodal position in the fluid domain and in the absorbing region. These quantities must be equal at the border between the solid and fluid according to the imposed boundary condition. Solutions which have higher values of Trr in the solid domain than -p in the fluid domain generally represent modes guided along

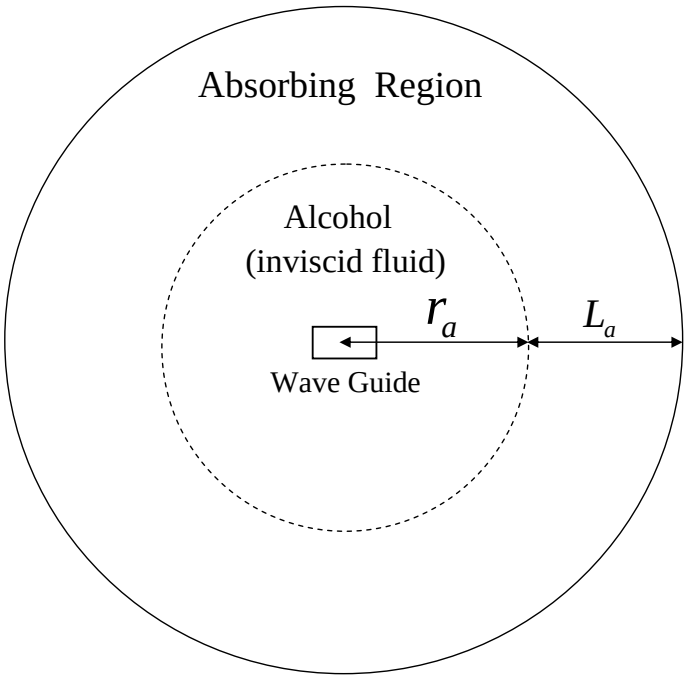

Figure 3.3: *Schematic of the FE model used for the rectangular aluminium bar immersed in alcohol .*

the bar and radiating into the fluid, while other solutions represent resonances of the whole system and so are unwanted.

Table 3.1: Mechanical properties for materials used in the SAFE modelling.

	Density (kg/m^3)	Bulk longitudinal velocity (m/s)	Bulk shear velocity (m/s)
Aluminium	2700	6320	3130
Copper	8900	4700	2260
Steel	7932	5959	3260
Magnesium	1700	5770	3050
Water	1000	1500	
Alcohol	800	1168	

3.3.2 Fundamental modes at single frequency

Fig. 3.4 shows the four fundamental propagation modes of guided waves propagating on the rectangular bar immersed in alcohol at 70 kHz, which are the longitudinal mode (a), the torsional mode (b) and two flexural modes (c) and (d). The radial stress in the bar and in the fluid is displayed as a grey scale. From the figure, it can be seen that the longitudinal mode and two flexural modes leak energy from the bar into the fluid, however the torsional mode does not have any attenuation.

Fig. 3.5 shows a zoom of the bar and nearby fluid in the torsional mode, as it is the most interesting mode for fluid density measurement. The displacement in the fluid and in the cross-section of the bar is plotted by arrows. It can be clearly seen that the fluid is trapped by the corners of the bar, thus it is to be expected that the propagating speed of the torsional mode along the bar should be influenced by the fluid. It should be noted that there is no radial component of the waves in the fluid, even though the fluid loads the bar and there is some local movement, so that the torsional mode on such a rectangular bar is a non-leaky mode.

3.3.3 Dispersion curve of the torsional mode

The dispersion curves can be generated by repeating the SAFE solution over a desired range of frequencies, and the fundamental torsional mode can be traced by comparing the mode shapes of all the propagating solutions at each frequency. Fig. 3.6 presents the phase velocity dispersion curve of the fundamental torsional mode of the aluminum rectangular bar immersed in alcohol, from 50 kHz to 90 kHz. For comparison, the phase velocity of the fundamental torsional mode of the same rectangular aluminum bar in vacuum is also plotted in the figure (line), also generated by the SAFE method but omitting the fluid [48]. It can be seen that the torsional speed of the waveguide with the rectangular cross-section decreases when it is immersed in the fluid. In addition, it is observed this particular mode has almost no dispersion over this frequency range, and is therefore useful for measurements.

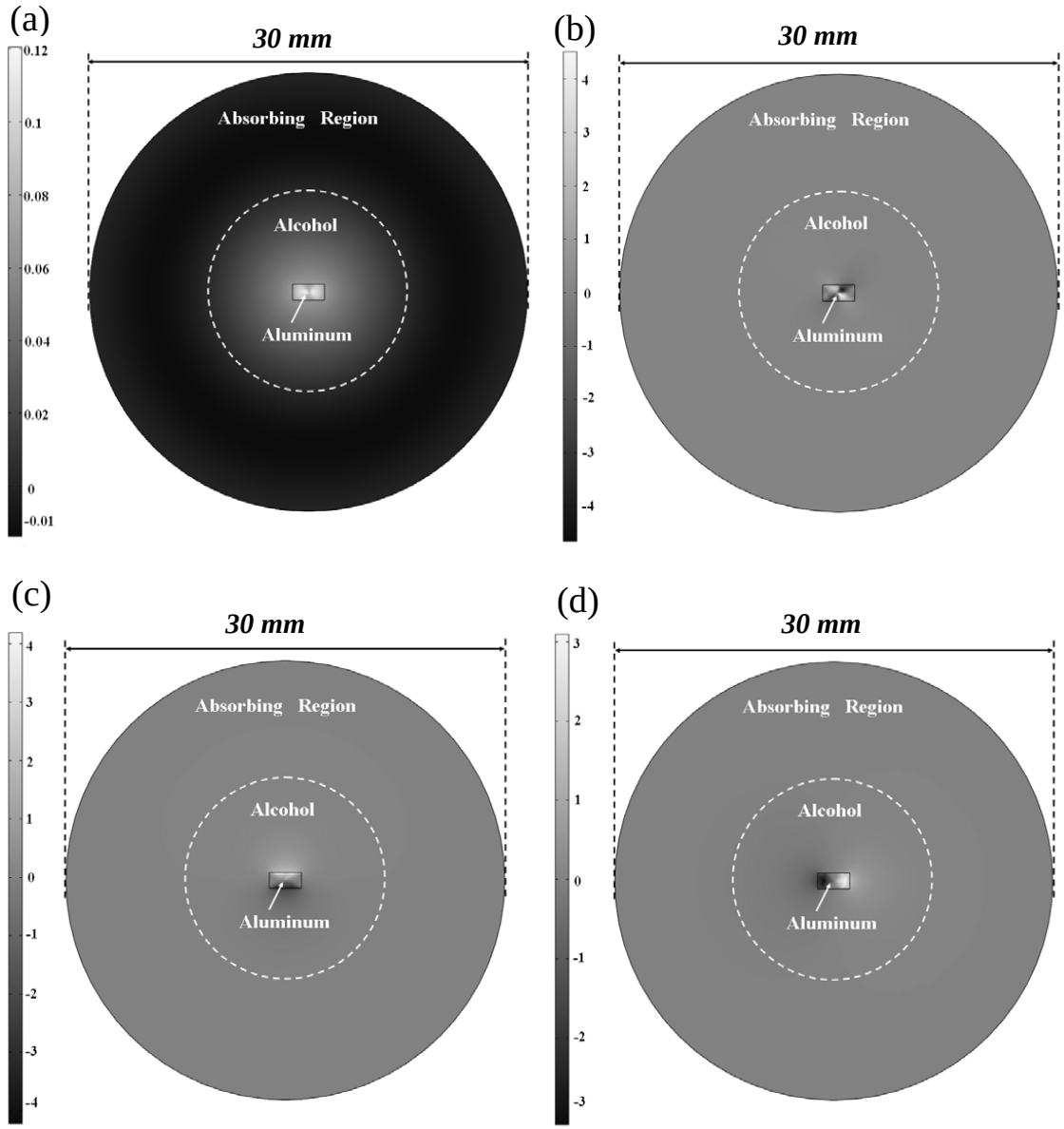

Figure 3.4: *Theoretical prediction of mode shape of four fundamental modes of aluminium bar with rectangular cross-section* ($1.1mm \times 2.2mm$) *immersed in alcohol, at* 70 *kHz: (a) Longitudinal mode (b) Torsional mode, (c) flexural mode 1 and (d) flexural mode 2. The radial (with respect to the center of the bar) stress in solid and pressure in fluid is displayed in a grey scale .*

From the calculation, we also confirmed that the attenuation of the torsional mode of the aluminum rectangular bar immersed in alcohol is zero, which means there is no leakage from the bar to the fluid in the above frequency range. Therefore, the

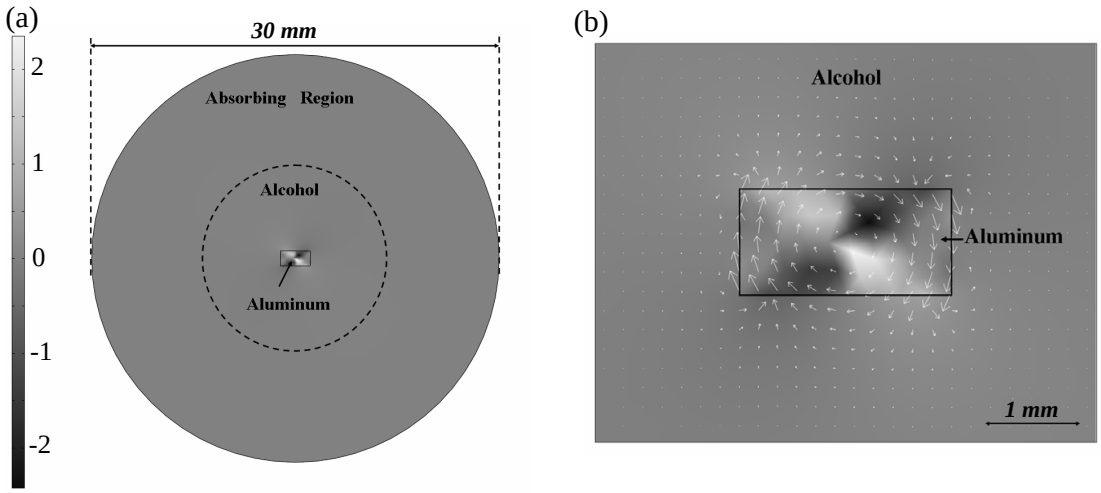

Figure 3.5: *A zoomed picture of torsional mode of aluminium bar with rectangular cross-section (*$1.1mm \times 2.2mm$*) immersed in alcohol at* 70 *kHz. The radial (with respect to the center of the bar) stress in solid and pressure in fluid is displayed in a grey scale. Arrows indicate displacements in cross-section of fluid and the bar .*

group velocity is identical to the energy velocity [54], the latter being the quantity which was actually measured in the experiments; the experiments will be discussed shortly.

3.3.4 Inverse model for density prediction

From the above modelling demonstration it can be seen that the properties of the propagation of the torsional mode on a rectangular bar immersed in a fluid can be calculated precisely. Therefore a precise inverse model relating the group velocity of the torsional wave and the density of the surrounding fluid can be established, by calculating the group velocity of the torsional mode in different fluids. The group velocity is easily obtained by doing a numerical derivation $C_{gr} = d\omega/dk'$. Fig. 3.7 shows the inverse model relating the group velocity of the torsional waves of the immersed rectangular bar and the density of the fluids. A number of inviscid fluids with densities from $0.8g/cm^3$ to $1.5g/cm^3$ with a step of $0.1g/cm^3$ has been modeled, and their corresponding group velocities are shown in the figure as circles.

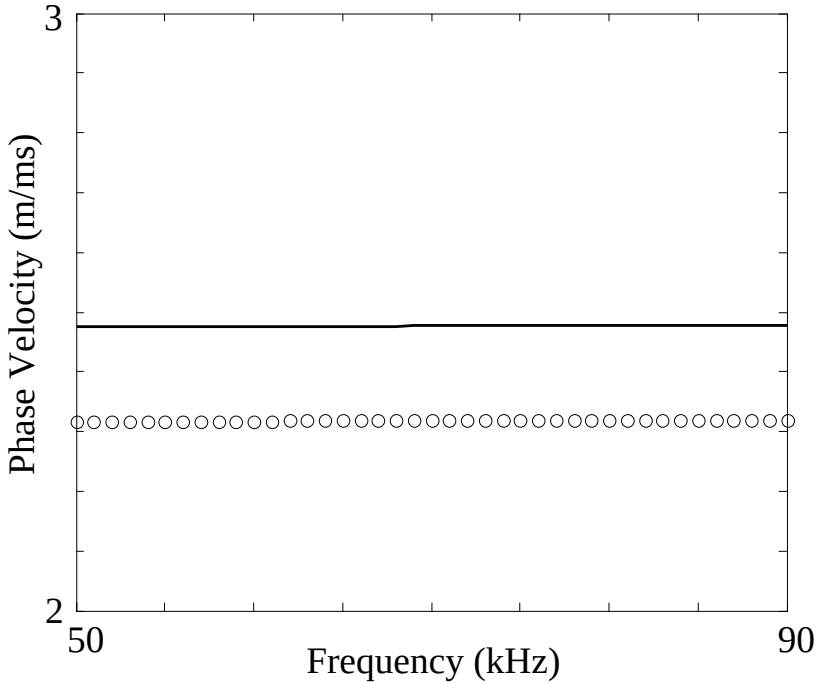

Figure 3.6: *Phase velocity dispersion curves of aluminium bar with rectangular cross-section (*$1.1mm \times 2.2mm$*) immersed in alcohol (circles) and in vacuum (line) predicted by the SAFE method .*

A linear relationship between the group velocity and the density of the fluid can be discovered from the figure, which agrees with the previous theory [20]. In the experimental measurement, the group velocity of the propagating torsional wave on a bar can be practically measured, hence the density of the fluid can be obtained via the inverse model. The comparison of this model with the experimental results and previous approximate theory will be shown in the next section.

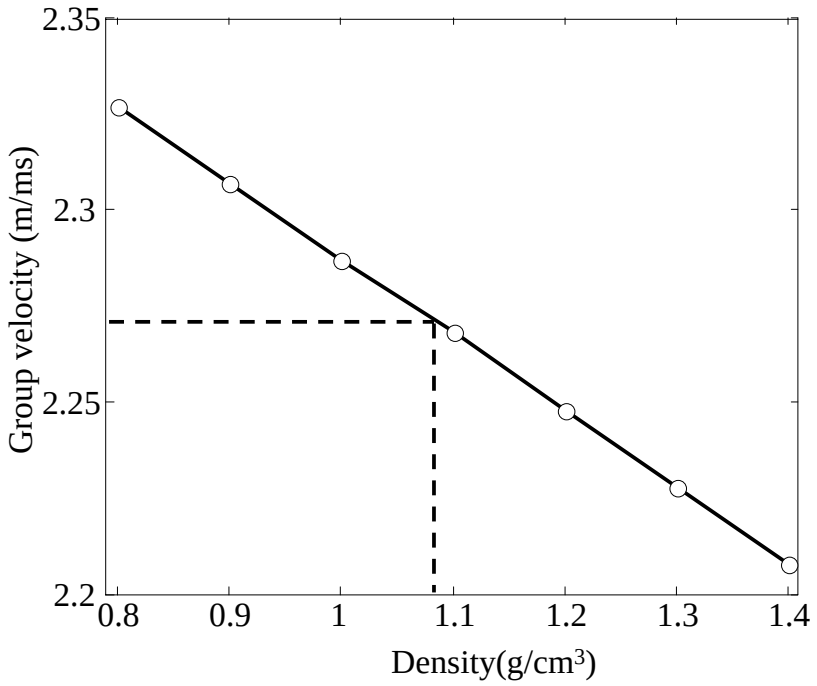

Figure 3.7: *Inverse Model relating the group velocity of the torsional wave of the immersed rectangular bar and the density of the fluids .*

3.4 Experiment

3.4.1 Experimental setup

An experimental setup was designed to validate the model by exciting the torsional mode in an aluminium rectangular bar immersed in a fluid and measuring its energy velocity (group velocity). Fig. 3.8 shows a schematic of the apparatus. The bar was 450mm long with rectangular cross-section ($1.1mm \times 2.2mm$), which had the same properties as were used for the model. A vessel containing a fluid sample was placed beneath the bar on a table of variable height. By changing the height of the table, the bar could conveniently be immersed in the fluid to different depths; the angle between the fluid surface and the axis of the bar was 90 degrees.

The signal was sent and received by a pulse generator and receiver unit (Macro Design Ltd.), a LeCroy 9400A Storage Oscilloscope was used to store the signal and data was then transferred to a computer for processing. A pair of standard shear

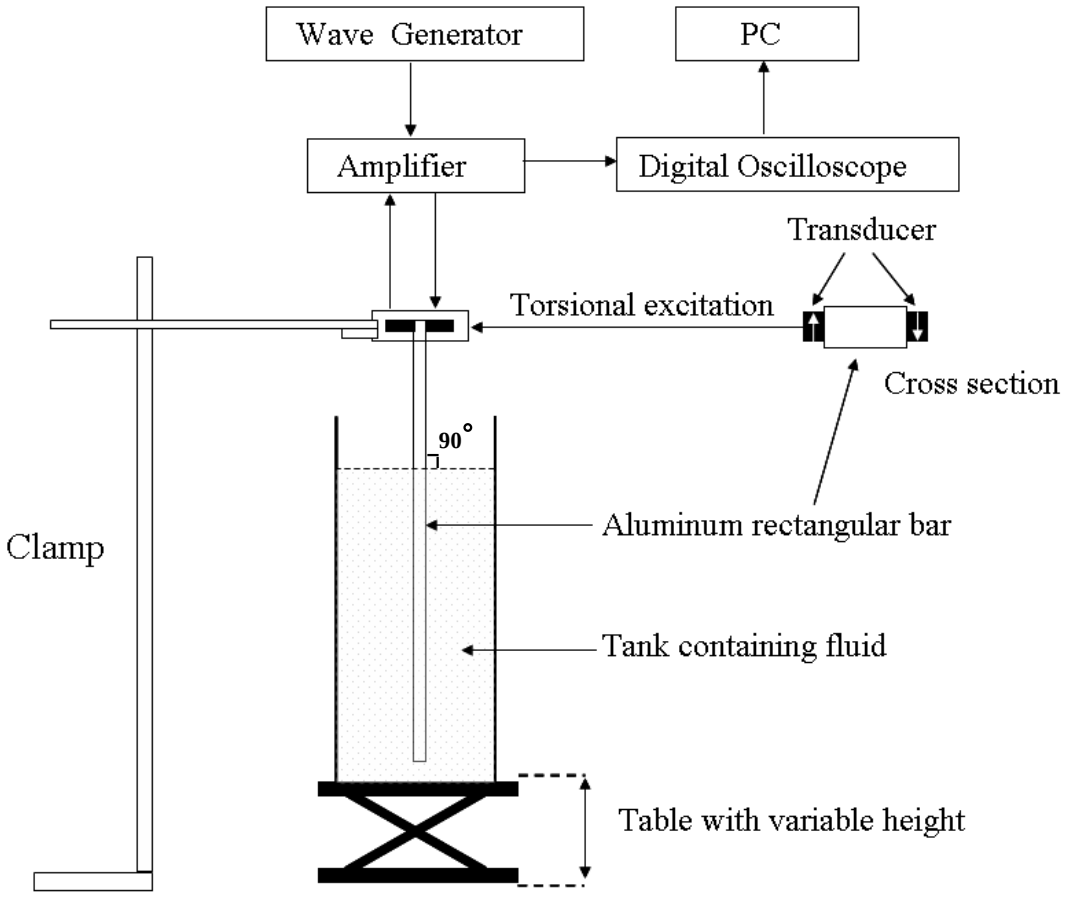

Figure 3.8: *Experimental setup .*

transducers made by Guided Ultrasonics Ltd. [63] was used to excite the torsional mode with a 5 cycle Hanning windowed tone burst. The signal was reflected from the end of the bar and traveled back to the transducer. It was then recorded after 50 averages to reduce the noise.

A typical time trace of this bar partly immersed in alcohol is displayed in Fig. 3.9(a) and for comparison the signal in air in shown in part(b). The first and second bar end reflections and reverberation in the fluid are clearly visible. ΔT is the flight time of the wave packages propagating twice the length of the bar, which can be determined by calculating the shift of the Hilbert envelope (shown in figure 3.9) of the measured signals. The phase of the measured signals is inverted after each

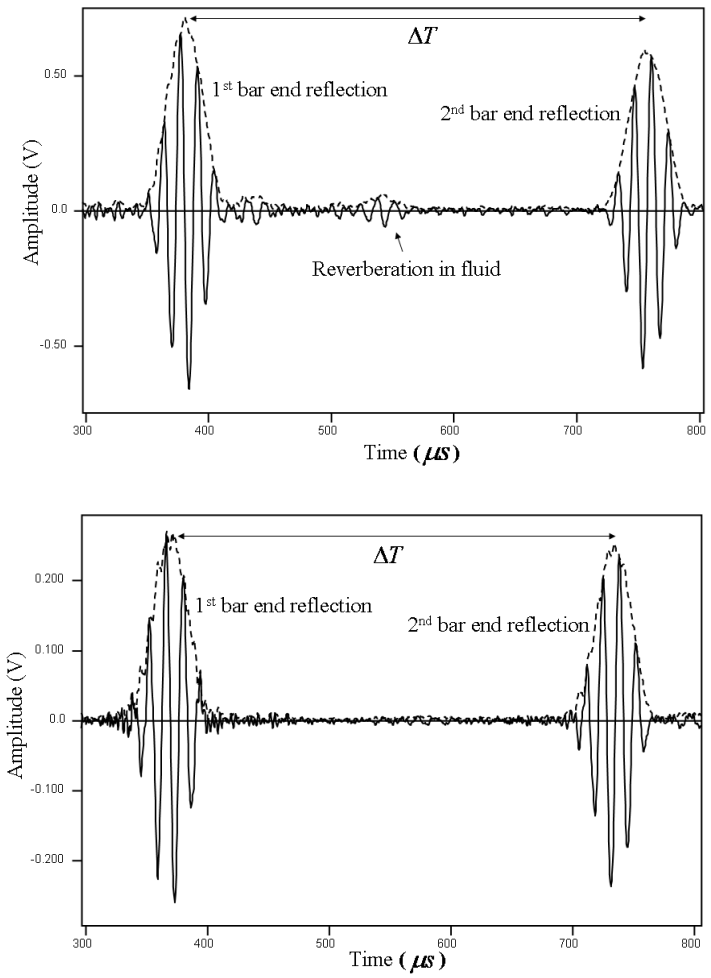

Figure 3.9: *Time trace at 70 kHz with aluminum rectangular bar immersed in alcohol at 170mm (a) and in air (b) .*

reflection because one end of the bar was clamped by the two transducers. Data for tone bursts at different centre frequencies and two different immersion depths were collected. The group velocity C_{gr} was extracted from the measured signals using:

$$C_{gr} = \frac{2(x_2 - x_1)}{(\Delta T_2 - \Delta T_1) + \frac{2(x_2 - x_1)}{C_a}} \tag{3.5}$$

where $x_2 > x_1$ are two different immersion depths, ΔT_1 and ΔT_2 are the flight time of the wave packages propagating twice the length of the bar with different immersion depths respectively. C_a is the group velocity of the torsional mode of the bar in air (which is considered to be a good approximation for group velocity in vacuum C_0).

3.4.2 Results

Alcohol

This first experiment was chosen to validate the dispersion curve using pure alcohol and the frequency range from 50 kHz to 90 kHz. The density of a sample of alcohol ($800kg/m^3$) was measured by a conventional measurement (by measuring the weight and volume of the liquid) and the aluminium bar properties were evaluated experimentally $\rho = 2700kg/m^3, C_l = 6320m/s, C_s = 3130m/s$. The temperature was recorded to be 25°C. Results were extracted from the time traces as described in subsection 3.4.1. Fig. 3.10 shows the measured group velocity of the torsional mode as a function of frequency, and the theoretically predicted curve by the SAFE method; this was obtained by doing a numerical derivation $C_{gr} = d\omega/dk'$ as was described in Sec. 3.3. From the figure we can see that the measured results agree very well with the theoretical predictions. There are small variations in the predicted curve of group velocity. They are due to the numerical differentiation and could be smoothed by fitting with a differentiable analytical function if higher resolution is required.

Density measurements

The second experiment was chosen to validate the inverse model for density prediction. A few fluid samples with density from $0.8g/cm^3$ to $1.1g/cm^3$ were chosen, the variation being achieved by changing the concentration of alcohol and salt with water. The centre frequency of the tone burst signal was selected to be 70 kHz. Fig 3.11 depicts the ratio $(C_a - C_{gr})/C_a$ as a function of the fluid density; these axes are chosen to match those used in the earlier published work in the approximated theory. The solid line shows the SAFE model results while the stars are the experimental results. The previous approximate theoretical prediction [20] (dashed lines) according to Eq. (3.3), is also shown in the figure. It can be seen that the SAFE method predictions agree very well with the measurements, and that this represents a substantial improvement with respect to the approximate model.

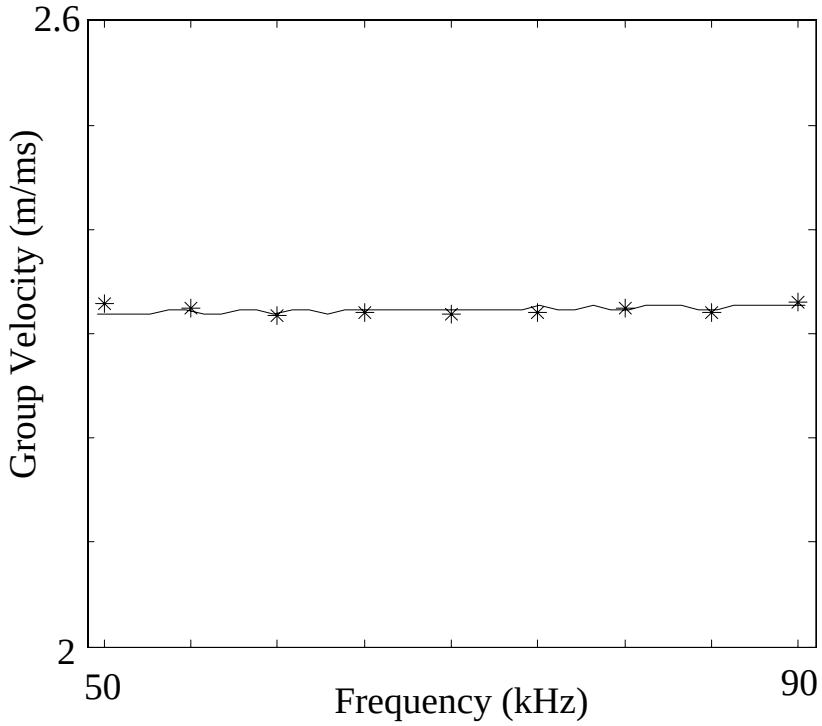

Figure 3.10: *Measured (stars) and theoretically predicted (line) group velocity of aluminium bar with rectangular cross-section immersed in alcohol .*

3.4.3 Error analysis

In order to further exploit this dipstick technology for the fluid density measurement, the sources of errors in the measurement need to be discussed. There are several key elements for the accuracy in the measurement. Firstly, the greatest error is believed to be introduced in the measurement of the immersion depth. In our experiment, the immersion depth was determined visually by means of a ruler, which suffered an accuracy of $\pm 0.5mm$, about 1% of the immersion depth. For future construction of an improved measurement, it is recommended to determine the immersion depth as accurately as possible. For example to shield the unimmersed part of the bar from the liquid by a cover could be one of the solutions.

The second error comes from the measurement of flight time in Eq. (3.5). The

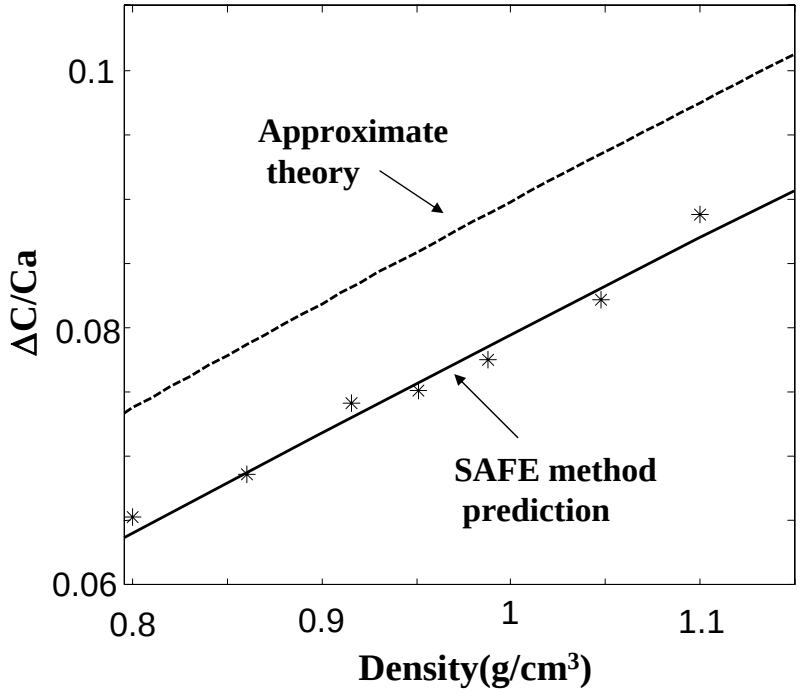

Figure 3.11: *Measured (stars) and theoretically predicted (line) group velocity of aluminium bar with rectangular cross-section immersed in different fluids compared with previous theory prediction (dashed line) .*

noise in the received time domain signals could cause shifting in the location of peak amplitude in the time domain signals, thus would affect the accuracy in the detection of flight time. The sampling frequency of the digitizer would cause another uncertainty of the measurement by limiting the temporal resolution of the signal recorded. However since the signal to noise ratio and the sampling frequency are both high in all measurements, the errors in the measurement of flight time were small.

The third error comes from the uncertainty in the properties of a solid bar, i.e. the density, mechanical properties as well as dimensions. The rectangular bar was produced by cutting a narrow strip from a plate and then bending it to be a straight bar. The material properties of the bar were measured on the plate, which could be slightly different from the material in the bar due to the bending procedure. The dimensions of the bar may also have errors in the FE modelling, for example it may

not be strictly constant along the bar. However the influence of the properties of the bar to the torsional speed was tested to be small, so that good accuracy can still be obtained from the inverse model.

3.5 Potential for Sensor Optimization

With the SAFE method, one can easily predict the torsional wave speed along bars with any arbitrary cross-sections immersed in fluids. Thus the model can be used as a powerful tool to optimize the sensitivity of the dipstick by changing aspect ratio, geometry of the cross section, and material properties of the bar. Compared to the previous simple theory, this cannot only improve the accuracy of the density prediction, but can also include the dispersion information. Therefore one can choose ideal shapes as well as frequencies for measurements according to the calculation.

Fig. 3.12 shows some examples of torsional mode on bars with different cross sections immersed in alcohol, which are the square shape, diamond shape, elliptical shape and hollow rectangular shape respectively. The displacements of the bars and the adjacent fluid are shown in arrows, which indicate the trapping of the fluid by the corners of each geometry. The group velocity of the torsional mode will be affected by the attached fluid, so that they can all be used as sensors of the fluid density.

Fig. 3.13(a) shows the measurement sensitivity of aluminum rectangular bars with aspect ratio from 1:1 to 1:4. Similar inverse models as shown in Sec. 4.6 were made by calculating the ratio $(C_a - C_{gr})/C_a$ as a function of the fluid density. From the calculations, it was found that $(C_a - C_{gr})/C_a$ is almost linear with density, therefore the sensitivity can be presented by the slopes of the lines. From the figure it can be seen that the sensitivity increases as the aspect ratio increases, thus it would seem desirable to operate with as large an aspect ratio as possible. However, the aspect ratio cannot be increased without limit. Fig. 3.13(b) presents the group velocity dispersion curves of these aluminum rectangular bars immersed in alcohol from 10 kHz to 100 kHz. It can be seen that as the aspect ratio increases the torsional mode becomes more and more dispersive, thus for bars with large aspect ratios

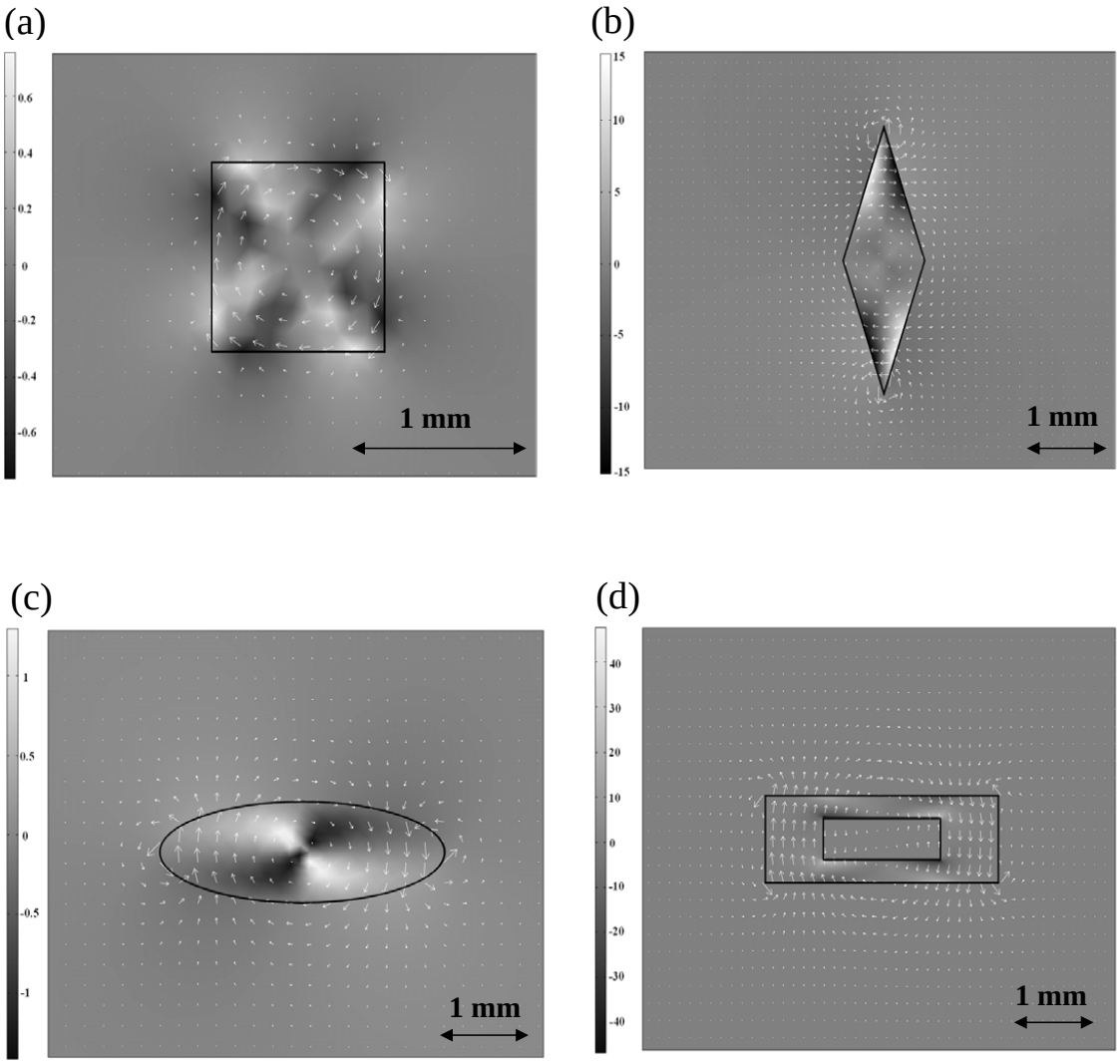

Figure 3.12: *Torsional mode on bars with different cross section immersed in alcohol: (a) square shape, (b) diamond shape, (c) elliptical shape and (d) hollow rectangular shape. The radial (with respect to the center of the bar) stress in solid and pressure in fluid is displayed in a grey scale .*

measurement are not practical at some frequencies. This conclusion has also been mentioned in the previous work by Kim and Bau [58]. With the SAFE method the dispersion characteristics of the waves can be accurately quantified, which helps to design the most practical aspect ratio.

For a given ratio, the sensitivity can also be optimized by the choice of geometrical configuration for the cross-section [58]. Fig. 3.14 compares the sensitivity of

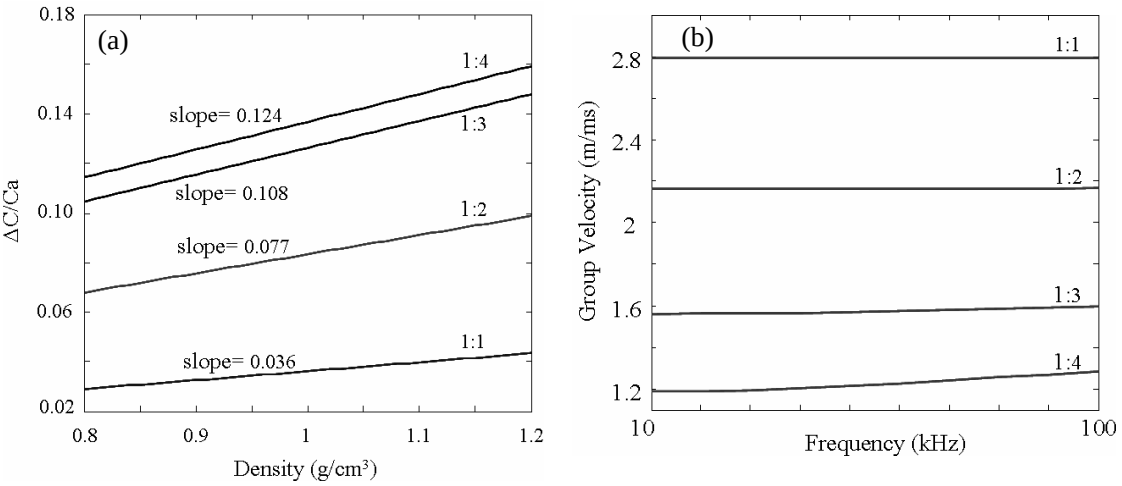

Figure 3.13: *(a) Measurement sensitivity comparison for aluminum rectangular bars with aspect ratio from 1:1 to 1:4. (b)Dispersion comparison for aluminum rectangular bars with aspect ratio from 1:1 to 1:4 .*

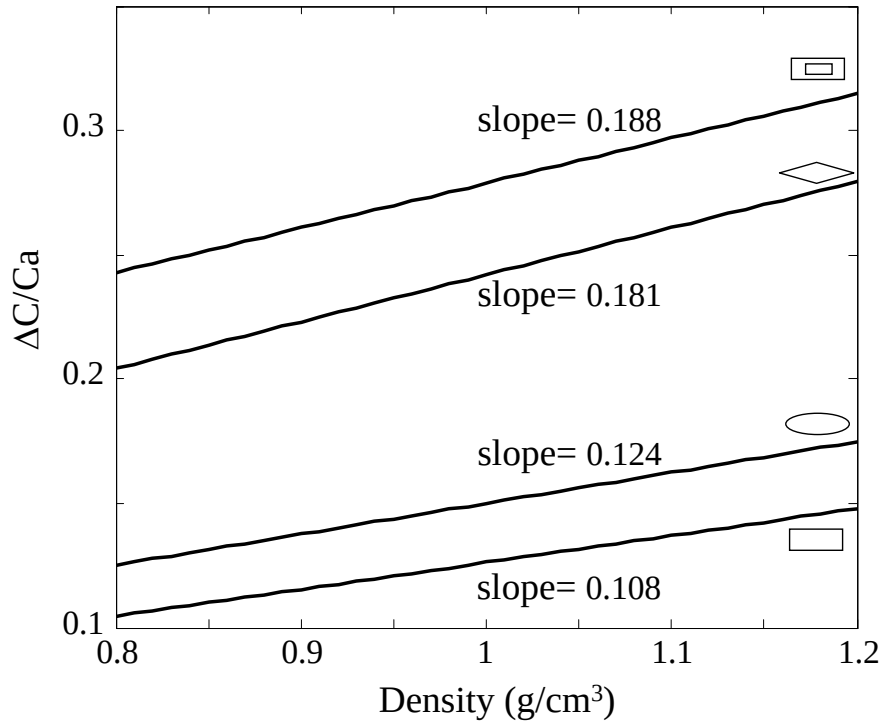

Figure 3.14: *Measurement sensitivity comparison for aluminum bars of rectangular, elliptical, diamond-shaped and hollow rectangular cross-sections with aspect ratio of 1:3 .*

aluminum bar of rectangular, elliptical and diamond-shaped cross sections with the same aspect ratio of 1:3. In addition the sensitivity of a rectangular waveguide ($1mm \times 3mm$) with a rectangular hole ($0.5mm \times 1.5mm$) in the middle is also shown in the figure. The results show that the diamond-shaped cross-section outperforms the elliptical one, and the elliptical one has better sensitivity than the rectangular cross-section. The hollow rectangular waveguide has similar sensitivity to the diamond-shape cross-section with the same aspect ratio.

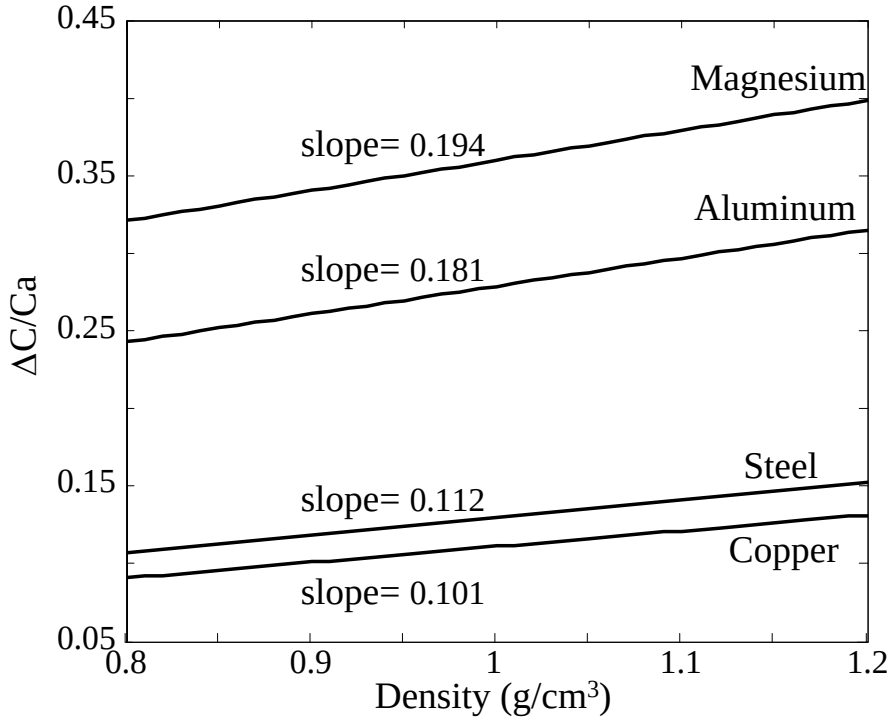

Figure 3.15: *Measurement sensitivity comparison for bars which are made of copper, steel, aluminum and magnesium of diamond-shaped cross-sections with aspect ratio of 1:3.*

The sensitivity also changes when different materials of the bar are chosen. Fig. 3.15 compares the sensitivity of bars with diamond-shaped cross-sections (with axes 1mm and 3mm) which are made of copper, steel, aluminum and magnesium. The parameters of the materials are shown in Tab. 3.1. It can be seen that the measurement becomes more sensitive when the density of the solid bar is closer to the fluid, which can also be explained by Eq. (3.4) from the approximate theory.

3.6 Summary

There are several ways to measure density ultrasonically. Conventional measurements use the time of flight and reflection coefficient methods. However for these methods the liquid compressibility has to be known and measurements have to be carried out in a test cell. For rapid field measurements "dipstick" sensors can be an alternative without the need for accurately machined test cells. A further advantage of "dipsticks" is the separation of the fragile transducer element from the measurement region so that fluids in harsh environments (high temperature, high radiation, corrosive etc.) can be tested.

The torsional mode of a non-circular dipstick waveguide has previously been employed in fluid density measurements but the accuracy was compromised by the lack of an accurate model. In this chapter, the semi-analytical finite element method has been applied for the study of solid waveguides immersed in fluids in which the guided waves propagate along the bar and are influenced by the fluid. The prediction of the model may include modes which attenuate by leakage of energy into radiating waves in the fluid. This has been achieved by using established absorbing region modelling techniques in order to absorb the leaking waves and thus simulate an infinite extent of the surrounding fluids. The method has been validated by studying a cylindrical bar immersed in water and comparing with analytical results. An accurate model has thus been developed to enable velocity measurements to be used to determine the density of the fluid. Experiments have been carried out to verify the model on a variety of fluids, showing very good agreement. This model also enables the optimization of the dipstick sensor by changing the material of the dipstick and the geometry of the cross section.

It should also be noted that only inviscid fluids were considered in the presented model. In practice, lots of fluids may have viscosity, which will undoubtedly affect the propagation of the torsional mode on an immersed solid waveguide. The SAFE method can be applied to predict guided modes in the solid bars immersed in viscous fluid, as it has been shown in Chapter 2. However it was challenging to develop an

inverse model. The main reason was that the velocity of the torsional mode was determined by both the density and the viscosity, thus it was required to solve a large number of SAFE models with different parameters to get the relationship between the velocity and two of the fluid properties. However, as it was shown in Chapter 2, the SAFE model for a solid bar immersed in a viscous fluid was very time-consuming to solve, therefore it was not practical to run many cases within the current computing capability.

Chapter 4

Investigation on feature guided waves

4.1 Discovery of the Feature Guided Wave

In the following three chapters, the discovery and exploitation of feature guided waves will be presented, applying the SAFE method as a tool for modal analysis.

As it is known, guided waves are interesting for large area inspections since they offer the potential for rapid screening from a single transducer position. Several successful applications have been made on one dimensional structures such as pipelines [11] and rails [64, 65]. Research work has also been carried out to study the possibility of applying the guided wave inspection to two dimensional plate-like structures such as storage tanks, pressure vessels and airframes [66–68], although this has resulted in little commercialization so far. This is mainly because in a two dimensional structure waves can propagate in an infinite number of directions from a single transducer position. In each direction the energy of the spreading wave decays with the distance away from the source, so that the inspection over a large area becomes difficult. Another challenge to inspect real plate-like structures is that there always exists some features such as welds and ribs which may cause extra coherent noise which interferes with the inspection signal.

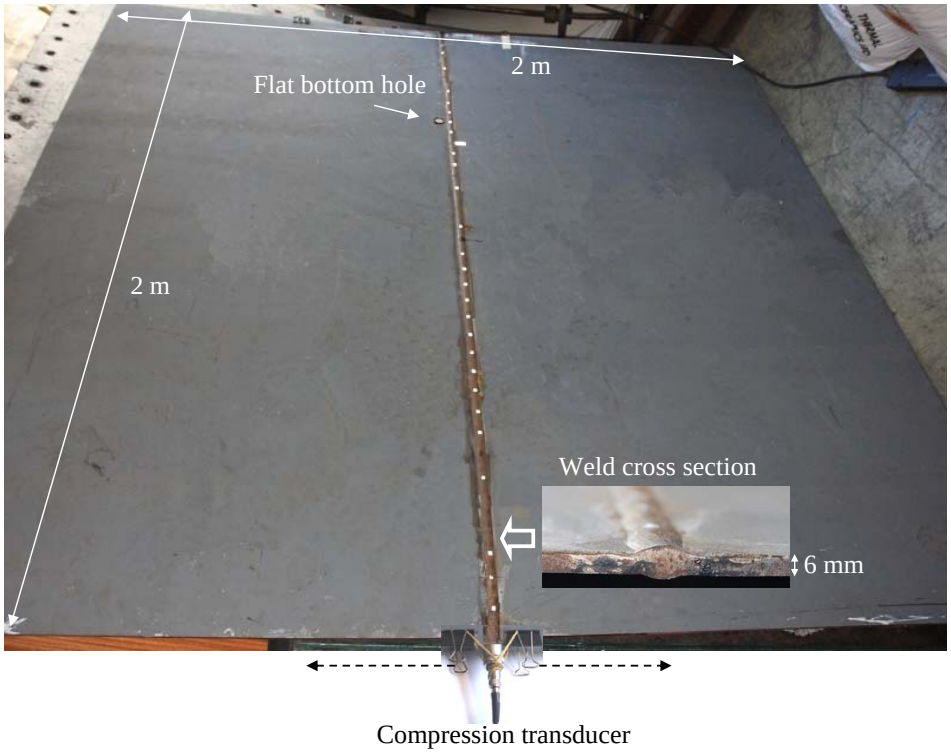

Figure 4.1: *Experimental discovery of feature guided wave.*

However, a recent experimental observation [21] on a large welded plate revealed that there existed "weld-guided" modes which can propagate along the weld and concentrate the energy in and around the weld. The experiments [21] were conducted by Dr. J. Sargent of BAe System, working in the NDT Laboratory of Imperial College. The tests were carried out on a $2m \times 2m \times 6mm$ thick steel plate with a butt weld in the middle, as shown in Fig. 4.1 . A flat bottomed part through thickness hole 20 mm in diameter was formed at a distance of 1.5 meters from the lower edge in the picture, and in a region adjacent to the weld. A single transducer (Ultra 200kHz, or a Panametrics 100 kHz - 500 kHz wide band transducer) was mounted on the edge of the steel plate in a number of locations, to excite an in-plane compression wave with a 20 cycle Hanning window tone burst with a center frequency of 200 kHz. The transducer was working in pulse-echo mode, and reflections from the hole and the far edge of the plate were monitored. It was observed that the reflection from the 20 mm hole was stronger and slightly delayed when the transducer was attached at the edge of the weld. This implied that a new wave mode was propagating along

the weld with energy concentrating close to the weld. This mode has a similar mode shape to the S0 mode in the plate but has slower velocity.

A simple explanation of this phenomenon is that the difference in the weld and plate thickness and material properties causes slower propagation velocities in the weld compared with the plate, therefore part of the energy is trapped in the weld and causes the weld to act a waveguide, which is analogous to that found in optical waveguides [69]. An illustration is shown in Fig. 4.2 but more details and a physical explanation of the trapping phenomenon will be discussed later in this chapter.

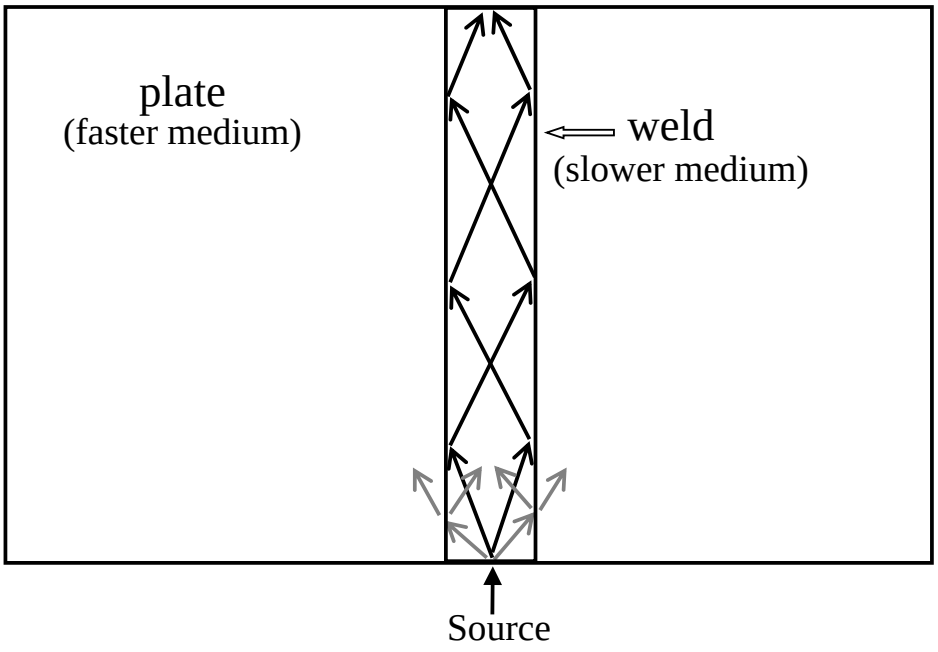

Figure 4.2: *Illustration of the trapped wave due to different propagation velocities in the weld compared with the plate .*

This is an attractive discovery as we know defects frequently occur preferentially in or near the weld due to the changes in microstructure, weld imperfection and presence of residual stress, and the same is true for other geometric features, such as joints and stiffeners. Therefore, instead of seeing the features as a problem, it may be possible to exploit them as waveguides to focus the energy of the guided wave. This offers the potential to quickly inspect for defects such as corrosion along long lengths of features on plate-like structures.

4.2 Time Step Finite Element Simulations

In order to exploit this feature-guided wave, it is necessary to understand its nature and propagation characteristics. Time step finite element simulations have been commonly used to illustrate the guided wave propagation on large and complex structures. Juluri has applied this method to demonstrate the trapped mode on an idealized weld (square bar) between two plates, which is a helpfully simple approximation to the actual welded plate [23, 70].

The model was simulated by FE analysis in the general three-dimensional domain implement using the commercial package ABAQUS [71]. The schematic of the model is shown in Fig. 4.3. The model plate was assumed to be 6mm thick and was connected by a rectangular bar with 12mm in width and 10mm in height.

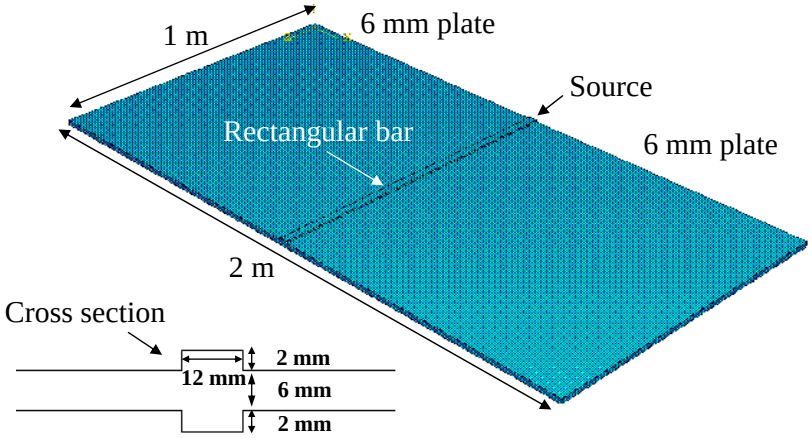

Figure 4.3: *Schematic of time-step finite element modelling of guided wave propagation on an idealized welded plate [23] .*

Fig. 4.4(a) shows a snapshot of propagation of the weld-guided waves at 100 kHz [23]. The image in the figure is a plain view of the plate with the model weld running top-to-bottom at the centre. The image shading denotes the amplitude of motion of the surface of the plate at some selected time after a tone-burst signal has been injected at the lower end of the weld. Thus the shading shows wave crests of the propagating signals. The signals labelled "Spreading S0 wave" and "Spreading SH wave" are those which would be expected from a localized source in a simple plate

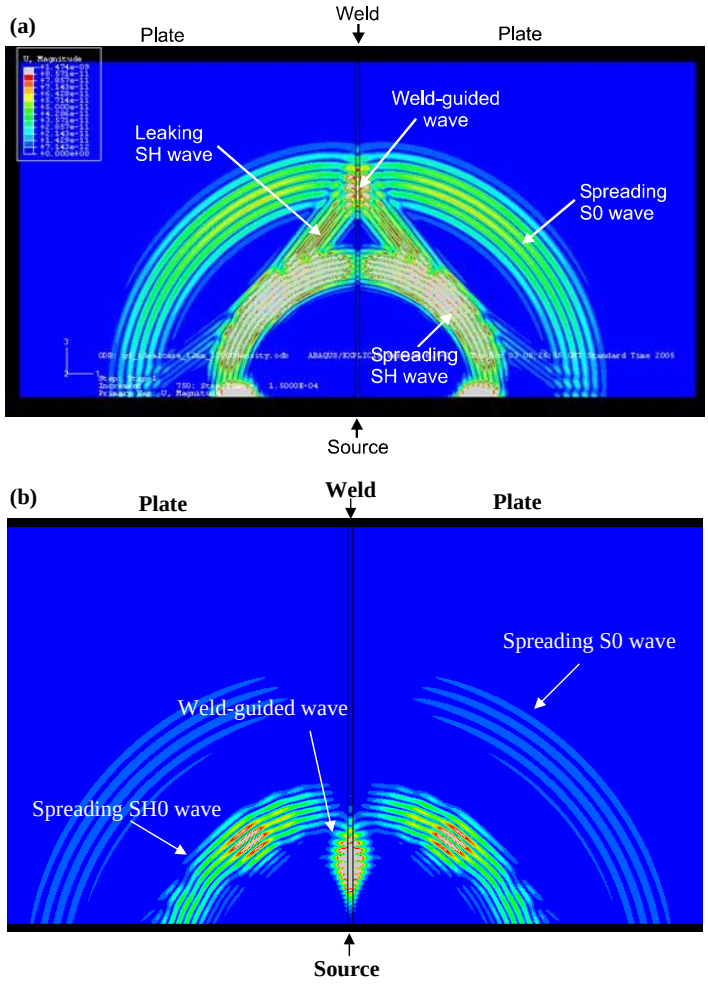

Figure 4.4: *Snapshot of propagation of the weld-guided waves at 100 kHz (a) and 500 kHz(b) [23].*

without a weld. The wave of particular interest, labelled "weld-guided wave" can clearly be seen to propagate strongly along the weld, with a speed slightly lower than the S0 wave (it has not travelled quite as far as S0 in this time). From the figure, it can be seen that the weld-guided wave in the thicker region of the weld runs more slowly than the S0 wave in the plate, and is then partially trapped, and so can propagate long distances with relatively little attenuation. There remains some attenuation in this example because the weld-guided wave is still faster than the SH0 shear wave in the plate and so can leak some energy into it. This can be seen as a wave spreading behind the weld-guided wave in the figure.

Fig. 4.4(b) shows the snapshot of propagation of the same mode at a higher frequency

of 500 kHz [23]. In this case the wave is found to be slower than the SH0 wave in the plate and so does not leak any energy into the adjacent plate. These two figures have clearly shown that a weld-guided wave exists and how it is guided.

However a major limitation of this 3D finite element model is its big size so that the simulations are always very time consuming. Therefore it is difficult to apply this method to investigate the properties of feature guided waves over a range of parameters and feature geometries.

4.3 SAFE Modelling

In order to further understand how the guiding is affected by the geometry and frequency, it is therefore necessary to perform a modal study of the welded-plate to fully predict the properties of the waves which are guided by the features. Therefore the Semi-Analytical Finite Element (SAFE) method, which uses finite elements to represent the cross section of the waveguide, plus a harmonic description along the propagation direction, becomes an ideal tool. It is a two dimensional model since only the cross-section which is normal to the direction of the wave propagation has to be meshed by finite elements and the wave is assumed to propagate harmonically. A typical calculation (calculation of all the propagation wave numbers at one frequency) in the model presented here only takes approximately one minute on a Pentium 4 PC with 2Gbyte memory, while it takes several hours to calculate one specific mode propagation at one frequency in the 3D time step FE model on the same computer. Therefore the SAFE model is much more convenient to obtain the dispersion curve of the weld guided mode, and is more flexible to study different geometries and parameters.

4.3.1 Model description

The schematic of the model is shown in Fig. 4.5, in which the profile has been measured from the welded steel plate shown in Fig. 4.1. Stress free conditions are

imposed at the outer limit of the system. Both the plate and the weld are assumed to have the same material properties (steel) as the adjacent plate. In order to model the wave propagation along the weld and leaking into the side plates, an absorbing region has been attached at each side of the plate to avoid reflections from the edges [50]. This region, shown in Fig. 4.5, has the same mass density and elastic properties as the side plate, but its damping properties gradually increases with the distance away from the central axis of the system. To achieve this, the imaginary parts of its viscoelastic moduli gradually increase according to the following law:

$$C_{ija} = C'_{ij}[1 + I\alpha_1(\frac{|r - r_a|}{L_a})^3], I = \sqrt{-1}, \tag{4.1}$$

where C'_{ij} represents the elastic stiffness of the side plate (coefficient in the strain-stress law [26]), r_a is the distance between the inner border of the absorbing region and the central axis, L_a is the length of the absorbing region, r is the position in the absorbing region with respect to the central axis, and C_{ija} are the resulting viscoelastic moduli of the absorbing region. α_1 is a coefficient that defines the proportion of the viscoelasticity at the outer limit of the absorbing region.

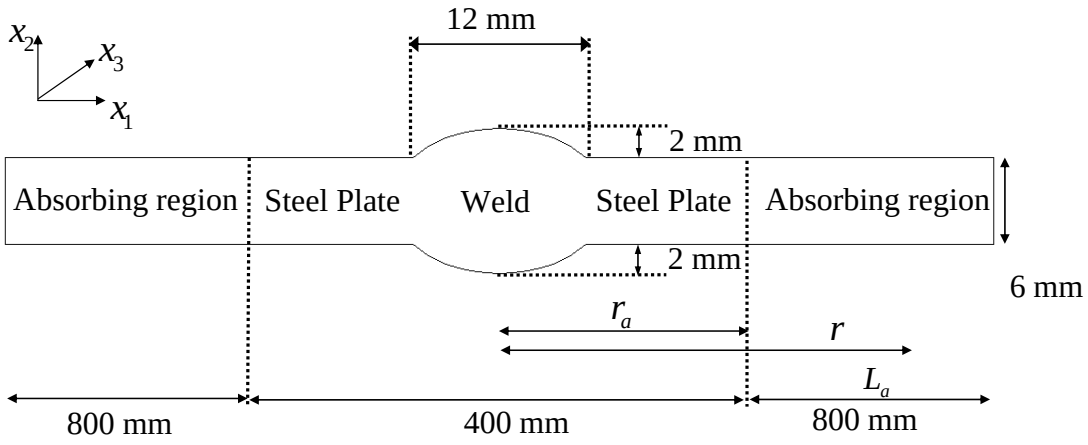

Figure 4.5: *The schematic of the two dimensional SAFE model of a welded plate.*

By introducing the imaginary part of the stiffness moduli, the propagation wave numbers, which are eigen solutions of the system, become complex ($k = k' + Ik''$). The imaginary parts (k'') represent the attenuation due to the leakage from the weld to side plates.

The length of the absorbing regions has been chosen to be 800 mm, which is twice the biggest wavelength of any radiated wave in the whole frequency range [50], and was proven to be efficient by a convergence check: when the length was increased the same solutions for the propagating modes in the waveguide was still obtained. The total width of the cross section is 2 m, including the absorbing region. The whole geometry is meshed by 1072 triangular elements of the first order, with sidelengths comprised between 1 and 6 mm. These elements are automatically generated by the software used, and are finer in the welded zone than in the adjacent plates. The number of degrees of freedom is 15882.

The system is solved using the SAFE method to find values of the wave number k at different frequencies. For each frequency, several solutions are obtained. For each solution, the axial component of the energy flow (Poynting vector) is calculated at each nodal position of the mesh, and the quantity is expressed by the following formula [26]:

$$P_{x_3} = -Re[(\frac{I\omega}{2})(u_1^*\sigma_{31} + u_2^*\sigma_{32} + u_3^*\sigma_{33})], \tag{4.2}$$

Where σ_{31}, σ_{32} and σ_{31} are the axial stress components; u_1^*, u_2^* and u_3^* are the complex conjugate of the vertical, horizonal and axial displacements respectively. Solutions with higher axial component of the energy-flow in the weld cap than in the side plates generally represent modes guided along the weld and possibly radiating in the plates, while other solutions represent resonances of the whole system and are unwanted.

4.3.2 Mode shapes at single frequencies

The first task of the investigation was to study the weld-guided compression (S0-like) wave which had been observed as described earlier in the chapter. The mode was identified by its mode shape. This is shown at 100 kHz in Fig. 4.6, with the eigenvalue $k = 115.486 - 3.034 \times 10^{-2}i$ /m, from which the corresponding phase velocity is: $C_{ph} = 5440.6$ m/s and the attenuation is: $\alpha = 0.263$ dB/m. A snapshot

of the axial component of energy flow is shown in Fig. 4.6(a), which indicates that the energy is concentrated in and close to the weld. The mode shape of this mode in the center of the weld along x_2 is shown in Fig. 4.6(b). From the figure it can be seen that the mode guided along the weld is dominated by axial displacement u_3 with respect to the vertical displacement u_2 and horizontal displacement u_1 , which is similar to a S0 (compression) Lamb wave in a plate. Thus this mode is named the compression weld guided mode.

According to the Snell-Descartes' law [26], only modes of the lateral plates having smaller phase velocities than that of the compression weld-guided mode could be radiated into the side plates. Thus the S0 mode, with its phase velocity of 5441 m/s [9] in a 6-mm-thick plate, cannot radiate, while in principle the other two fundamental modes, A0 and SH0 could. However, since this compression weld-guided mode is symmetric with respect to the mid-plane of the plates and weld, the A0 mode, which is anti-symmetric, cannot be launched. Therefore, the SH0 mode is the only mode that can be leaked into the plates at 100 kHz, and is radiated at an angle equal to $\theta_{leak} = sin^{-1}(3260/5440.6) \approx 36.8°$, with respect to the direction normal to the plates-weld interface. The axial displacement u_3 which dominates this compression weld guided mode in the center of the plate along x_1 is shown in Fig. 4.6(c). From the figure it can be seen that the axial displacement quickly decays with distance away from the center, which indicates the energy is concentrated in and around the weld. The oscillation of u_3 represents the leakage of the SH0 wave in the plate. It can be seen that the separation distance of the oscillation peaks agrees with the projection of the wavelength of the leaky SH0 wave along the x_1 direction, using $\lambda_{proj} = \lambda_{SH0}/cos\theta_{leak} = 40.7$ mm.

Fig. 4.7 shows zoomed energy flow snapshots for the compression weld guided mode, from frequency 50 kHz to 300 kHz. It can be seen that the lateral extent of the weld guided mode decreases as the frequency increases. At lower frequencies, the weld guided mode propagates along both the weld and the heat affected zone, thus it offers potential to inspect the heat affected zone by choosing a frequency lower than 150 kHz. However the sensitivity decreases exponentially as the lateral distance of the

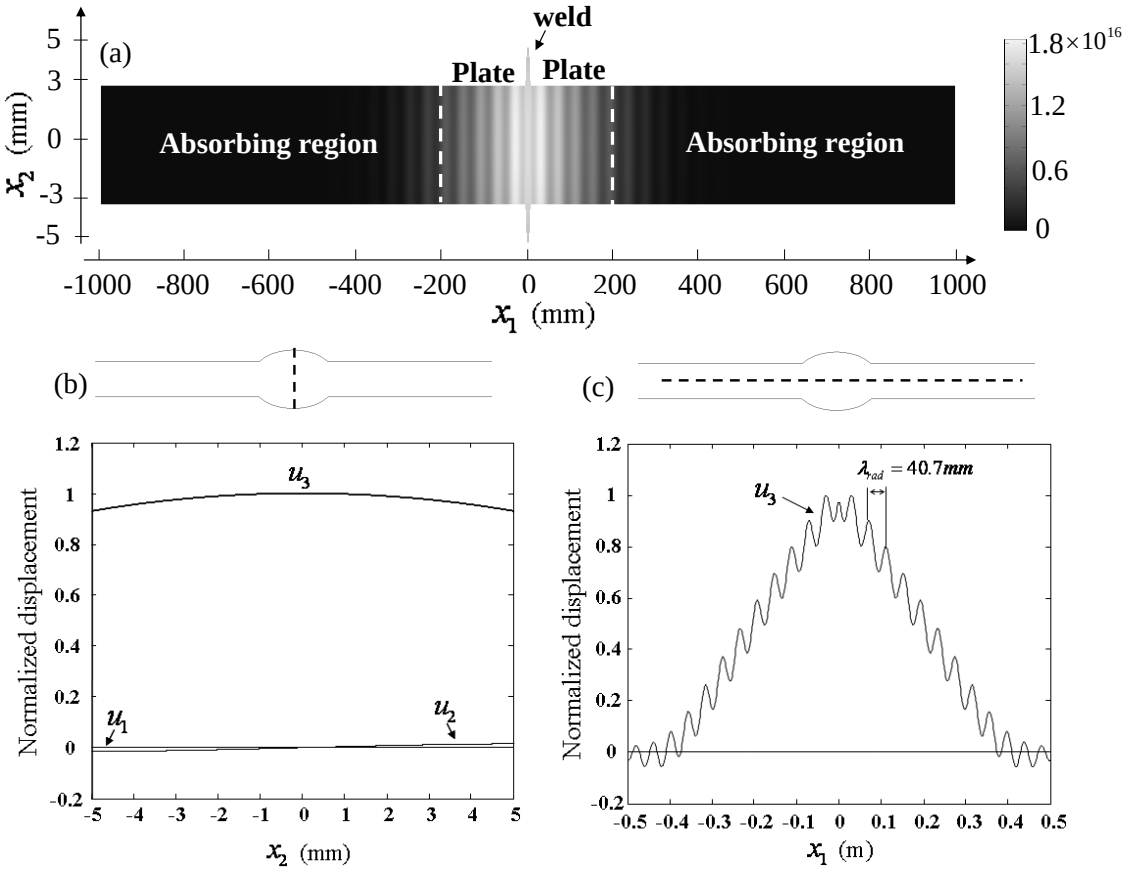

Figure 4.6: *Compression weld guided mode at 100 kHz: (a) snapshot of the axial component of energy-flow (white=high energy-flow, black=low energy-flow), (b) the mode shape in the center of the weld along x_2 (u_1, u_2, u_3 represent displacements of x_1, x_2 and x_3 respectively) (c) the axial displacement in the center of the plate along x_1.*

defect from the weld increases. At frequencies higher than 200 kHz, the compression weld guided mode exists only inside the weld and the energy concentrates on the surface of the weld cap as the frequency increases, which suggests that the sensitivity of this mode to small surface breaking cracks on the weld cap should increase.

4.3.3 Dispersion curve

The dispersion curves can be obtained by repeating the eigen calculations over a desired frequency range and the various modes identified by comparing the mode shapes as shown in Chapter 2.

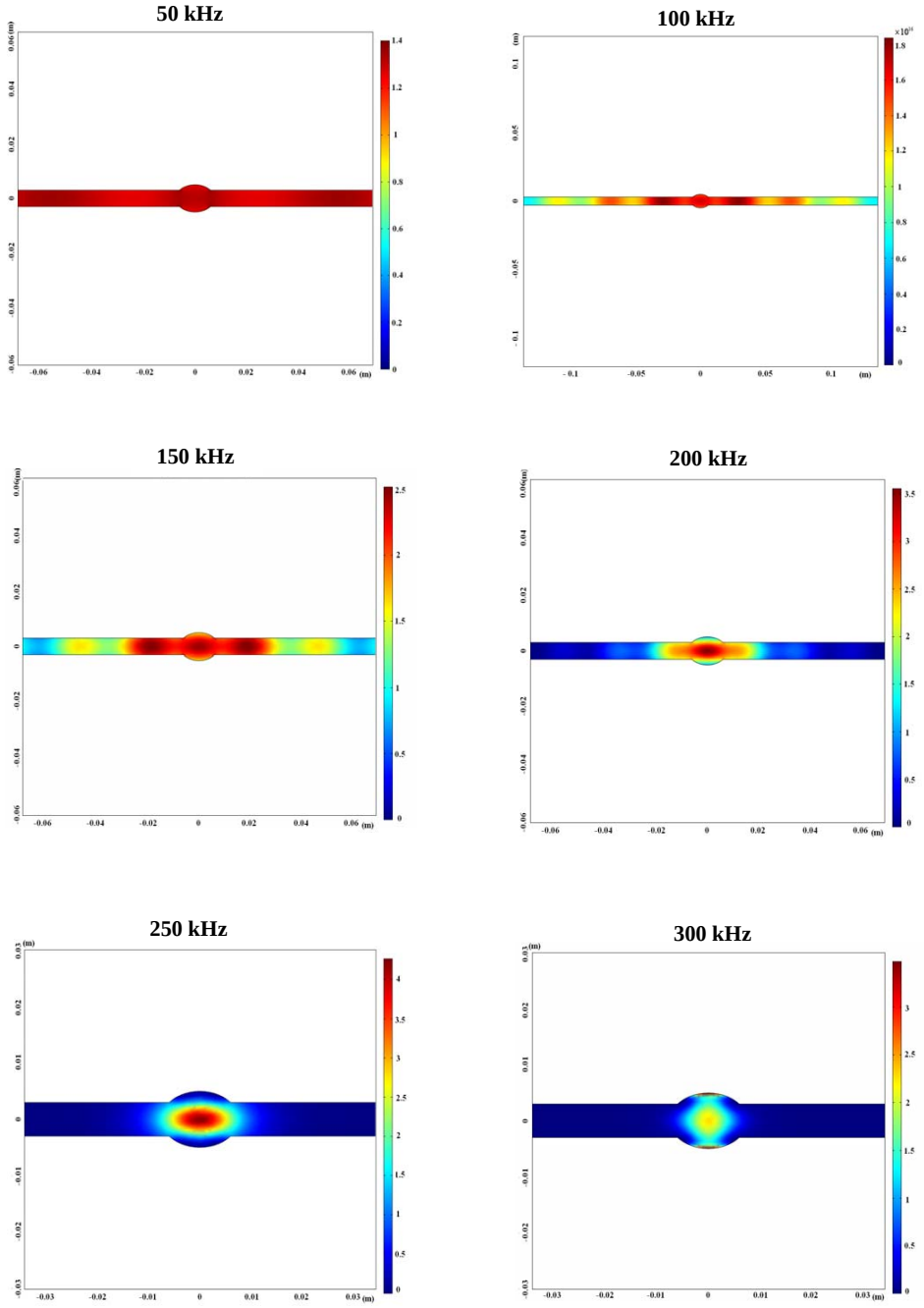

Figure 4.7: *Energy flow snapshots for the compression weld guided mode from frequency 50 kHz to 300 kHz.*

Fig. 4.8 shows the phase velocity and attenuation dispersion curve of the compression weld guided mode from 50 to 500 kHz produced by the SAFE method. The phase velocity dispersion curves of simple flat plates with 6 mm and 10 mm thickness are also plotted in Fig. 4.8(a) for comparison, confirming the similarity of the

weld guided mode to the S0 Lamb mode in the plate. As discussed earlier, this compression mode leaks the SH0 wave in the side plates when the phase velocity of this mode is higher than that of the SH0 wave in the plate; however, according to the Snell-Descartes' law, after 410 kHz it becomes a non-leaky mode when its phase velocity is lower than that of the SH0 wave in the plate, thus the zero attenuation after 410 kHz in Fig. 4.8(b) can be expected. In the attenuation dispersion curve in Fig. 4.8(b), there can be seen two peaks at 200 and 350 kHz and a dip at 250 kHz. A similar phenomenon has also been observed by Castaings and Lowe [50], who showed that it can be explained by studying the normalized energy-flow through the weld-plate interface which shows a similar curve.

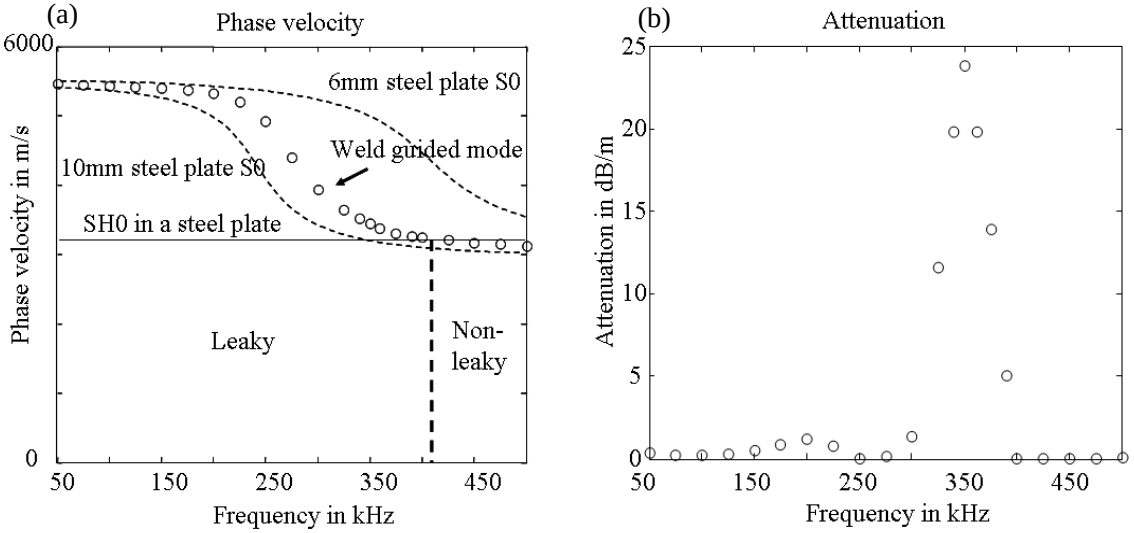

Figure 4.8: *Phase velocity (a) and attenuation (b) dispersion curve of compression weld guided mode predicted by SAFE method.*

4.4 Discovery of Shear Feature Guided Wave

The SAFE method calculates all the propagation modes at one frequency, thus it creates the possibility of finding other feature-guided modes which could be candidates for inspection but have not yet been discovered. During the modal study, another interesting mode, which has particle displacement perpendicular to the plane

of propagation, has been discovered. The schematic of this new mode is shown in Fig. 4.9. As can be seen from the figure, the mode shape of this newly discovered mode is very similar to the SH0 mode in the plate, this mode is therefore named the shear feature guided mode.

It is believed that this mode has not been observed before, and it is very interesting for long distance inspection since it is found to be non-leaky and almost non-dispersive. The properties of this mode will be discussed in detail in the following paragraphs.

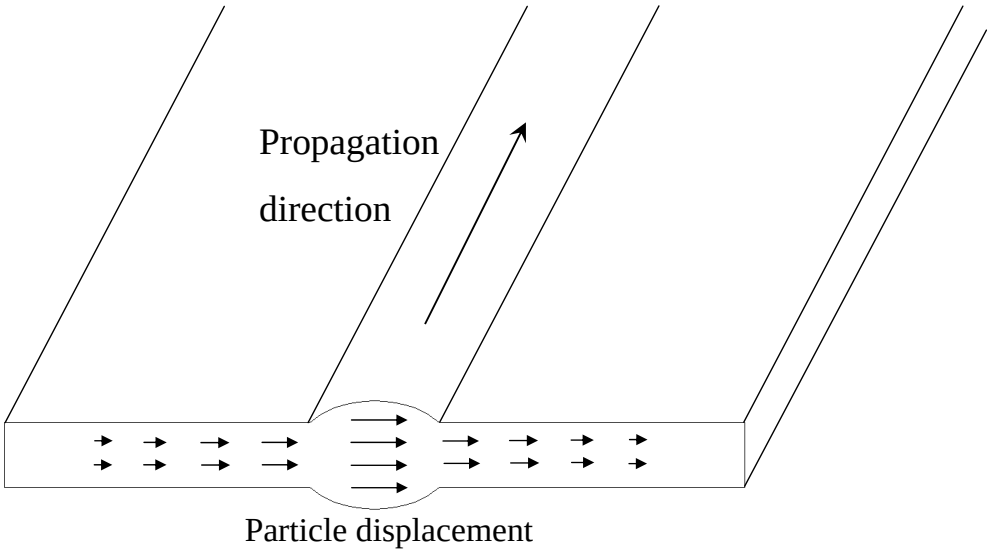

Figure 4.9: *Schematic of the shear weld guided mode.*

4.4.1 Mode shapes of the shear mode at single frequencies

The shear mode at 100 kHz is shown in Fig. 4.10 with the eigenvalue $k = 194.86 - 1.3 \times 10^{-7}i$ /m. The imaginary part of the eigenvalue is numerical error which is effectively zero. This shows that the attenuation of this mode is zero, which means there is no mode leaking to the lateral plates. The phase velocity can be calculated from the real part of the eigenvalue: $C_{ph} = 3224.5$ m/s. A snapshot of the axial component of energy flow is shown in Fig. 4.10(a), which indicates that the energy is concentrated in the weld. The mode shape of this shear mode in the center of the

weld along x_2 is shown in Fig. 4.10(b). From the figure it can be seen that the mode guided along the weld is dominated by horizontal displacement u_1 with respect to the vertical displacement u_2 and axial displacement u_3, which is similar to a SH0 wave in a plate. Fig. 4.10(c) shows the horizonal displacement u_1 in the center of the plate along x_1, which indicates that the energy is concentrated in the weld, but this mode has no leakage and thus no oscillation in the adjacent plates.

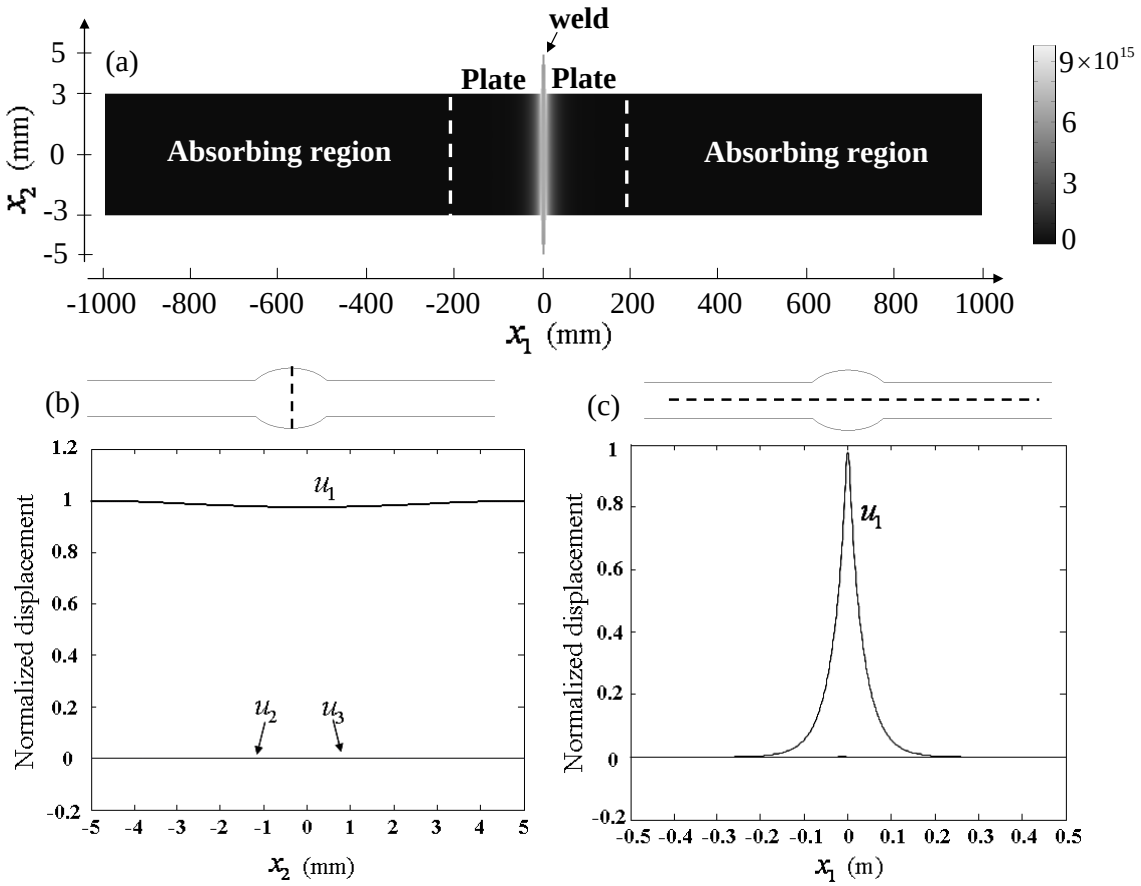

Figure 4.10: *Mode shape of shear weld guided mode at 100 kHz: (a) snapshot of the axial component of energy-flow (white=high energy-flow, black=low energy-flow), (b) the mode shape in the center of the weld along x_2 (u_1, u_2, u_3 represent displacements of x_1, x_2 and x_3 respectively) (c) the horizontal displacement in the center of the plate along x_1 .*

Fig. 4.11 shows zoomed energy flow snapshots for the shear weld guided mode, from frequency 50 kHz to 300 kHz. As it can been seen from the figure, similarly as the compression weld guided mode, while the frequency increases the energy becomes more and more concentrated in the weld. This suggests that at lower frequency the

shear weld guided mode is more sensitive to defects in the heat affected zone, but the sensitivity decreases as the frequency increases. At higher frequency, the mode becomes more sensitive to defects inside the weld.

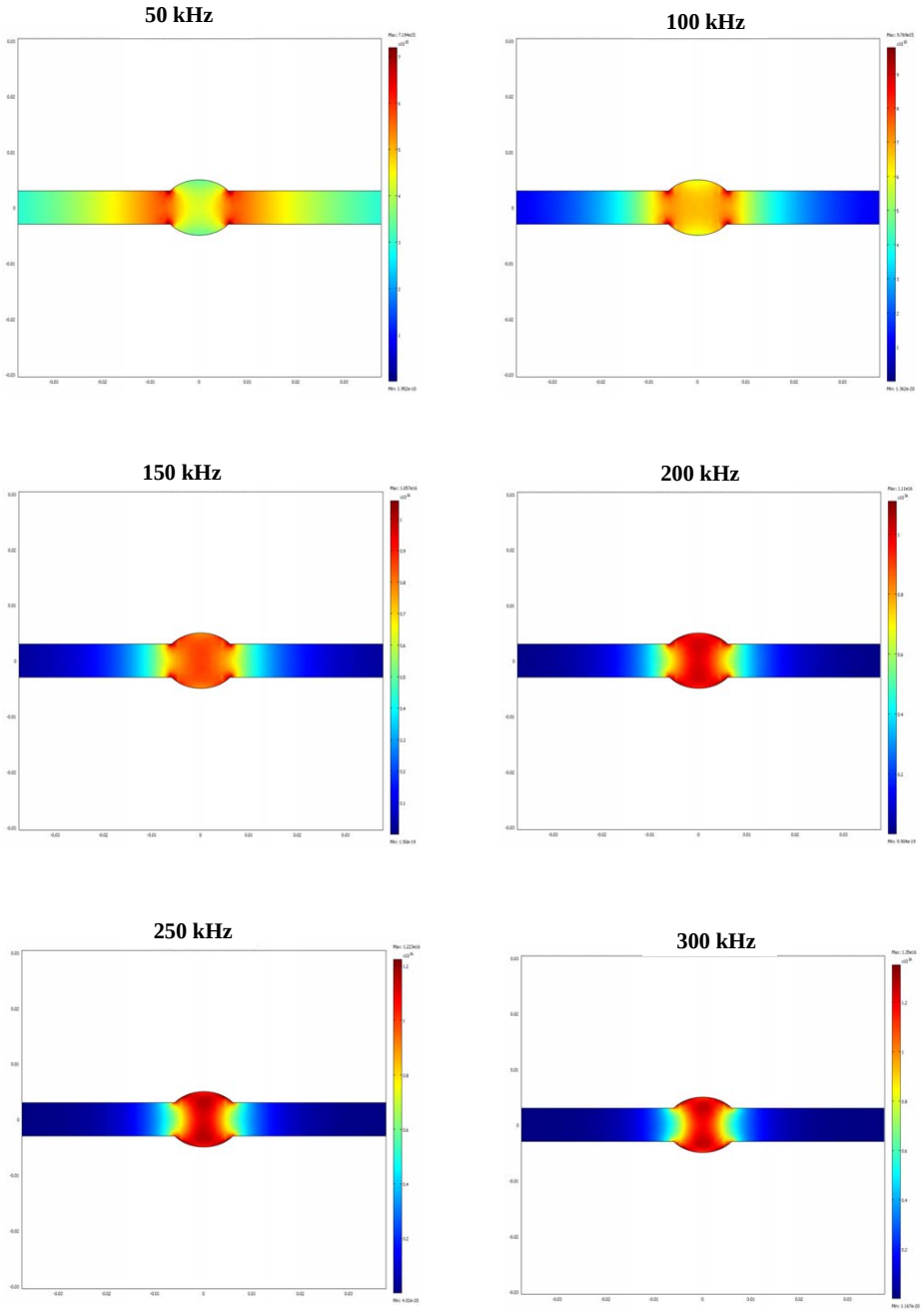

Figure 4.11: *Energy flow snapshots for the shear weld guided mode from frequency 50 kHz to 300 kHz.*

4.4.2 Dispersion curve of the shear weld guided mode

Fig. 4.12 shows the phase velocity dispersion curve of the shear welded-guided mode from 50 to 250 kHz. As is known, the SH0 mode in a plate is a non-dispersive mode, thus the phase velocity is constant at all frequencies, which is shown by the dashed line in the figure. From the figure it can be seen that the shear weld-guided mode has lower phase velocity than the SH0 mode in the plate at all values of frequency. Also, this mode is very much less dispersive than the compression weld-guided mode, which is another advantage for applying this mode to long range weld inspections. The imaginary part of the wavenumber of this mode stays zero at all frequencies which confirms that this mode is non-leaky.

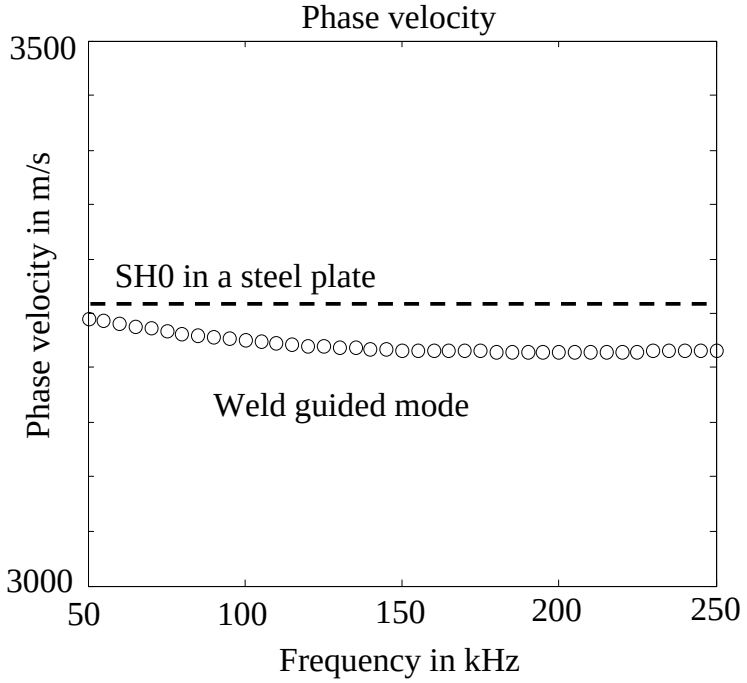

Figure 4.12: *Phase velocity dispersion curve of shear weld guided mode predicted by SAFE method.*

From the discussion above, it can be seen that the non-leaky and almost non-dispersive characteristics of the shear weld guide mode are particularly attractive for NDE, so this is a significant new finding. In addition, the particle displacement of this mode is perpendicular to the plane of propagation and therefore it is expected to be more sensitive than the compression mode to the fatigue cracks that are typ-

ically aligned along the weld in the heat affected zone. The sensitivity of this mode to different type of defects will be discussed in the next chapter.

4.5 Energy Trapping Effect

In order to explain the reason for the energy trapping effect of the weld guided mode, the geometry has been separated into two parts, which are the steel weld and a 6-mm-thick steel plate. The fundamental propagation modes in these two geometries have been calculated separately.

The dispersion curves and the mode shape of the propagation modes in the weld can be calculated by the SAFE method while in the plates they can be calculated by well-established analytical methods [7,9]. There are four fundamental modes which may exist in the weld, and the displacements in the cross section (mode shapes) at 100 kHz are plotted in Fig. 4.13. It can be seen from the figure that at low frequency the torsional mode is dominated by the circumferential displacement; flexural modes 1 and 2 are dominated by the horizontal and vertical displacement respectively. The longitudinal mode is dominated by the axial displacement. Comparing the mode shapes of these four modes in the weld and the fundamental modes in the plate, it can be found that the longitudinal mode and flexural modes 1 and 2 have similar mode shapes as the S0, SH0 and A0 modes in the plate respectively, while the torsional mode does not have any similar modes in the plate.

The phase velocity dispersion curves of the fundamental propagation modes in the weld are shown in Fig. 4.14 by the solid lines, and compared with the dispersion curves of the S0, SH0 and A0 modes of a 6-mm-plate, which are shown in dashed lines. From the figure, it can be seen that the phase velocity of the longitudinal and flexural mode 1 are slower than their similar modes in the plate, which are the S0 and SH0 mode respectively. The Snell-Descartes' law [26] would impose the condition that, when the weld and plate are joined up, the waves must have the same axial velocity in both parts. The combined axial velocity should be expected to be something between the velocity in the weld and that in the plate. Thus, if the

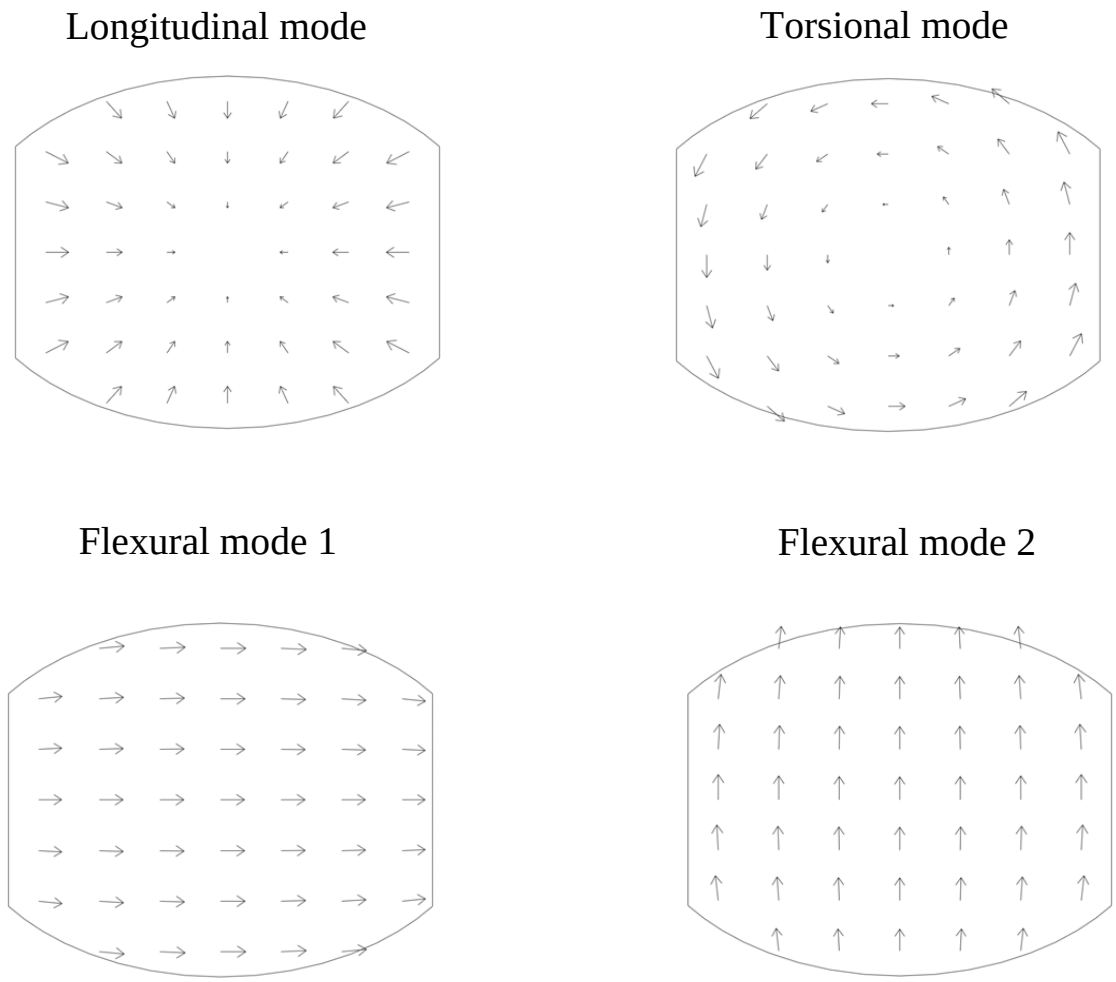

Figure 4.13: *Mode shapes of four fundamental propagation modes of the weld at 100 kHz. Arrows indicate displacements in the cross section.*

velocity in the weld mode is less than its similar mode in the plate, the combined velocity should be less than the plate velocity. It is also known from the Snell-Descartes' law [26], that if a wave is constrained by the boundary conditions at an interface to have a slower phase velocity than that in the adjoining medium, then it can propagate energy only along the interface, not away from it. Therefore while the combined mode, which could be the compression mode or the shear mode, is propagating along the weld, the energy of the mode will be trapped in and around the weld. The phase velocity of the flexural mode 2 is higher than its similar mode (A0 mode) in the plate, thus it cannot be trapped.

Therefore it can be summarized that the condition of the trapping effect should follow the rule: the propagation modes in the weld should have similar mode shapes to the corresponding modes in the plate, but have slower phase velocity. It should be noted that the geometry of a weld could be less regular than that which is discussed in our model and the material of a weld could be different from the adjacent plate. However, the weld guided modes can always exist as long as the phase velocity of those modes in the weld are slower than their similar modes in the plate, so that the energy is trapped in the welded zone.

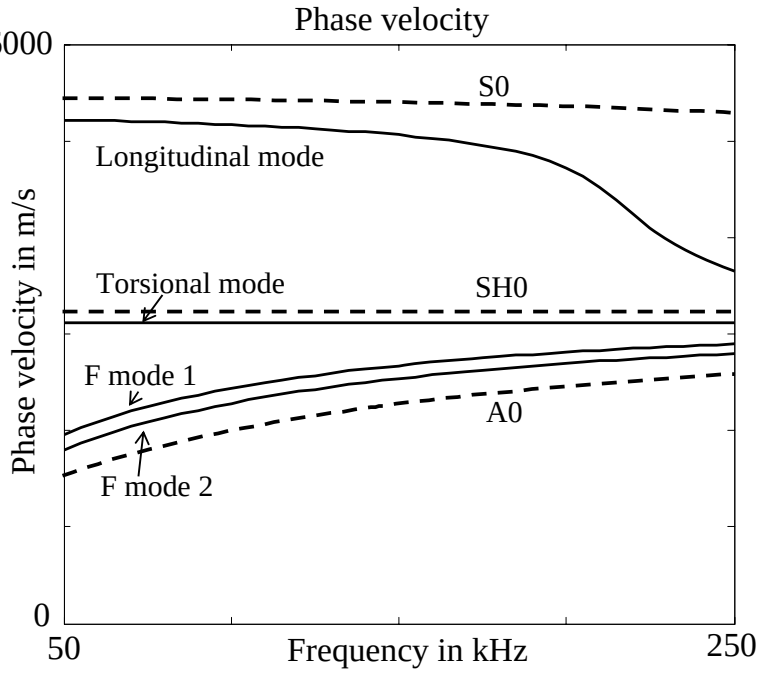

Figure 4.14: *Phase velocity dispersion curves of the fundamental propagation modes in the steel weld and in the 6-mm-thick steel plate.*

From the physical explanation of the energy trapping effect, it is known that the feature guiding phenomenon is geometrically oriented, therefore it is necessary to discuss how the change of the weld geometry (the height or the width of a weld) effects the energy distribution of a weld guided mode. In order to describe it quantitatively, a concept of Full Width Half Maximum (FWHM), which is also called the 6 dB Width (W6dB), is borrowed from imaging theory [72]. It can be described graphically by Fig. 4.15, which shows a zoomed energy flow snapshot for the shear weld guided mode on a geometry shown in Fig. 4.5 at 100 kHz, and the axial energy

distribution along the center line of the cross-section. The FWHM is marked in the figure, which is measured by identifying the points on the curve which are half the maximum value. The smaller the value of the FWHM is, the more energy is concentrating in and around the weld.

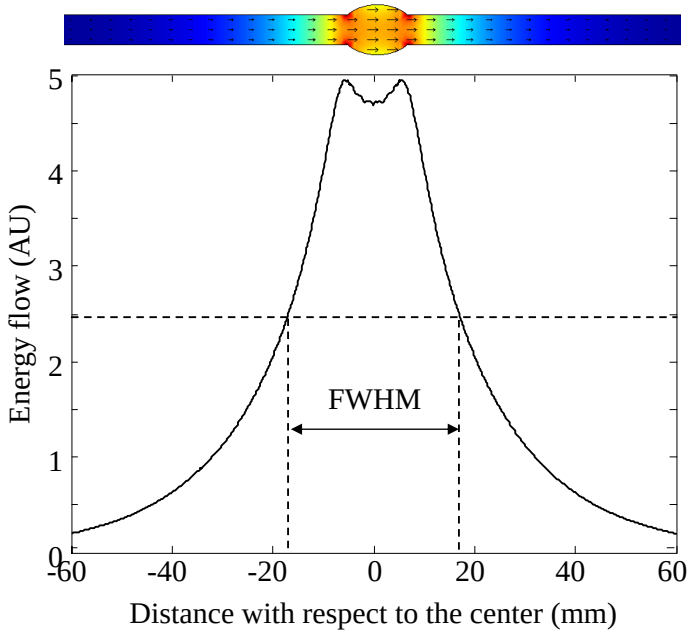

Figure 4.15: *The FWHM of the shear weld guided mode at 100 kHz.*

Fig. 4.16 discusses the change of the energy distribution with the variation of the weld geometry. Fig. 4.16(a) shows that the energy of the shear weld guided mode becomes more and more concentrated to the weld when the height of the weld increases. (Here the weld is assumed to be symmetric with respect to the center of the plate, while the non-symmetric case will be discussed in the next chapter.) Fig. 4.16(b) suggests that the width of the weld has less influence in the energy distribution of a weld guided mode than the height of the weld.

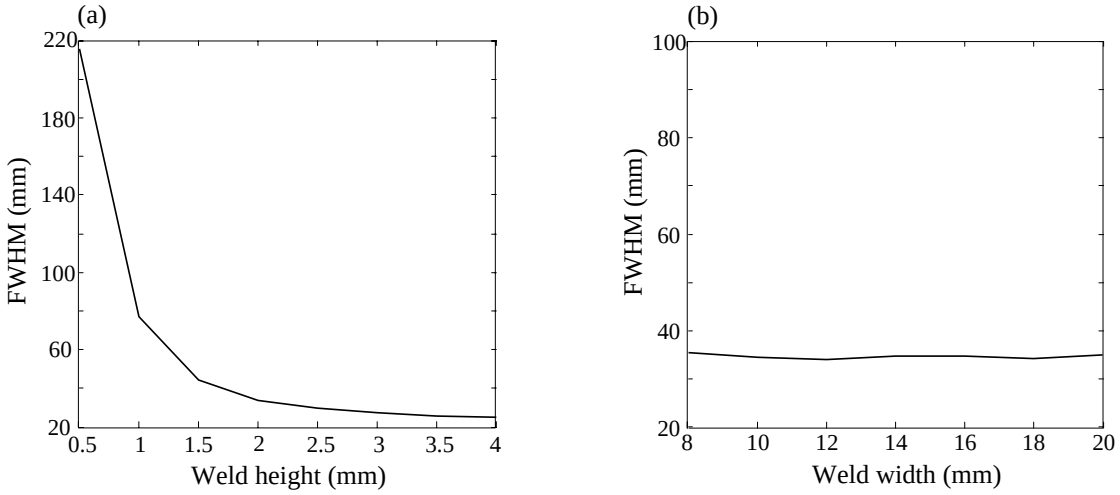

Figure 4.16: *The energy distribution (FWHM) with different height (a) and width (b) of the weld.*

4.6 Experiment on the Shear Guided Mode

4.6.1 Experimental setup

An experimental setup was designed to validate the shear weld guided mode since it is particularly attractive for NDE. In order to achieve an accurate experimental validation with low noise, a machined 600 mm by 1200 mm aluminum plate ($\rho = 2700kg/m^3, C_l = 6474m/s, C_s = 3051m/s$, at temperature 20°C) was used instead of using the actual welded plate. The plate was originally 10 mm thick, and was machined to be 3 mm thick with a 10 mm by 10 mm square bar in the center. Although it was not a welded plate, this simple idealized geometry enables the same principle of the energy trapping effect to be examined as a validation. A picture of the experimental setup is shown in Fig. 4.17.

A wide-band piezoelectric shear transducer(Panametrics V154) was attached on the top of the bar at the edge, as shown, to excite the shear mode with a 5 cycle Hanning windowed tone burst. Its orientation was such to impose its oscillation force in the horizontal direction in this view (lateral to the bar). The signals were generated using a Wavemaker (Macro Design Ltd, UK) instrument. A laser interferometer

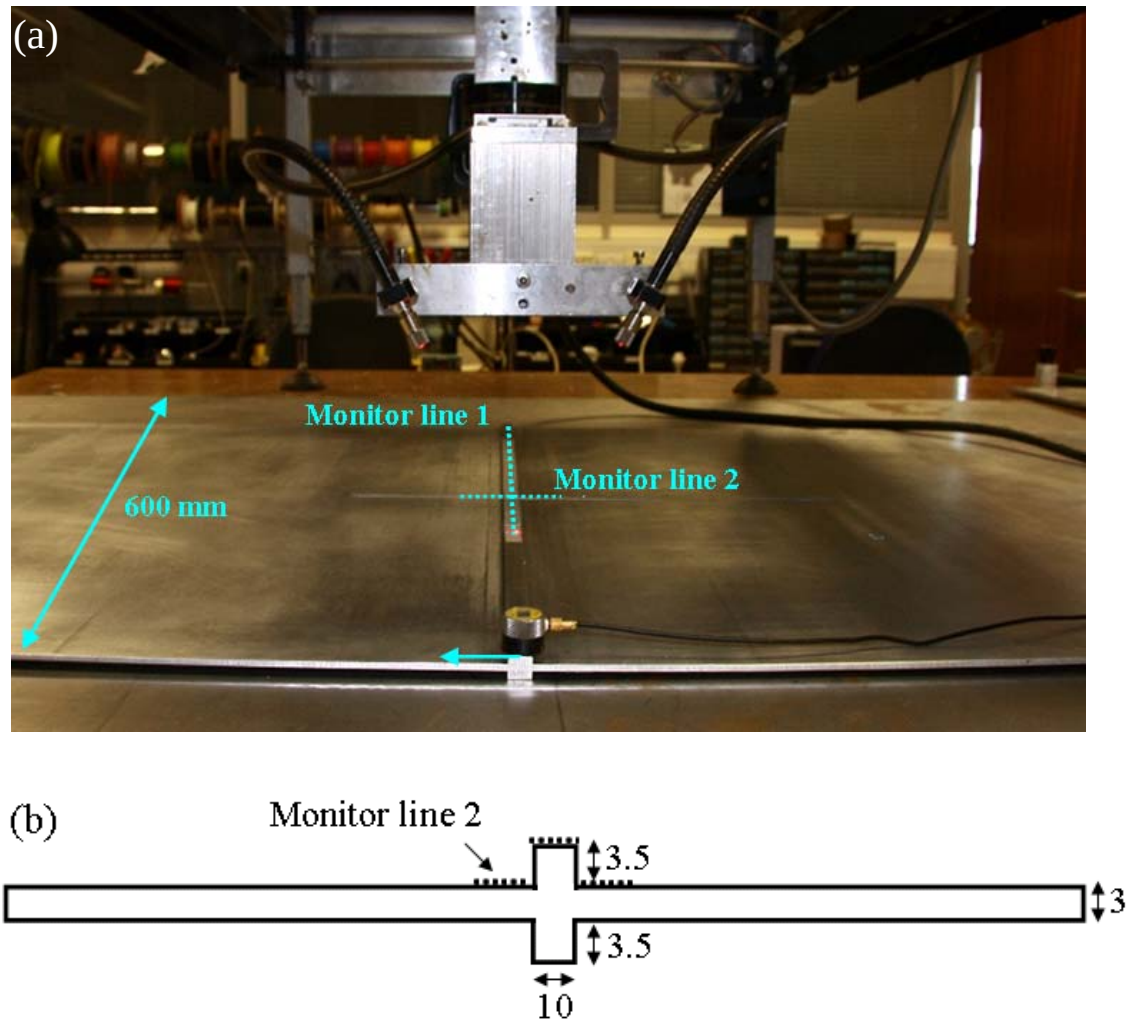

Figure 4.17: *Experimental setup. (a) plan view, (b) side view .*

(Polytec OFV 2700, with dual differential fiber optic lines) was used to pick up the horizontal displacement at positions along two monitor lines. One was along the center of the bar 200 mm to 500 mm from the source, and the other was across the bar 300 mm from the source, as shown in the figure. A LeCroy 9400A Storage Oscilloscope was used to store the time trace of the signal and the data was then transferred to a computer for processing.

4.6.2 Validation of group velocity and attenuation

The group velocity C_{gr} can be extracted from the measured signals by $C_{gr} = \Delta S/\Delta T$ at any chosen frequency. Here ΔT is the flight time of the wave packets propagating along the bar at two different locations on monitor line one, which can be determined by calculating the shift of the Hilbert envelope of the measured signals, and ΔS is the distance between the different locations. The accuracy of the results was enhanced by measuring at several different locations and taking averages.

A similar SAFE model as described in Sec. 4.4 but with different geometry and material was developed to compare with the experimental results, and the shear guided mode which was measured in the experiment was picked up.

Fig. 4.18 shows the dispersion curve of the group velocity measured in the experiment, and the theoretically predicted curve by the SAFE method, which was obtained by doing a numerical derivation $C_{gr} = d\omega/dk'$ of the SAFE phase velocity results. From the figure we can see that the measured results agree very well with the theoretical predictions.

Fig. 4.19 shows the displacement amplitude measured at different locations along monitor line one normalized by the displacement amplitude at 200 mm from the source at 120 kHz. For comparison, the beam spreading wave on a plane plate from a point source is also plotted in the figure, following the well known amplitude decay of approximately $1/\sqrt{r}$ [73]. From the figure it can be seen that the measured shear weld-guided mode has slight attenuation, which might come from scattering or material damping, although theoretically the attenuation should be zero, but this is very much less than the attenuation of the beam spreading wave.

4.6.3 Validation of energy concentration effect

In order to validate the trapping effect of the weld guided mode, a series of points on line two, shown in Fig. 4.17, 300 mm from the source, were monitored, and the maximum amplitude of displacement of these points at 120 kHz was recorded

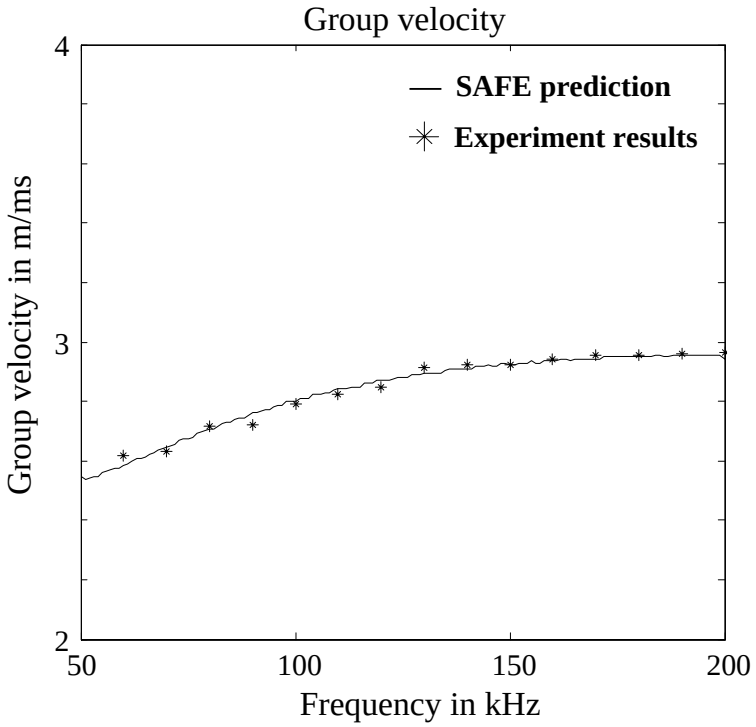

Figure 4.18: *Measured (stars) and theoretically predicted (line) group velocity dispersion curve of the shear weld-guided mode.*

and plotted in Fig. 4.20. From the figure it can be seen that the amplitude of displacement quickly decays with distance away from the central axis of the bar. Comparing to the displacement distribution of a beam-spreading wave from a point source on a plane plate without a weld, which is a circular crested wave [26] and appears to be straight in the figure because it is a long way from the source, it can be confirmed that the energy is concentrated in and around the weld region in the weld guided mode. The SAFE prediction is also plotted in the figure which shows near-perfect agreement with the experimental data.

4.7 Summary

Feature guided waves are interesting for large area inspections, and the particular case of a compression wave in a weld has previously been found experimentally, and also theoretically, by time step FE simulations. In this chapter, the Semi Analytical

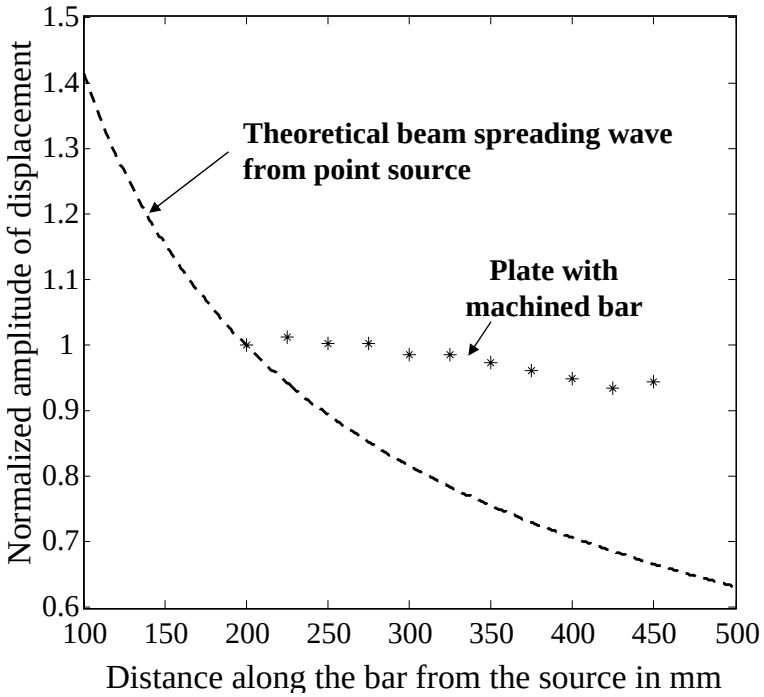

Figure 4.19: *Normalized displacement amplitude measured at different locations along monitor line one (stars) and comparison with the beam spreading wave from a point source on a plate (dashed line).*

Finite Element method has been applied to study the wave propagation along the weld and possibly leaking into the surrounding plates. Also a non-leaky and almost non-dispersive mode, named the shear weld-guided mode, has been discovered during the modal study and compared with the compression weld-guided mode observed earlier. It can be explained that the propagation mode can be trapped in the weld when it has a similar mode shape as in the side plates but with lower phase velocity. Experiments have been undertaken to validate the existence of the shear weld-guided mode and the accuracy of the FE model, showing very good agreement.

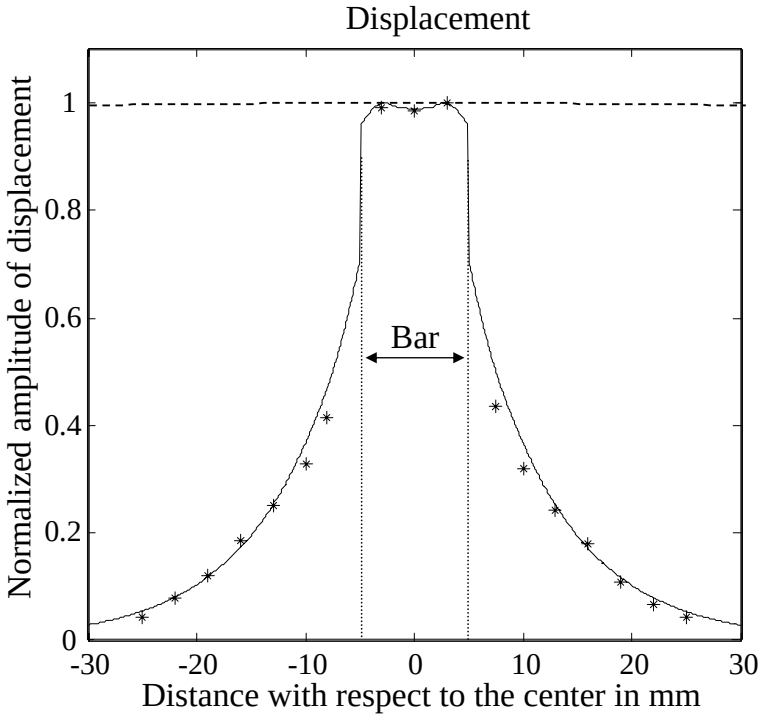

Figure 4.20: *Measured (stars) and theoretically predicted (solid line) normalized amplitude of displacement monitored along monitor line two, 300 mm from the source, and comparison with the beam spreading wave from a point source on a plate (dashed line). The width of the bar is also shown.*

Chapter 5

Scattering of Weld Guided Modes from Defects Located Around the Weld

5.1 Background

The conventional ultrasound inspection of a long length of weld is very time consuming and expensive as it requires scanning point by point over the whole length of the weld. Chapter 4 demonstrated that there existed weld guided modes which could concentrate the energy in or around the weld, and propagate along the weld with no or little attenuation. This kind of wave may be reflected by some defects when they are located on the path of the propagation. Thus it is possible to use a simple pulse-echo arrangement with a single transducer which is aligned to generate waves along the weld then receive reflections from any defects in or around the weld. In this case further knowledge regarding to the scattering of weld guided waves from different types of defects needs to be obtained, in order to exploit the idea of using weld guided waves as a screening tool to inspect long lengths of welds.

The interaction of guided waves with defects on a regular geometry such as a plate

has been widely studied by researchers. Several methods have been developed to understand the reflection and transmission of the guided waves when incident at defects. For example, Alleyne and Cawley have used finite element simulations and experiments to study the interaction of the A0, S0 and A1 modes with a surface breaking notch, emphasizing on establishing the transmission coefficient [74]. Lowe *et al* have studied the reflection of the S0 [66] and A0 [75] mode from cracks and notches, assuming a plain strain two-dimensional domain. The reflection behavior has been studied in terms of a frequency domain ratio of the resultant displacement of the reflected signal to that of the incident signal. Besides the Lamb modes, the shear horizontal mode is also interesting for inspection, especially because it is a non-dispersive mode and it is unaffected when the plate is loaded by fluids. Rajagopal and Lowe [76] have applied a plane stress assumption on a two-dimensional domain to study the SH0 wave scattering when normally incident at a finite crack. Ratassepp [77] *et al* have extended the study to address cracks which are aligned in the propagation direction of the mode. Three dimensional models have also been applied to study cracks with part-through thickness [78] and flat-bottomed circular holes [79].

The procedure to study the interaction between the weld guided modes with defects in or next to the weld was similar to the study mentioned above. A three dimensional model was required and reflections of the weld guided waves from the defects were studied in the frequency domain. There were also some differences. For example there is no need to consider the beam spreading effect as the energy of the weld guided waves is concentrated in and around the weld, not spreading away. In contrast, the amplitudes of guided waves on simple plates decay cylindrically away from the source, which needs to be compensated before calculating the reflection modulus. Moreover, the properties of the weld guided modes such as mode shapes and group velocity are frequency dependent, thus it is necessary to choose a proper operation frequency.

5.2 Experiment

5.2.1 Experiment preparation

In order to demonstrate the guiding effect of the weld guided wave, and its interaction with different defects, it is important to choose a weld which has a relatively smooth weld cap, so that the coherent noise level from the scattering on the surface of the weld cap can be kept low. The welded plate in our experiment was provided by Dr. Norrie McPherson from BVT Surface Fleet Ltd. [80]. His kind support for our project is highly appreciated. In the production process, two large plates with dimensions of $2400mm \times 800mm \times 6mm$ each were welded together by the submerged arc welding technique, which provided a relatively constant weld cap on both side of the plate. The weld was measured to be 19-21 mm wide, 1.5-2.5 mm high on one side of the plate and 15-17 mm wide, 2-3 mm high on the other side. The welded plate was cut into three pieces with equal weld lengths of 800 mm each for three different types of defects.

In our study, the artificial defects were all chosen to be close to the weld, in the region which is commonly named the heat affected zone (HAZ). This was done not only because they are easier than defects inside the weld to be introduced experimentally in the lab, but also because in reality defects such as cracks or corrosion are commonly located in the HAZ due to the heat from the welding process and subsequent cooling causing the change of the properties and microstructure in this area. Three types of defects were introduced in the experiment, which were located 2 mm away from the edge of the weld on the plates: through thickness slits with different lengths parallel to the weld; through thickness slits with different lengths perpendicular to the weld; 10 mm diameter flat-bottom hole with different depths. The slits were 2 mm wide cut by a milling machine; this was at least 10 times smaller than the wavelength of the incident wave for all of the frequencies used. Therefore they can approximately be considered as cracks [81].

5.2.2 Experimental setup

Fig. 5.1 shows a photograph of the experimental setup. A shear transducer was clamped on top of the weld cap. Two types of transducer were used in the experiment for different frequency ranges. One was a wideband piezoelectric in-plane transducer (Panametrics V301, 0.5 MHz center frequency) which worked properly in between 80 kHz to 150 kHz, and the other was a specially designed low frequency shear transducer by Guided Ultrasonics Limited [63], which worked well at lower frequencies between 40 kHz to 80 kHz. The transducer was coupled to the weld cap through a thin and small (3mm diameter) brass disc, so that the excitation can be assumed as a point-like source. The excitation signal consisted of a several cycles Hanning windowed toneburst which was generated by a Wavemaker (Macro Design Ltd., UK).

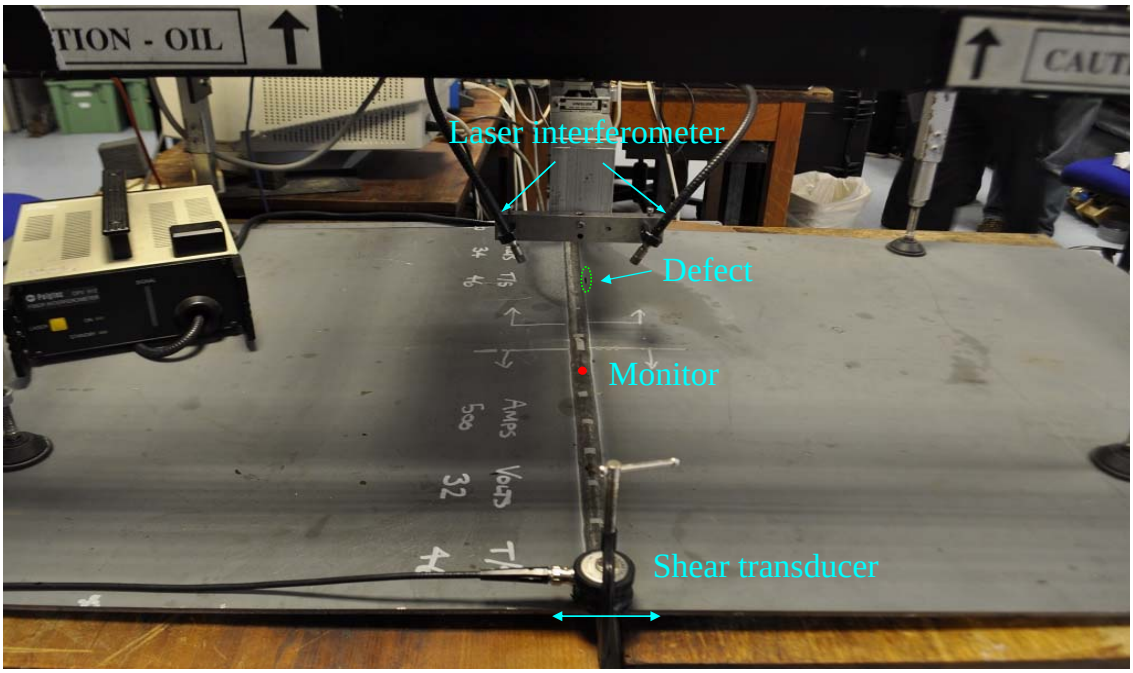

Figure 5.1: *Experimental setup .*

The defects were located at 600 mm away from the transducer, and the signal was monitored at 300 mm away. The monitoring point was more than $6\lambda_{shear}$ (wavelength of the shear guided modes at the center frequency of the toneburst signal) from both the generator and the defect so that it can be considered as far

field. The S0 wave was also generated in the side plates, however this signal could be time gated out by the choice of the defect location.

The monitoring of the incident signal and the detection of the reflected signal was achieved using a laser interferometer with dual differential fiber optic lines (Polytec OFV 2700). The two laser beams were on the same spot, but aligned at an angle of 60 degrees to the surface of the plate, so that the difference between the two signals gave the in-plane displacement. The mode shape of the shear weld guided mode is dominated by the horizontal displacement which is perpendicular to the edge of the weld; figure 5.1 shows the set up. A thin reflective tape was attached to the surface of the weld cap to enhance the optical backscatter. The signal was recorded after 500 averages to improve the signal to noise ratio.

The aligner holding the optical fibers was rotatable, thus it can also measure the compression mode which is dominated by the axial (parallel to the weld) displacement by turning it 90 degree to the current position. However it is not practical to measure the compression weld guided mode, because the wavelength of the this mode is twice that of the shear mode (the wavelength of the compression mode at 60 kHz is around 90 mm). Thus with the current length of the plate (800 mm), it would be impossible to find a location for the defect to avoid the near field effect.

5.2.3 Typical results

Fig. 5.2 shows a typical measured time trace of the signals of a 5-cycle toneburst at 100 kHz and a 3-cycle toneburst at 60 kHz respectively. The defect was a 30 mm slit parallel to the weld and 600 mm away from the location of the transducer. From the figure, the incident wave directly from the source and the reflection signal from the defect can be clearly seen. It can also been found that another toneburst signal appears after the defect reflection. This was the reflection of the S0 wave from the edge of the plate, as this wave was generated simultaneously in the side plates with the current setup. The last signal in the time trace corresponds to the reflection from the end of the plate.

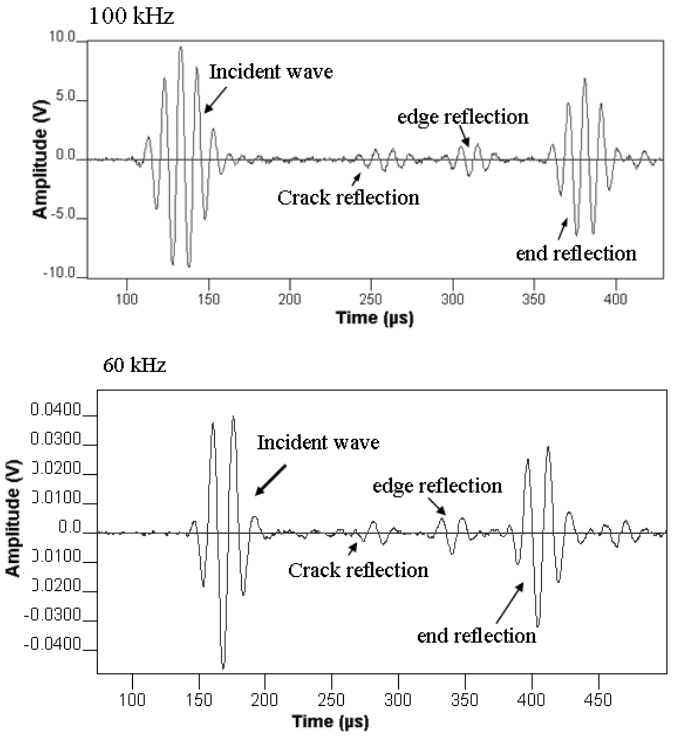

Figure 5.2: *Time trace of the shear weld guided mode monitored at 300 mm away from the source at 100 kHz (a) and 60 kHz (b) .*

The reflection behavior of the defect was studied in terms of a frequency domain ratio of the displacement of the reflected signal to that of the incident signal. Fig. 5.3 shows the experimental results from 40 kHz to 135 kHz. It can be seen that the amplitude of the reflection generally decreases with increasing of the frequency. Some oscillations can also be seen in the figure, and the reason will be discussed later in detail in Sec. 5.4.

5.2.4 Calibration experiment

The welded plate will later be considered to have a constant cross-sectional shape in our modelling for simplicity, however in reality the weld cap has slight variations in the geometry as shown in Sec. 5.2.1. In order to use the finite element simulations to compare the results with the experimental data, it is necessary to choose the most representative geometry of the weld. Therefore a calibration experiment has

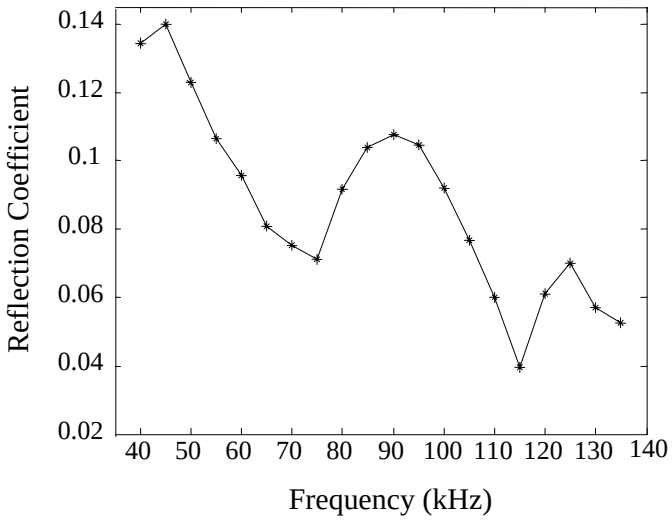

Figure 5.3: *Experimental results of the reflection ratio spectrum of the shear weld guided mode obtained from 30 mm slit parallel to the edge of the weld.*

been carried out to measure the properties of the weld guided mode propagating along the weld. As it was discussed in chapter 4, the shear mode is non-leaky and has little dispersion, therefore its mode shapes as well as group velocities on this geometry were measured for calibration.

The same experimental setup as described above was used. A 5 cycle toneburst signal at 100 kHz was generated on the edge of the weld by a shear transducer, and was monitored at two different lines (shown in Fig. 5.4(a)): one was along the center of the weld cap 150 mm to 400 mm away from the source; the other was across the weld at 300 mm away from the source. The work was similar to the experiment described in Chapter 4, but on this different geometry.

Fig. 5.4(b), (c) and (d) show the measured mode shapes (the signal amplitude across the weld), group velocity dispersion curve and the attenuation in terms of the signal amplitude along the weld respectively. It can be seen that the shear wave propagating along the weld is almost non-dispersive in this frequency range, and has very little attenuation compared to the beam spreading plane wave on a simple plate. The mode shapes in terms of displacements across the weld quantitatively presents the concentration of the energy to the center of the weld, and can be considered to

represent the geometry of the weld, thus they will be compared with the FE results to find the most similar geometries.

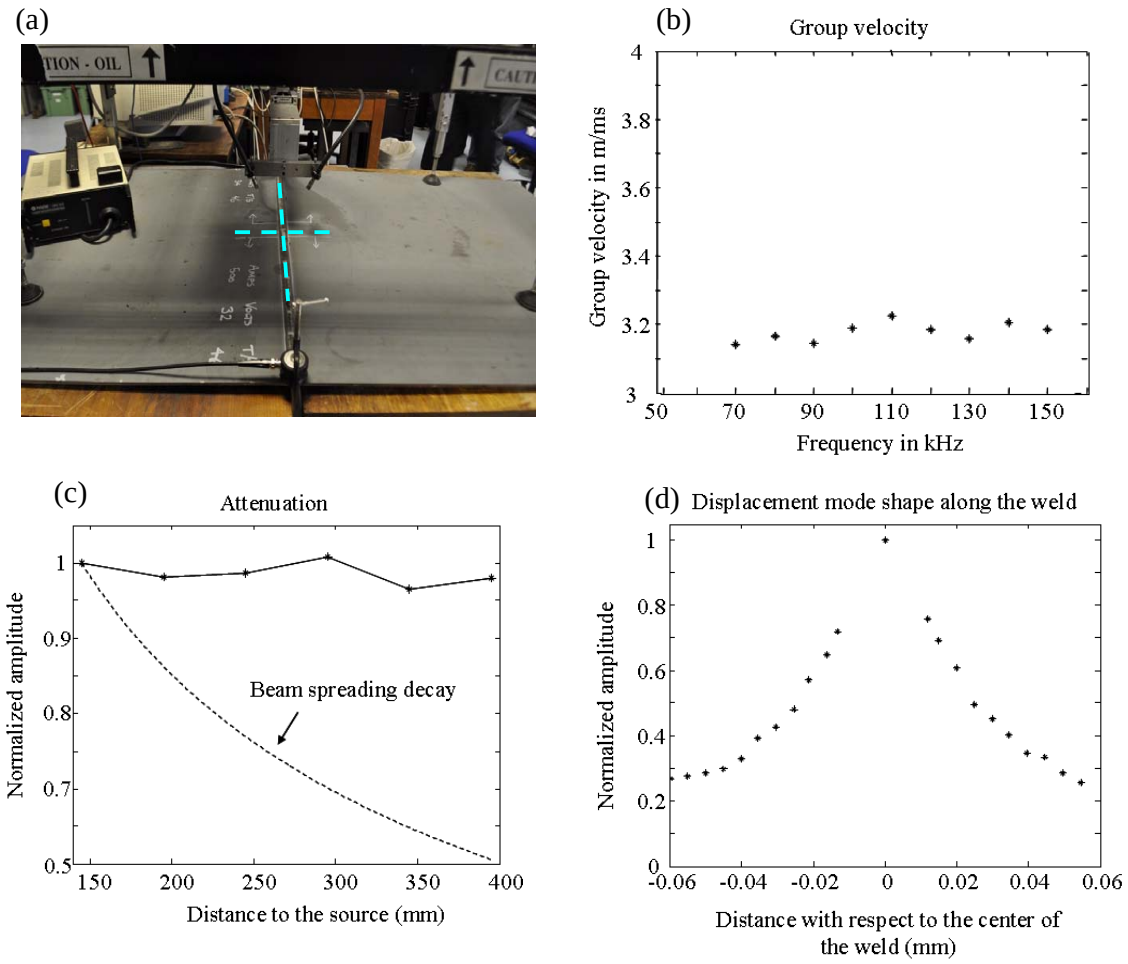

Figure 5.4: *Calibration experiment setup (a) and the results of group velocity dispersion curve (b), attenuation (c) and displacement mode shapes (d).*

5.3 Finite Element Modelling

5.3.1 SAFE modelling

SAFE models similar to those described in chapter 4 were carried out, in order to find the most representative cross-section. The geometry of the model is presented in figure 5.5. It is assumed that the material of the weld is steel (shown in Tab. 3.1),

which is considered to be the same as the plate. These models all have the same width of the weld cap (20 mm on one side of the plate and 16 mm on the other side), because it was measured to be fairly constant, and the small variation of the width has been tested in the models to have very little influence on the properties of the propagation mode. The height of weld, on the other hand, significantly influences the mode shapes of the weld guided mode, therefore it needs to be calibrated with the experimental results. In each of the models, the height of the weld cap varied from 1.5-2.5 mm on one side (h_1) and 2-3 mm on the other side (h_2).

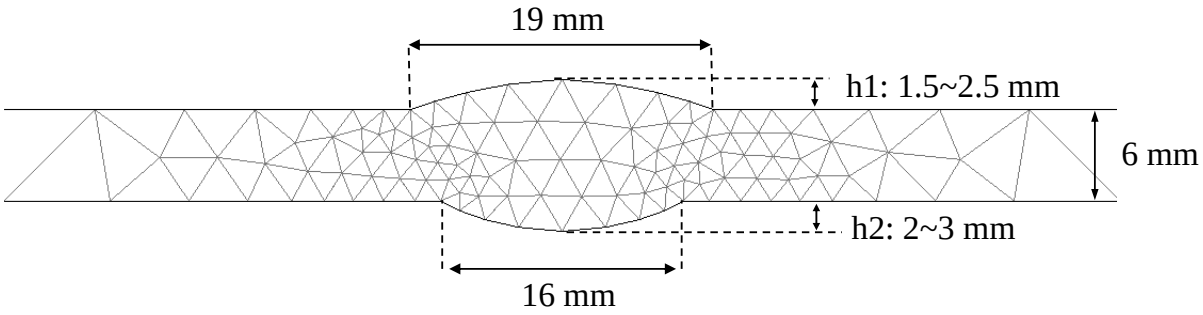

Figure 5.5: *Schematic of the calibration modelling using the SAFE method .*

In order to suppress the unwanted reflections, an absorbing region has been modeled at each side of the steel plate, in a similar manner as in the case in Chapter 4. In these models, the maximum possible wavelength of leaky waves is that of the SH0 wave at the lowest frequency of the investigated frequency range, i.e., $\approx 80mm$ at 40 kHz. Since the geometry of the weld is not symmetric with respect to the mid-plane of the plates and weld, it is possible for the A0 mode to radiate, but its wavelength is smaller than the wavelength of the SH0 wave. The length of the absorbing region was therefore set equal to 800 mm, which allowed good absorption of all the possible radiating SH0 and A0 modes at almost any possible angles between 0° and 84°, in the frequency range of interest, which was chosen from 40 to 150 kHz.

The models were meshed and solved in the same way as shown in Chapter 4. The modes which have higher energy flow in the weld than in the side plates corresponded to the weld guided mode, thus were picked up. At 100 kHz, the mode shape of the shear weld guided mode, which is the maximum displacement across a line on the

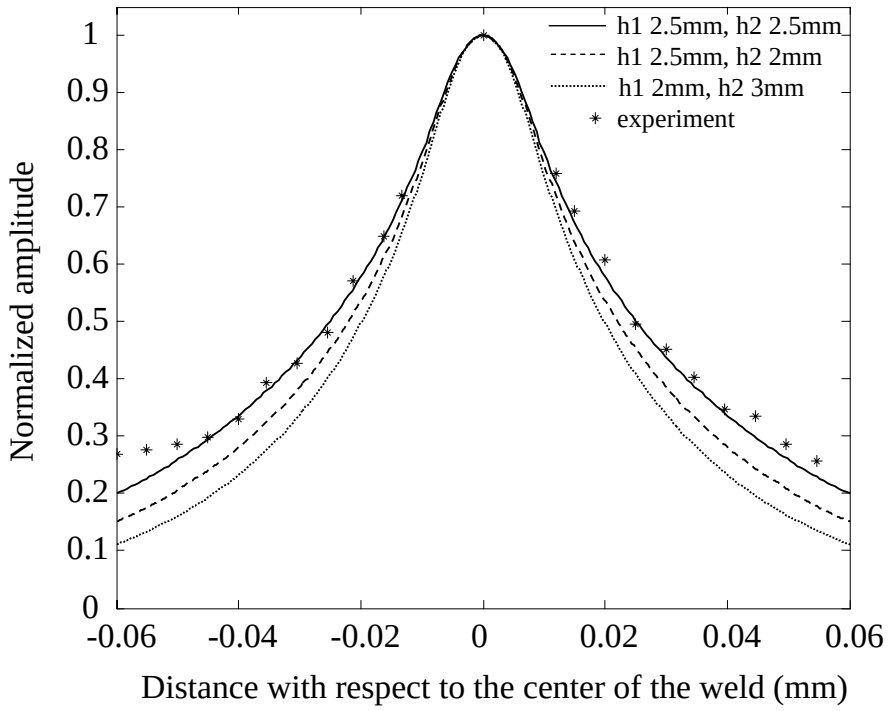

Figure 5.6: *Mode shapes in terms of displacement monitored in a line across the center of the weld for different geometries, predicted from the SAFE method (lines) and measured from the experiment (stars).*

surface of the weld cap and the plate, was obtained and plotted in figure 5.6. Three curves with different height of the weld cap have been shown in the figure, and it can be discovered that the curve with $h1 = 2.5mm, h2 = 2.5mm$ agrees the best with the experimental data, thus the above profiles can be considered to be representative.

Fig. 5.7(a) shows the variation of the group velocity and the attenuation dispersion curve at frequency from 50 kHz to 150 kHz of the shear mode on the representative weld geometry found above. The experimental results of the group velocity measured between 70 kHz to 150 kHz are also presented in the figure, showing good agreement. Fig. 5.7(b) shows that the shear mode on this geometry has some attenuation, due to the leakage of A0 mode on the side plates. However the amplitude of the attenuation is very small, almost negligible. This is confirmed by the calibration experiment which is shown in Fig. 5.4(c).

Since the defects investigated in this work were all located in the HAZ close to the

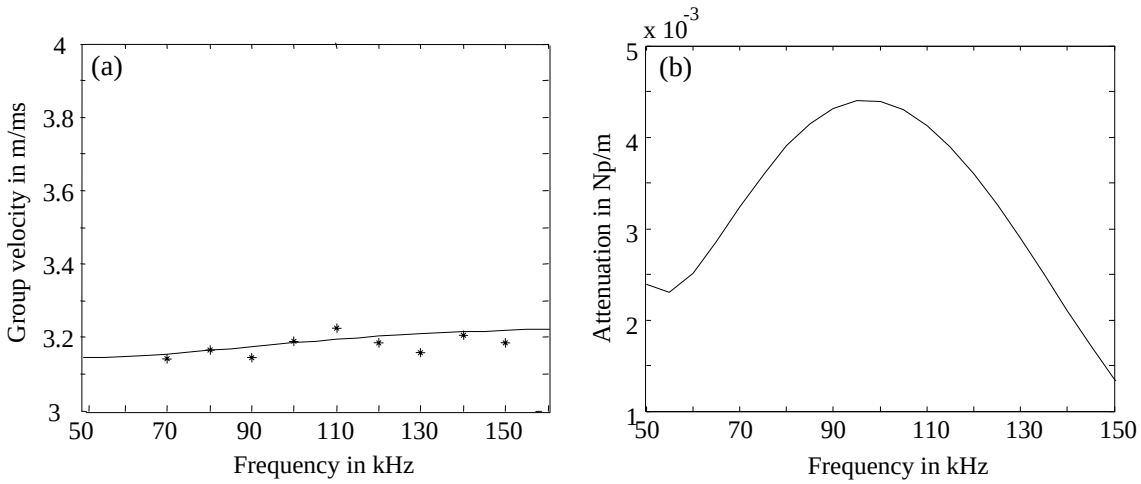

Figure 5.7: *(a) SAFE predictions (−) of the group velocity dispersion curve of shear weld guided mode on the geometry with $h1 = 2.5mm, h2 = 2.5mm$ and compares with experimental results (∗); (b) SAFE predictions (−) of the attenuation velocity dispersion curve.*

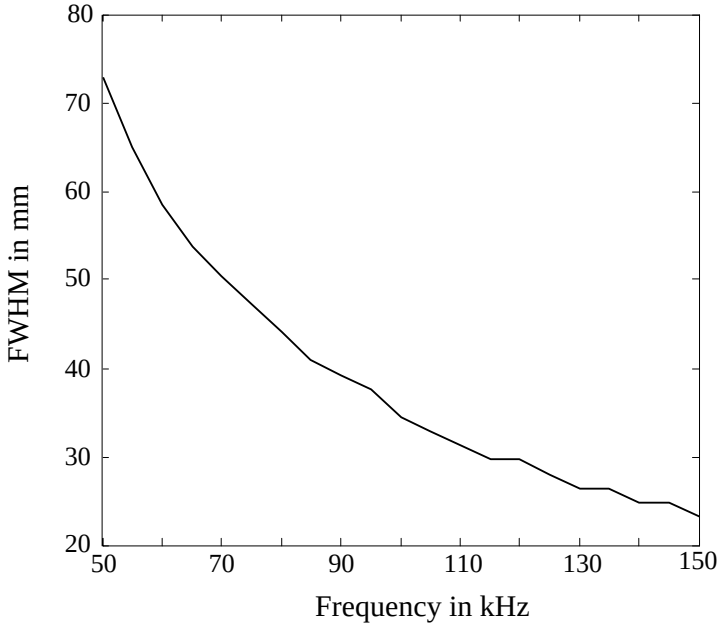

Figure 5.8: *The spectrum of the FWHM from 50 kHz to 150 kHz.*

weld, the energy distribution of weld guided modes across the weld is important to understand their interaction with defects. Fig. 5.8 shows the spectrum of the FWHM of the shear mode from 50 kHz to 150 kHz. It can be confirmed that while the frequency increases the FWHM decreases which means the energy concentrates

more and more in the centre of the weld. Therefore it should be expected that the sensitivity of the weld guided mode to defects located in the heat affected zone will decrease while the frequency increases. This will be shown by examples later in this chapter.

5.3.2 Time step finite element simulation

The two dimensional SAFE method assumes that the wave propagates on a geometry with constant cross-section, thus it is not capable of modelling discontinuities. Therefore in order to numerically study the interactions of the weld guided mode with different types of defects, it is necessary to apply a three-dimensional time step FE simulation. In our work, it was performed by the commercial software package ABAQUS/Explicit [71].

The schematic of the model is shown in Fig. 5.9, the profile of geometry is the same as the one in the SAFE method calibrated by the experiment. The mesh of the center of the cross-section is also shown in the figure. The model uses a standard three-dimensional spatial discretisation composed of linear cubic shaped 3D brick elements (C3D8R), where each node has three degrees of freedom with respect to displacement. The elements used in the modelling have two sizes. The ones in the region of the plate are 2mm in the x (width) and z (length) direction, and 1 mm in the y (thickness) direction; Others in the region of the weld are shown in Fig. 5.9; they have smaller dimensions to achieve a better representation of the shape of the geometry.

The wavelength of the shear weld guided waves at 100 kHz is around 32 mm, and the wavelength of the S0 wave propagating on the side plate is around 54 mm. Therefore the element size along the z direction guarantees that there are more than 15 elements per wavelength of the propagation, in order to minimise erroneous wave propagation distortions and inappropriate dependence of wave speed upon direction of propagation. The time step was chosen to be $1 \times 10^{-7} s$ in order to satisfy the guidelines given by [10].

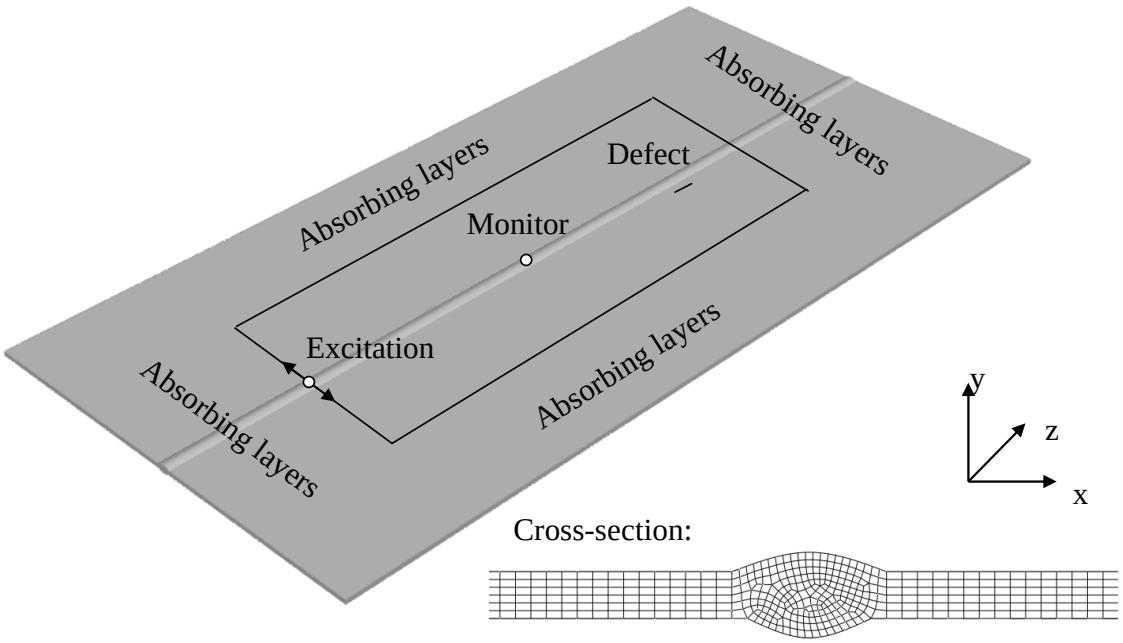

Figure 5.9: *Schematic of the three-dimensional time step simulation.*

This three-dimensional modelling with large size of the plate is very time consuming to solve. One way to reduce the model size is to define a relatively small region for the steel plate and apply an absorbing region around the plate (shown in figure 5.9). This is a modelling technique named ALID (Absorbing Layers with Increasing Damping) which has been recently introduced into the time step FE simulations [82]. Since the energy of the weld guided modes exists only in a small area around the weld, and our study focused on the interaction with defects in this area, it was possible to model only a short width of the plate with the weld in the center and apply the absorbing region outside the plate; thus we assumed the infinite width of the plate but significantly reduced the calculation time.

Three types of defects were introduced in the model 600 mm away from the source, including cracks normal or parallel to the weld and flat-bottomed holes. All of the defects were located in the Heat Affected Zone (HAZ) close to the weld, as in the experiment. The cracks introduced in the FE model were made simply by disconnecting adjacent elements representing zero-stress; this method has been widely applied in the previous FE studies of guided wave interactions with defects [76, 77]. The holes with different depths were achieved by defining partitions of the geometry

in the direction of the thickness, and mapping the elements. Since the elements of the 6 mm-plate had dimension of 1 mm in the y (thickness) direction, it was more convenient to define the holes with six different depths varying from 1 mm to 6 mm (through thickness).

A 3 cycle Hanning windowed toneburst signal was applied as an in-plane force on a single node on top of the weld cap, which is assumed to be a point source as in the experiment. This generates mainly the shear mode with the displacement direction perpendicular to the weld (x direction), or the compression mode with the displacement direction parallel to the weld (z direction).

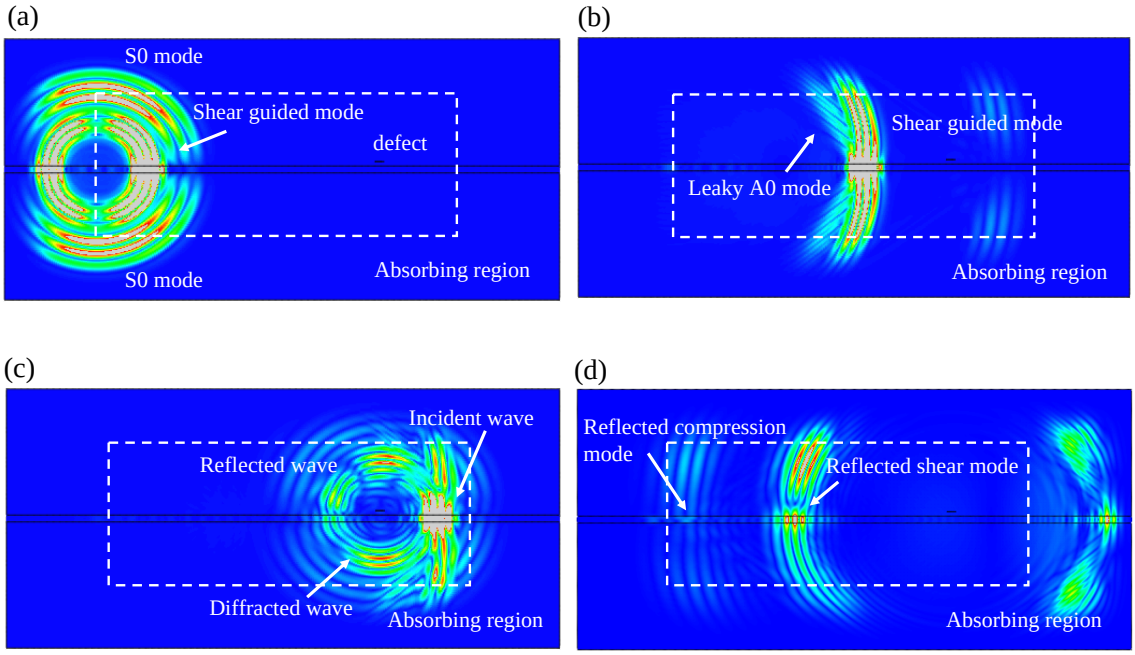

Figure 5.10: *Time snapshots of the shear weld guided mode propagation along the weld: (a) and (b) show the incident wave; (c) and (d) show the reflected wave.*

Fig. 5.10 presents typical time snapshots of the contour of the magnitude of resultant displacement from the FE simulations. Fig. 5.10(a) shows an instant soon after the excitation: the S0 wave on the plate is also generated and propagates mainly in the x direction while the shear guided mode travels towards the crack. Fig. 5.10(b) shows the snapshot after the wave propagates for a distance before it meets the defect. Small leakage of the A0 wave due to the non-symmetric geometry of the weld can be seen from the figure. The S0 wave which propagates towards the edge

of the plate has been completely damped by the absorbing region. Fig. 5.10(c) shows the mode interaction with the crack. The local interaction is very similar to the SH0 wave scattering from a axial crack [77]. The scattered field consists of the diffracted SH0, S0 wave on the plate and the reflected shear and compression weld guided mode along the weld. Fig. 5.10(d) shows the snapshot of the reflected signal which is also guided by the weld. The reflected energy is dominated by the shear weld guide mode, although a weak compression weld guided mode can also be seen in the figure.

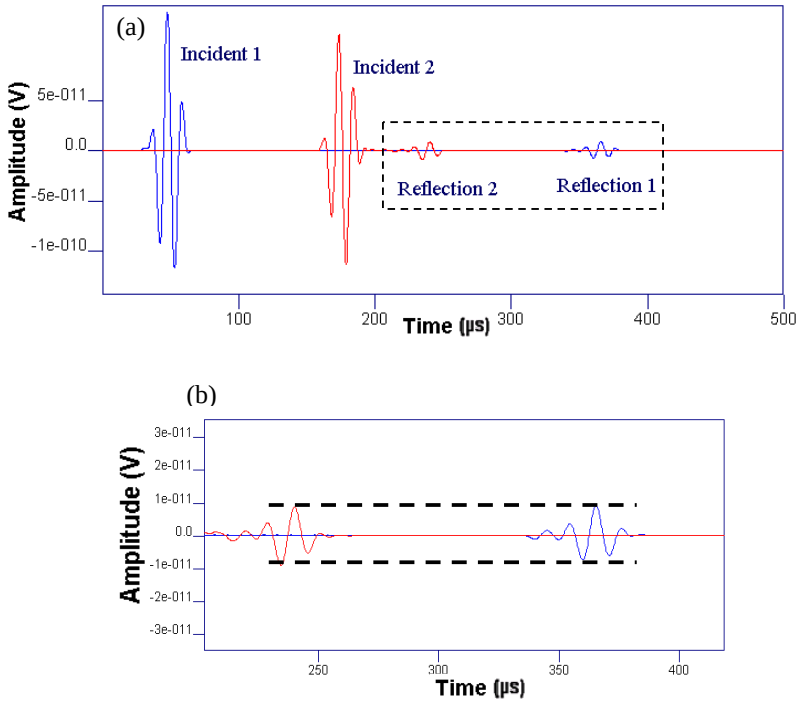

Figure 5.11: *(a) Time trace of a 3 cycle toneburst signal monitored at 100 mm and 400 mm away from the source. (b) Zoomed picture of the reflected waves.*

The signal was monitored at several locations on the surface of the weld cap. Fig. 5.11(a) shows the monitored 3 cycle toneburst signal at 100 kHz center frequency at 100 mm and 400 mm away from the source. Both the incident wave directly from the source and the reflected wave from the defect scattering are shown in the figure. Due the performance of the absorbing layers, the reflections from the edge of the plate as well as from the end of the weld were damped in the absorbing region, thus do not appear in the figure. It is noted that the amplitude of the incident signal at

100 mm away from the source is larger than that at 400 mm. This is because 100 mm is only about three wavelengths of the shear weld guided mode at 100 kHz, thus it is in the zone of near field and has larger signal amplitude. Fig. 5.11(b) presents a zoomed picture of the reflected signal, which can confirm that the reflected signal does not decay much during propagation due to the weak attenuation characteristics of the shear weld guided mode. Moreover the shape of the reflection signal almost remains the same in the propagation, which confirms that the propagation mode has little dispersion. Therefore it can be suggested that the shear weld guide mode is an ideal candidate mode for screening defects along the weld.

5.4 Interaction of Shear Weld Guided Mode with Defects Around the Weld

The scattering of the shear weld guided mode by cracks parallel to the weld has been qualitatively investigated in Sec. 5.3.2 of this chapter. In order to further exploit this mode for the selection of different types of defects, and suggest the best frequency range for inspection, it is necessary to quantitatively study its reflection behavior. This can be done in terms of a frequency domain ratio of the reflected signal by the incident signal. Experimental results on the same type of defects are also shown in this section and compared with results from FE simulations.

5.4.1 Cracks parallel to the weld

The first study considers cracks aligned parallel to the weld, which is a very common concern in industry.

In order to calculate the reflection coefficients over a range of frequencies, the model has been excited with tonebursts with different center frequencies. Cracks were assumed to be zero width, and located 2 mm away from the edge of the weld and 600 mm away from the source. Three different lengths of the cracks were investigated

both by FE simulations and experiments. The resultant reflection ratio as a function of frequency is shown in Fig. 5.12. The defect length (L) was expressed as a fraction of the input wavelength (λ). The amplitude of reflection coefficient was calculated in the frequency domain by dividing the maximum amplitude of the reflected signal by the maximum amplitude of the incident signal, which were both monitored 300 mm away from the source.

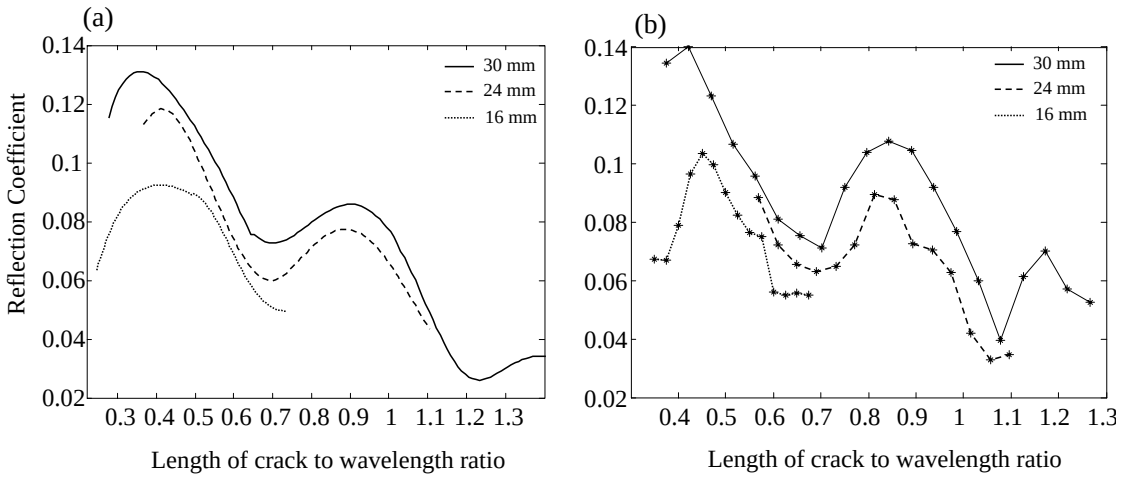

Figure 5.12: *Reflection coefficient spectrum with cracks of different lengths (solid line 30 mm, dashed line 24 mm and dotted line 16 mm) parallel to the edge of the weld: (a) FE results (b) experimental results .*

It can be seen from the figure that, from low frequency, the reflection coefficient rises as the wavelength decreases (frequency increases) and reaches a maximum value when the length of the crack is around 40% of the incident wavelength. While the frequency keeps increasing, generally the reflection coefficient decreases. This is because the energy of the weld guided mode becomes more and more concentrated in the weld while the frequency increases as was shown in Sec. 5.3.1. Therefore less energy strikes the defects which results in smaller reflection coefficient. There are also oscillations on the curve which shows a large peak point at 90% and two low points which are located at 70% and 120% respectively. The reason of the oscillation is the interference between the reflection from the near tip and the far tip of the crack. The reflection from the far tip of the crack is retarded with respect to the signal from the near tip, so their superposition in the resulting reflected wave packet

may be constructive or destructive, depending on the duration of the delay.

Similar oscillation phenomena were also discovered for rectangular notches [81] and axial (aligned in the propagation direction) cracks [77] in plates. The location of the oscillation peaks appear at similar places as figure 5.12(a), which suggests that the local interference at cracks is similar in both cases. However there are also differences. Firstly in uniform plates there is no overall decreasing while the frequency increase because the mode shape of the SH0 wave is independent of the frequency. It should also be noted that the reflection coefficient in plates was calculated after performing the compensation for the beam spreading effect. As the SH0 waves decay cylindrically away from the source and also assuming the crack to act as the emitter of cylindrical waves, then the reduction of the amplitudes in both cases is inversely proportional to the square root of the propagation distance from the source [73]. However the amplitude of the shear weld guided mode can be considered to be independent of the propagation distance because it has very little attenuation.

Experimental work has been carried out on the three crack lengths mentioned above, and compared with the FE modelling. It is shown in Fig. 5.12 that the experimental results showed the same trend as the FE results, however they had slightly larger amplitude, and the first oscillation peak shifted to a higher value of the crack length to wavelength ratio. The difference might be caused by different shapes of the defects in the FE modelling and in the experiment. In the experiment, the milled slit (notch) has a finite width of about 2 mm, however in the FE modelling the defect was defined as a zero-width crack. Therefore a slight difference of the amplitude as well as the phase of the reflected signal from the notch and the crack can be expected. More detailed discussion of the scattering from notches and cracks can be found in [81].

Fig. 5.12 shows that in general the reflection coefficient is higher at low frequency, since the energy is concentrating in the weld as the frequency increases. The maximum reflection appears when the wavelength is about 0.4 of the crack length. Therefore low frequency shear weld guided waves are attractive to inspect cracks parallel to the weld.

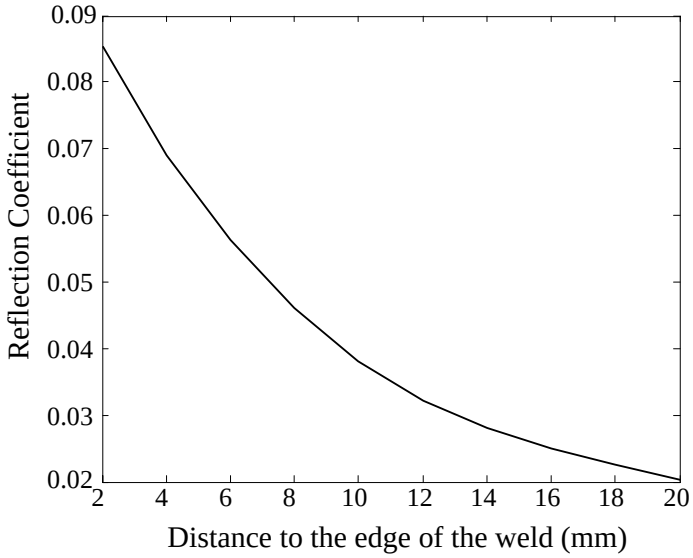

Figure 5.13: *Variation of reflection coefficient with location of the cracks parallel to the weld.*

Fig. 5.13 shows the influence on the reflection coefficient of the location of the crack with respect to the edge of the weld, in the range from 2 mm to 20 mm. The crack was 30 mm long and a 3 cycle toneburst signal at 100 kHz was used in the model. The reflection coefficient at 100 kHz with respect to the location of the crack is presented in the figure. The results show that the shear weld guided mode is more sensitive to target defects in the region near the weld than far away from the weld, which is expected from the mode shape studies explained in Sec. 5.3.1.

5.4.2 Cracks normal to the weld

The second study was carried out on cracks which were aligned normal to the direction of the wave propagation (parallel to the wavefront).

Rajagopal [76] has studied the specular reflection of the low frequency SH0 wave from the crack face and the diffraction at its tips. The incident wave has been considered to be a cylindrical crested wave, and in the far field it can be approximately considered as a plain wave in which the energy is homogeneously distributed along the wavefront.

The weld guided mode behaves differently since the energy is concentrated in and around the weld. In FE simulations, two lengths of cracks were modeled; one 20 mm long and the other 40 mm long. Both of them are located 600 mm away from the source, and defined as zero width cracks. In both cases, one end of the crack is 2 mm away from the edge of the weld. The measurement was taken at 300 mm away from the source.

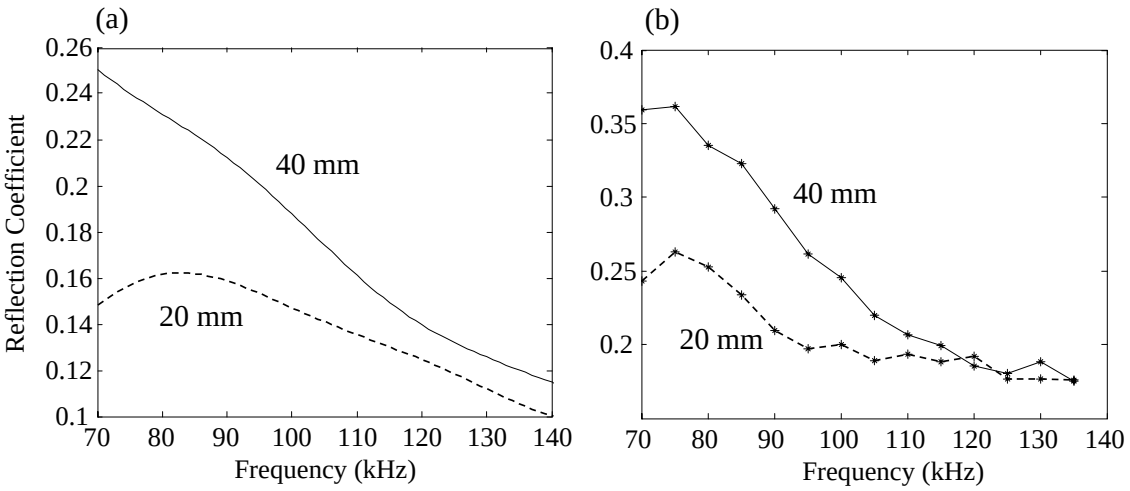

Figure 5.14: *Reflection coefficient spectrum for cracks normal to the edge of the weld: (a) FE predictions (b) experimental results.*

Fig. 5.14 shows the reflection spectrum for different crack lengths, in which (a) shows the FE predictions and (b) shows the experimental measurements. From Fig. 5.14(a), it can be seen that the energy reflected from the crack decreases as the frequency increases. This is due to the decrease in lateral extent of the shear weld guided mode as the frequency increases. At low frequencies, the shear weld guided mode has a larger lateral extent and therefore a large portion of the mode strikes the crack which results in larger reflection coefficients. At high frequencies, a relatively small extent of the shear guided mode strikes the crack and therefore results in smaller reflection coefficients at these frequencies.

At low frequencies, there is a substantial difference between the two reflection coefficients (reflection coefficient from 20 mm crack and reflection coefficient from 40 mm crack), but this difference decreases as the frequency increases. The reason can

again be explained by the mode shape of the shear weld guided modes shown in Sec. 5.3.1. While the frequency increases, the energy of the mode becomes more and more concentrated near to the weld. Therefore only part of the crack which is close to the weld scatters the weld guided mode. This results in the small difference of the reflection coefficient between different lengths of cracks at higher frequencies.

Fig. 5.14(b) shows the experimental results for the corresponding defects. The shape of the curve is similar to the FE predictions, which shows higher reflection at low frequency than high frequency. However the amplitude of the curves were significantly larger than the FE predictions. One likely reason for this is that the shape of the geometry used in the FE model is derived from the calibration experiment, which measures the mode shape of the shear weld guided mode at one location of the weld. However, the shape of the weld is not strictly the same along the total length of the weld. From Fig. 5.6 it can be seen that a small change in the height of the weld will result in a relatively large change of the mode shapes. It is possible that at certain locations the lateral extent of the weld guided modes is larger than predicted by the FE model. This would cause the reflection from the defects at the HAZ measured experimentally to be larger than in the FE prediction.

5.4.3 Flat-bottom holes

Corrosion in the heat affected zone around the weld is another defect of concern in industry. The scattering of guided waves from corrosion patch defects on a plate has been studied by many researchers. Diligent and Lowe [79] presented finite element and experimental results for the reflection of S0 waves from flat bottomed circular holes. Fromme and Sayir [83] used Kirchhoff and Mindlin theory to study the scattering of flexural A0 waves from a through thickness circular hole. More recently, Ma and Cawley [84] theoretically and experimentally studied the scattering of SH0 waves from part-thickness elliptical defects including circular holes.

In our work, for simplicity a circular hole with a diameter of 10 mm with different depths was modeled as the corrosion. The hole was located 600 mm away from

the source, and the edge of the hole was 2 mm away from the edge of the plate. Fig. 5.15(a) shows the magnitude of the reflection coefficient spectrum obtained from holes with six different depths with their diameter normalized to the input wavelength.

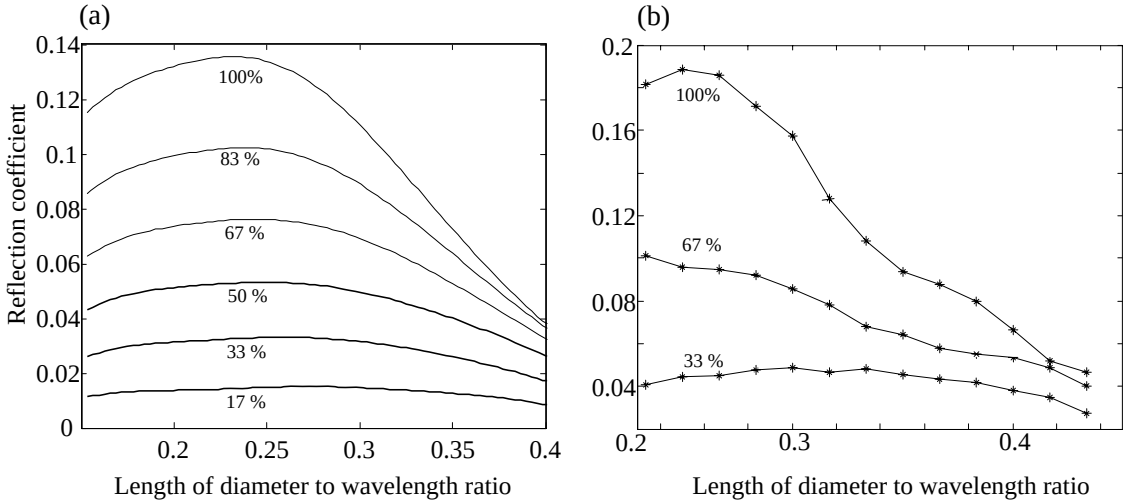

Figure 5.15: *Reflection coefficient spectrum for flat-bottom holes with different depths: (a) FE predictions (b) experimental results.*

Given that the plate was 6 mm thick and the element length was 1 mm in the depth, six different depths from 16.7% to 100% of the total depth were studied. At each depth, the reflection coefficient was extracted in the same way as before and these are plotted respectively in Fig. 5.15. From the figure, it can be seen that at low frequency the reflection coefficients increase with the increasing of frequency, They all reach a maximum value while the diameter of the hole is 23% of the wavelength. After that, the reflection coefficients decrease as the frequency increases. Similarly as discussed above, the reason for this shape of reflection function is that the energy becomes more and more concentrated in the centre of the weld while the frequency increases, therefore a smaller amount of the energy will strike the defects at the HAZ.

The peak of the reflection coefficient is caused by the interference between the direct reflection from the front of the hole and secondary reflections composed of circumferential creeping waves, as has been observed previously [79, 85]. Their superposition

in the reflected wave packet results in the oscillation of the curve. The constructive interference occurs when the second reflection is half a cycle behind the leading edge reflection, which is when the defect length is around a quarter of a wavelength, as can be confirmed from the figure.

It can also be noted that at low frequency there is good resolution of the reflection coefficient with respect to the depth of the hole. For example, the maximum value of the reflection coefficient is approximately linear with the depth of the hole. However the difference decreases at higher frequencies, since the energy is more concentrated in the weld and only part of the hole which is close to the weld scatters the weld guided mode.

Experimental results are shown in Fig. 5.15(b) for holes with depth of 2 mm, 4 mm and 6 mm (through thickness) respectively. It can be seen from the figure that these results have similar shapes as the finite element results, however the amplitude is again higher. The reason is believed to be the same as discussed in Sec. 5.4.2.

5.5 Interaction of Compression Weld Guided Mode with Defects Around the Weld

From the discussion above, it is shown that the fundamental shear mode can be a good candidate as a screening tool to inspect for defects. On the other hand, the compression weld guided mode, whose properties were discussed in Chapter 4, also has some interest in detecting defects at low frequency. Juluri [70] has discussed the interaction of the compression (S0-like) weld guided mode with cracks or notches normal to the weld in the HAZ on an idealized welded plate. The interaction of the compression (S0-like) weld guided mode with the flat-bottom hole was also investigated experimentally.

In this section, FE simulations were performed using the compression mode and the same geometry of the cross section. The typical wavelength of the compression

mode at low frequency was relatively large. For example at 100 kHz the wavelength is around 54 mm, which is twice as much as the wavelength of the shear mode at the same frequency. As it is known, in order to get an accurate result, the monitor point has to be located outside the zone of the near field, which is approximately 5 wavelengths away from the source. Consequently the length of the welded plate has to be longer than it is in the model of the shear mode to avoid the near field effect. Moreover the size of the absorbing region also needs to be larger than it is in the other model to be effective.

However the current modelling capacity restricts the size of the geometry in the FE model. Hence the near field effects are unavoidable and the modelling accuracy has to be compromised. Therefore the scattering study carried out on the compression welded guided mode interacting with different defects remains qualitative. For the same reason, no experimental work has been carried out on this mode due to the small size of the plate.

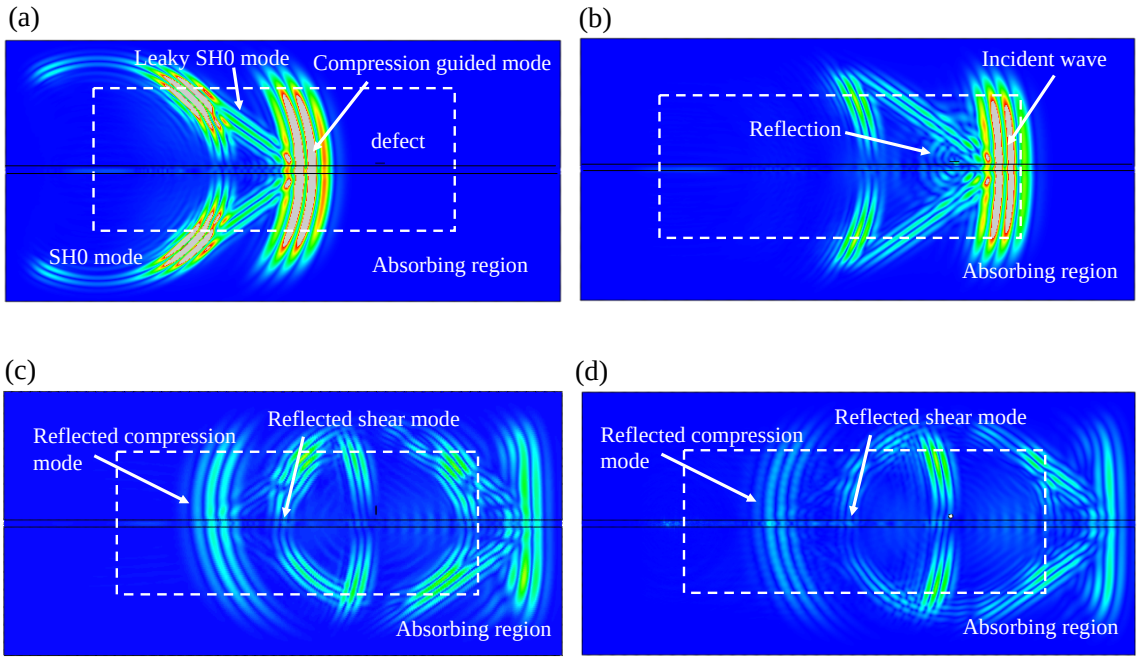

Figure 5.16: *Time snapshots of the compression weld guided mode propagation along the weld (a), and scattering from a crack parallel to the edge of the weld (b), a crack normal to the edge of the weld (c) and a flat-bottom hole in the heat affected zone (d).*

Fig. 5.16(a) shows a snapshot of the propagation of the compression weld guided mode before it reaches the defects. It is shown that energy of the compression weld guided mode is concentrating around the weld and a wave is spreading behind the guided wave, which corresponds to the leaky SH0 wave in the plate.

Fig. 5.16(b) shows a snapshot of the compression weld guided mode at 100 kHz interacting with a 30 mm crack parallel to the weld in the HAZ. Since the mode shape of the compression weld guided mode is dominated by the axial displacement (parallel to the weld) at low frequency, it is expected not to be sensitive to the crack shown in the figure. However it can be seen from the figure that there still exists a small reflection from the defect. This reflection is believed to be caused by the interaction between the crack and the leaky SH0 wave from the weld guided mode. Rajagopal and Lowe [86] have discussed the angular influence on scattering of the SH0 wave by cracks. However it is not necessary to perform the study here as the overall amplitude of the leaky SH0 wave is small, thus the reflection from the defect is small correspondingly. Therefore, compared to the shear guided mode, this compression mode is less interesting to detect cracks aligned parallel to the weld.

Fig. 5.16(c) and (d) show respectively the snapshots of the scattering of the compression weld guided mode by cracks perpendicular to the weld and through-thickness flat-bottom holes. The local interaction was found to be similar to the S0 wave interacting with certain types of defects [66, 85]. Relatively strong reflections of the the compression mode can be seen from the figure and some of the reflected energy was converted to the shear weld guided mode. Moreover the reflected compression mode also leaked the SH0 mode into the side plates, thus the remaining energy decreases with the propagation distance. Therefore for inspections over long distances it is less interesting than the low attenuative shear mode.

5.6 Summary

In this chapter, a study of the pulse echo reflection of the weld guided wave from defects in the heat affected zone on a welded plate is presented. Three different

types of defects: cracks parallel or normal to the edge of the weld, and flat-bottom holes were studied both by time-step FE simulations and by experiments.

It can be seen that the shear weld guided mode, which is little-attenuative and little dispersive, is more interesting than the compression weld guided mode to be applied as a screening technique to inspect welds over long distances. The nature of the scattering of the shear weld guided mode by defects located around the weld is similar to the SH0 wave interacting with defects on a plate. However the amplitude does not decay with the distance of wave propagation. Moreover, the mode shape of the weld guided mode is frequency dependent, i.e. the energy distribution of the cross-section gets more and more concentrated in the center of the weld with the increasing of the frequency.

The study on the reflection ratio with respect to frequency suggests that the weld guided mode is more interesting at low frequency than at high frequency to inspect defects located in the heat affected zone of a welded plate. The experimental measurements show good agreement with the trend of the reflection coefficient spectrum predicted by FE simulations, however there is a significant difference in the the amplitudes of curves. This is believed to be due to the variation of the cross-section of the geometry, thus the mode shape of the weld guided mode is not consistent along the weld. Therefore it might be difficult to apply the weld guided mode to size the defect at this stage, although it has been shown to be attractive to screen for defects.

Chapter 6

Feature Guided Waves on Other Geometries

Chapters 4 and 5 have demonstrated that there exists weld guided modes in a welded plate, which can be exploited as screening tools to inspect long lengths of welds. However, it has been proved from previous chapters that the SAFE method is capable to model geometries with any cross-sectional shapes. It is also clear from the revealed principles of the weld guiding effect that feature-guiding should be expected in any geometric feature whose effect is to lower the phase velocity of the waves. Therefore a similar opportunity for long distance feature-guided propagation may be possible in many other kinds of structural features.

In this chapter, the SAFE method will be applied to the example geometries of lap joints, stiffened plates and tube plates. The existence of the feature guided modes (trapped modes) will be discussed, as well as their properties and potential applications.

6.1 Lap Joints

6.1.1 Introduction

The first application is related to the inspection of the adhesively bonded lap joints, which are common in industry. Fig. 6.1 (a) shows a schematic of the geometry and possible defects such as voids in the adhesive layer or the disbond of the adhesive from one of the adherends. Conventional techniques to inspect for defects and the bonding quality rely on the point-by-point ultrasonic scanning, which is usually time consuming. Lowe *et al* [87] have discussed a technique to rapidly check the quality of the bonding, based on calculating the transmission of Lamb waves across the lap joints. However, according to the discussing of the reason for the trapping effect in Chapter 4, and considering the geometry of the lap joint, it can be expected that there may exist similar feature guided modes in this geometry which can concentrate the energy in the joint, and propagate along the joint. If so, it would offer an attractive alternative to inspect a long length of the joint by the pulse-echo or pitch-catch feature guided wave method, thus significantly increasing the speed of inspection of large regions.

6.1.2 Geometry and model description

The geometry of the model is shown in Fig. 6.1 (b). The two plates are both made of aluminum with thickness of 1.6 mm each, with their density and elastic properties given in Tab. 6.1. There is a 1-mm-thick and 10-mm-wide layer of adhesive between the two plates, and its mechanical properties are also shown in Tab. 6.1. The adhesive has viscoelasticity which is presented in terms of attenuation per wavelength of the longitudinal (α_L) and transverse (α_T) waves. In order to suppress unwanted reflections from the border of the plate, an absorbing region is modeled at each side of the plate, in a similar manner as described in the weld case discussed in Chapters 4 and 5. The absorbing region has the same mass density and elastic properties as the plate, but its viscoelasticity, i.e. the imaginary part of its

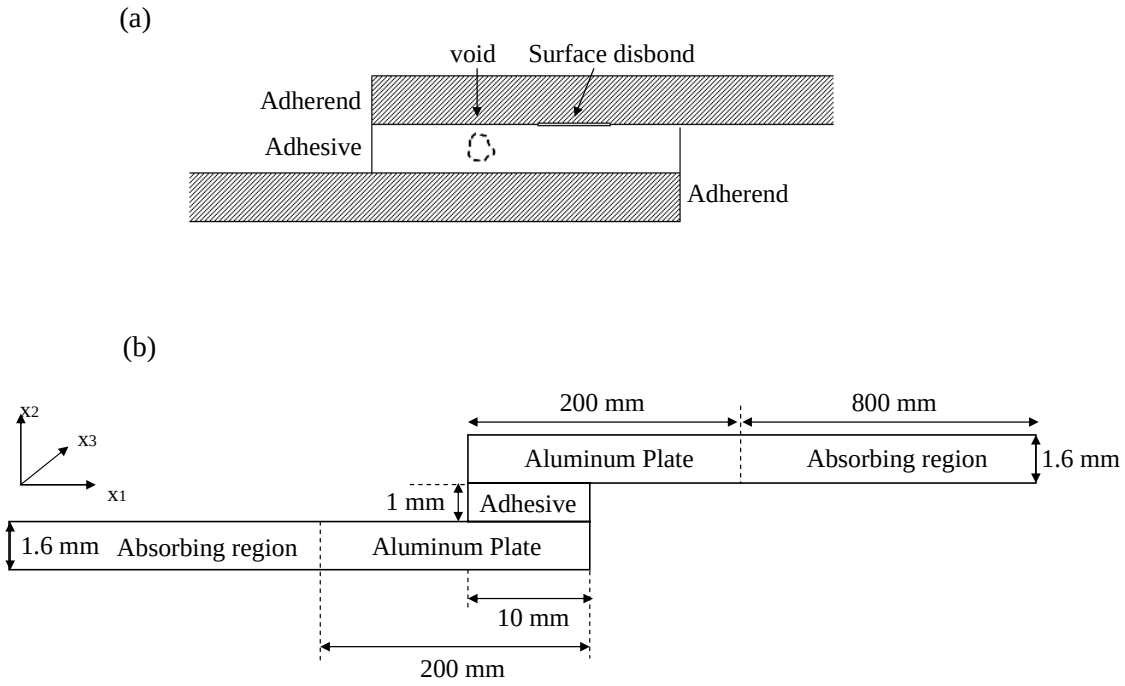

Figure 6.1: *Schematic of a lap joint showing the possible defects (a) and the SAFE modelling of this geometry (b) .*

Table 6.1: Mechanical properties for materials used in the SAFE modelling.

	Density (kg/m^3)	Bulk longitudinal velocity (m/s)	Bulk shear velocity (m/s)	α_L and α_T (dB/λ)
Aluminium	2700	6320	3130	...
Steel	7932	5959	3260	...
adhesive	1100	2523	1044	1.637

elastic moduli, gradually increases with distance away from the joint. The width of the absorbing regions was chosen in the same way as discussed in Chapter 4, which can provide accurate solutions if it is more than twice the projection along the x_1 axis of the maximum wavelength of the guided waves that could be radiated along the plates.

In our model, the width of the absorbing region is set to be 800 mm, so that it guarantees valid solutions from most of the range of radiation angle. For example, the wavelength of the SH0 wave in the adjacent plate at 30 kHz is approximately

110 mm, thus the 800 mm length of the absorbing region is greater than twice the projection along x_1 of the maximum wavelength, up to radiation angle of 74°.

The displacements and stresses are considered to be continuous between the plate and the adhesive. Stress-free conditions are imposed at the outer border of the geometry. The geometry is meshed by 1895 triangular elements of first order and the number of degree of freedom is 33522. The system is solved for all the possible wavenumbers that can propagate harmonically at different frequencies. At each frequency, those modes which have energy concentrating in the joints and radiating into the side plates correspond to the feature guided modes.

6.1.3 Results and discussion

In order to pick up the solutions of interest among all the solutions obtained, the axial component of the energy flow is calculated along a cross-section line in the middle of the upper plate.

Fig. 6.2 shows the energy flow distribution for several solutions obtained at 100 kHz. It can be seen that two modes (in solid lines) have their maximum energy in the area of the joint, with decay towards the outsides of the absorbing region. These two modes are the feature guided modes at this geometry, whose energy is concentrated in the joint, and radiating into the lateral plates. For comparison, Fig. 6.2 also shows the modes which are resonating in the plates and the absorbing region, thus are unwanted.

Fig. 6.3 shows the properties of feature guided mode 1. Fig. 6.3(a) presents a snapshot of energy flow at 100 kHz which confirms that the energy of this mode is concentrated in the center of the joint. Fig. 6.3(b) presents the mode shape of the displacement of mode 1 along a through thickness line shown in Fig. 6.3(a), which suggests that this mode is dominated by the axial in-plane displacement (u_3), similar to the S0 mode in a free plate. The eigenvalue for this mode at 100 kHz is 119.13-0.2158i /m, from which the corresponding phase velocity is 5274 m/s. Thus, it is possible to radiate the SH0 mode and A0 mode in the side plate, at radiation

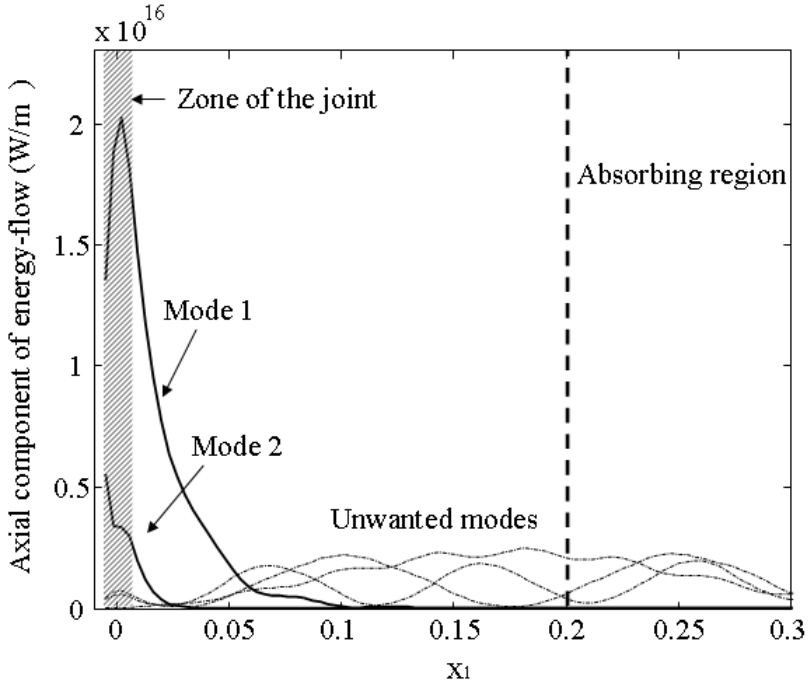

Figure 6.2: *Cross-section distribution of axial energy flow for several eigen solutions obtained for the lap joints at 100 kHz. The solid lines show two feature guided modes, while the dashed lines show unwanted plate resonance solutions. The grey zone indicates the joint area.*

angles of about 36.4° and 13°, respectively. Fig. 6.3(c) shows the phase velocity dispersion curve of mode 1 from 30 kHz to 100 kHz, which suggests a similarity to the S0 mode in the plate, and this mode does not have much dispersion at low frequency. Fig. 6.3(d) presents the attenuation dispersion curve of this mode, which shows an increasing attenuation while the frequency increases.

The properties of mode 2 are shown in Fig. 6.4. Fig. 6.4(a) shows the snapshot of energy flow at 100 kHz of this mode and (b) shows the mode shape of the through-thickness displacement, which indicates a similarity to the SH0 mode in a plate as they are both dominated by the horizontal in-plane displacement u_1. At 100 kHz, the phase velocity of this mode is 2784.6 m/s and the attenuation is 1.641 dB/m, both of which are obtained from the eigenvalue 225.639-0.189i /m. The A0 mode in the aluminium plate is the only possible wave to radiate, at an angle of about 23.7°. Fig. 6.4(c) and (d) shows the phase velocity and the attenuation dispersion curves

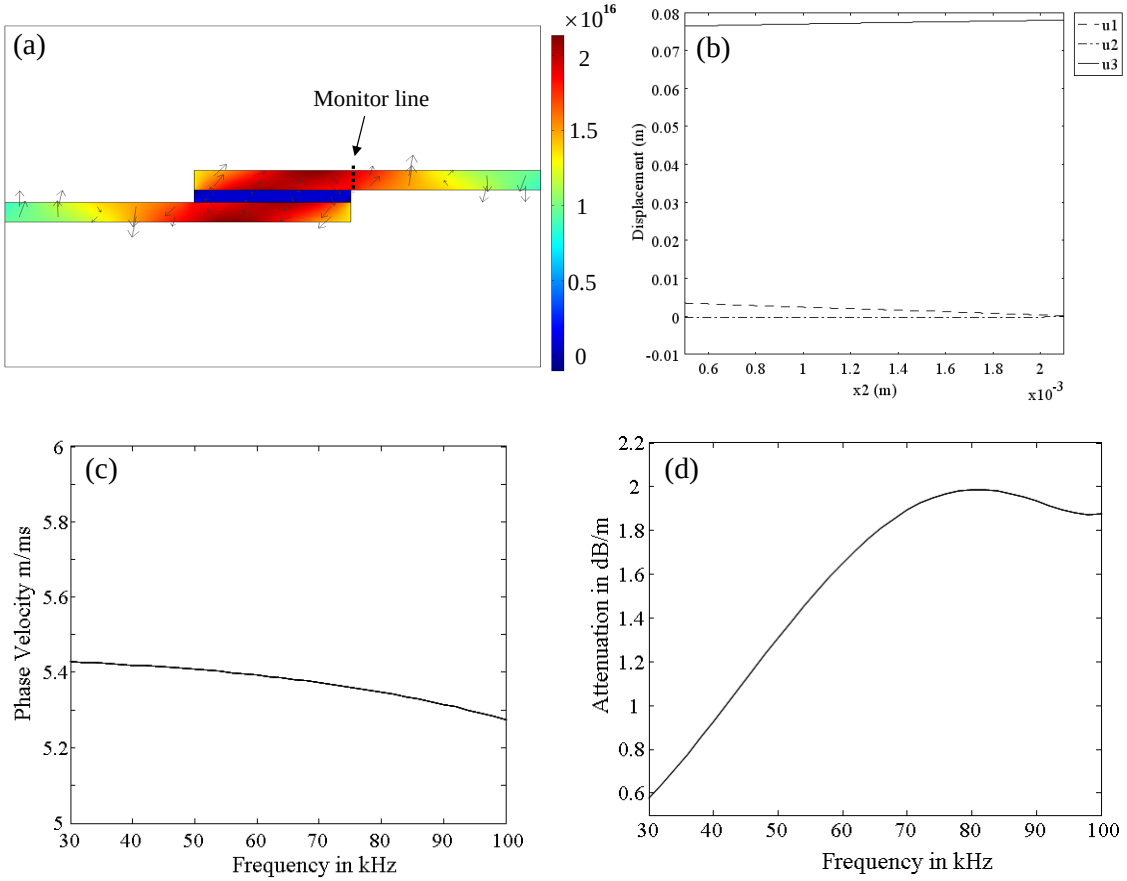

Figure 6.3: *(a) Energy flow snapshot for the feature guided mode 1 at 100 kHz, with arrows indicating displacements of the cross-section, (b) the mode shape of displacement through the thickness of the plate, (c) the dispersion curve of phase velocity from 30 kHz to 100 kHz, (d) the dispersion curve of attenuation from 30 kHz to 100 kHz .*

from 30 kHz to 100 kHz, respectively. It can be noticed that mode 2 has very little dispersion in this frequency range, similar to the shear weld guided mode discussed before. This mode is radiating more energy to the side plate as the frequency increases, and the attenuation is at about the same level as mode 1.

To explain the reason for feature guiding in this geometry, propagation modes on the geometry of the joint part were investigated and compared with the plate modes. Phase velocity dispersion curves of the joint part as well as a 1.6 mm thick aluminum plate are presented in Fig. 6.5(a). It can be seen from the figure that there exists four modes in the joint, which are the Longitudinal mode, Torsional mode, Flexural mode 1 and 2, and their modes shapes (displacements of the cross section) and the energy

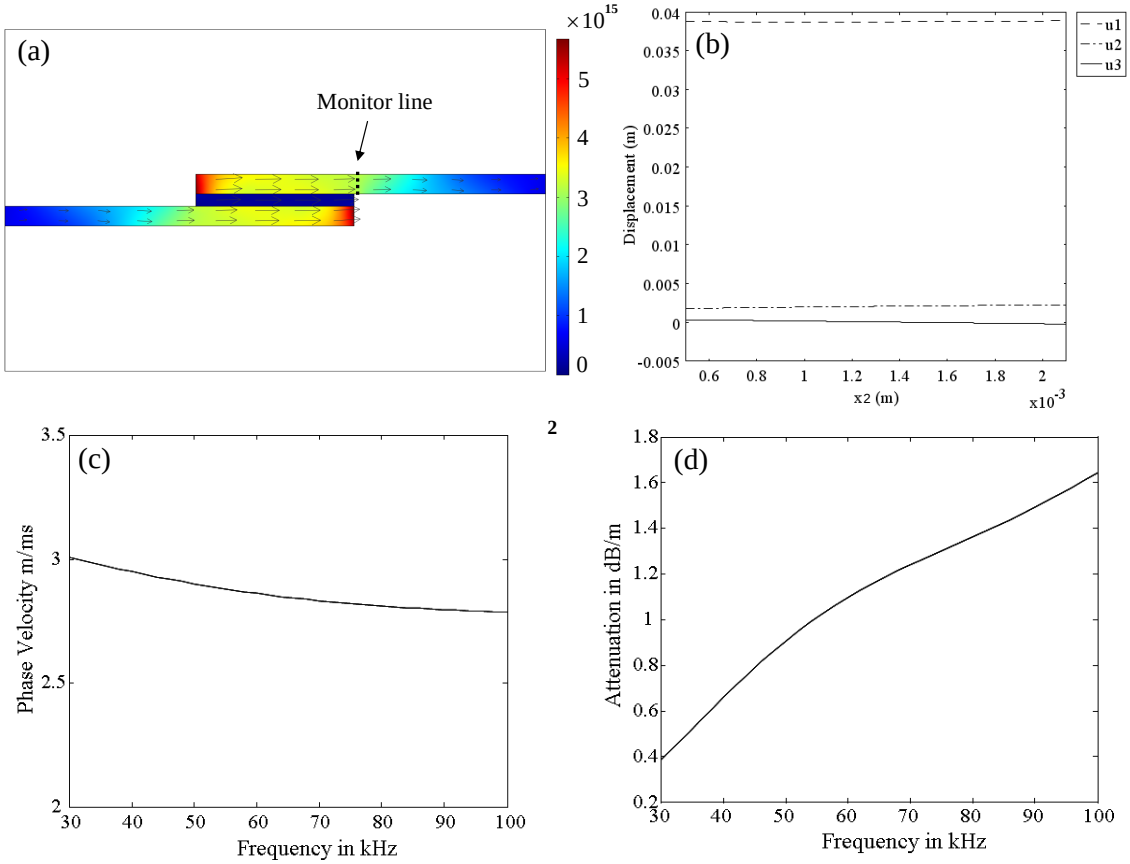

Figure 6.4: *(a) Energy flow snapshot for feature guided mode 2 at 100 kHz, with arrows indicating displacements of the cross-section, (b) the mode shape of displacement through the thickness of the plate, (c) the dispersion curve of phase velocity from 30 kHz to 150 kHz, (d) the dispersion curve of attenuation from 30 kHz to 150 kHz .*

flow snapshot are presented in Fig. 6.5(b). Comparing with the three fundamental plate modes existing at this frequency, the Longitudinal mode and the Flexural mode 1 of the joint has similar mode shapes to the S0 and SH0 mode in the plate respectively. Moreover their phase velocities are slower than their corresponding modes in the plate, therefore the energy of these two modes is concentrated within the joint area when the whole lap joint geometry is considered. This is similar to the case of the welded plate discussed in Chapter 4. On the other hand, the phase velocity of Flexural mode 2 is higher than the A0 mode in the plate, although their mode shapes are similar; the torsional mode does not have any similar modes in the plate, thus neither of them is able to form a trapped mode (feature guided mode).

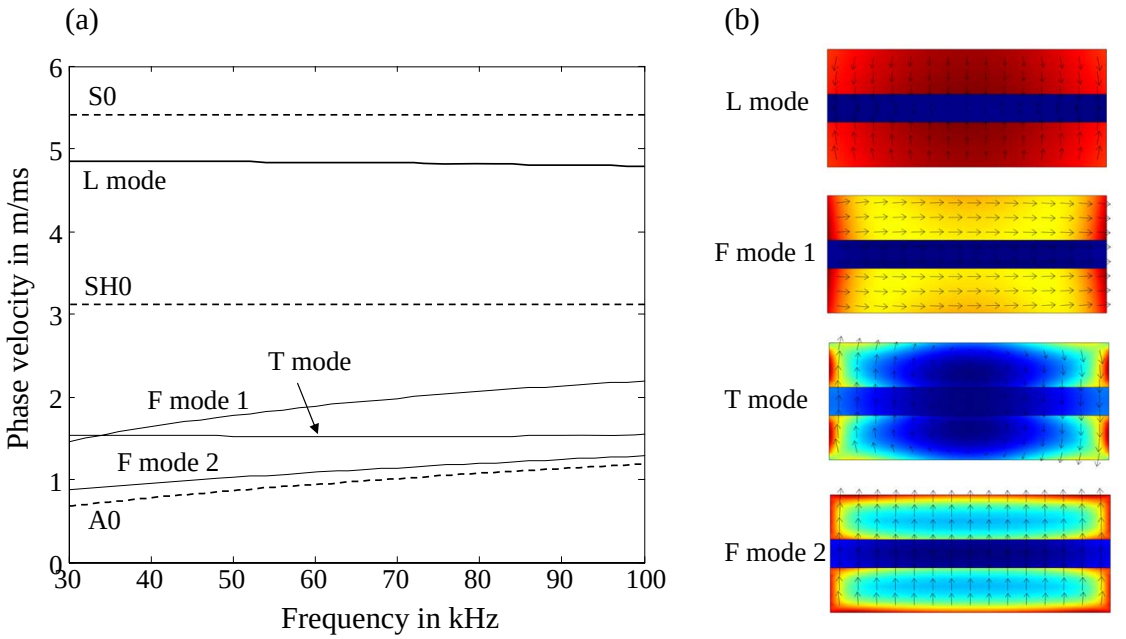

Figure 6.5: *(a) Phase velocity dispersion curves of the propagation modes in the joint geometry and in the 1.6-mm-thick aluminium plate, (b) mode shapes of four propagation modes of the joint geometry at 100 kHz. Arrows indicate displacements in the cross section*

.

To summarize, two feature guided modes have been found on the lap joint geometry, which may have the potential to inspect for defects in or around the joint according to their properties. Moreover, it is also possible that the bonding conditions such as the bonding strength, length and thickness may be evaluated by examining the properties of the guided modes. However, in order to apply these two feature guided modes in real applications, it would be necessary to perform parametric studies on mode properties as well as on defect scattering. Since the purpose of this chapter is just to illustrate the existence of feature guided wave on some geometries other than welded plates, the studies on the application of the guided modes have not been carried out, and would be left for future work upon request from industry.

6.2 Plate with Stiffener

6.2.1 Introduction and model description

The second geometry concerned in this chapter is a large aluminum plate with a T-shaped aluminum stiffener bonded onto one face. Feature guided modes, which propagate along the stiffened region and radiate into the side plates, are possible to exist due to the geometry change in the stiffened area, similar to the welded plate and the lap joint. Castaings and Lowe [50] have investigated one sample of the stiffened plate and discussed the existence and application of one feature guided mode. However due to the complex shape of the stiffener, the discussion was brief. In fact, there exists more than one feature guided modes in such a geometry. In this section, the properties of these modes and the reason for feature guiding in this geometry will be discussed in detail.

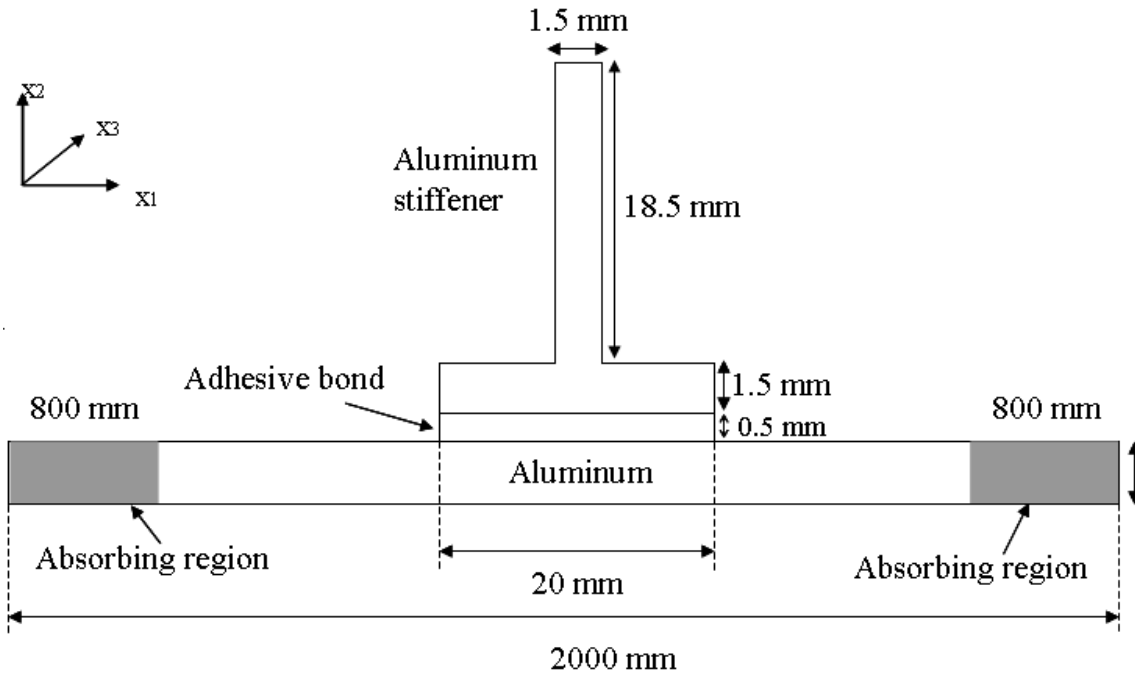

Figure 6.6: *Schematic of 2D model of a aluminium stiffener bonded on a aluminium plate.*

The geometry of the model is shown in Fig. 6.6. The plate is 3 mm thick and the adhesive has a thickness of 0.5 mm. The stiffener has a T shape and it is also

made of aluminium. Material properties are all listed in Tab. 6.1. Similarly as discussed, a 800 mm wide absorbing region is applied in the model to suppress the reflections from the outer border of the geometry. Continuity of displacement and stresses are imposed at the internal border between the stiffener, the adhesive layer and the aluminium plate. Stress free conditions are applied at the outer border of the geometry. The geometry is meshed by 1374 triangular elements of first order. These elements are automatically generated by the software used, and are finer in the stiffened zone than in the adjacent plates. The number of degrees of freedom is 15882.

6.2.2 Results and discussion

The system was solved using the SAFE method in the same way as in the previous examples, to find values of the wave number k at different frequencies. For each frequency, several solutions were obtained, including the feature guided modes and also unwanted modes corresponding to the resonance of the whole system. To pick up the feature guided modes, the axial component of the energy flow was calculated for each solution along a cross-section line across the center of the plate. Modes which have their maximum energy flow in the stiffened region with decay in the lateral plates correspond to the feature guided modes. Fig. 6.7 presents the distribution of the axial energy-flow component for one selected mode, at 100 kHz, showing that the energy is concentrating in the stiffened region, and quickly decays outside the region.

Fig. 6.8 presents snapshots of the three feature guided modes discovered at 40 kHz, which have higher energy flow in the stiffened area than in the side plates. Fig. 6.8(a) shows a guided mode which is dominated by the axial displacement u_3, similarly to the longitudinal (S0) mode in the plate. The eigenvalue for this solution is $k = 46.296 - 0.0884i/m$, from which the corresponding phase velocity is: $C_{ph} = 5428.7$ m/s and the attenuation is: $\alpha = 0.768$ dB/m. It is possible to radiate the SH0 and A0 modes in the side plate, at radiation angles of about 35.2° and 11.04°, respectively. Fig. 6.8(b) shows a guided mode which is dominated by

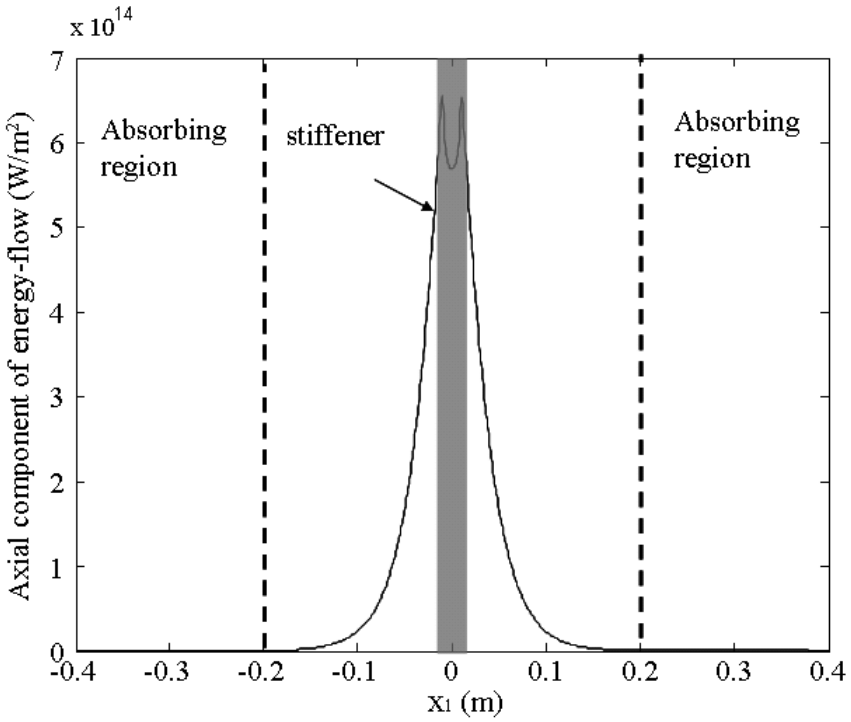

Figure 6.7: *Cross-section distribution of axial energy flow for one eigen solution selected corresponding to a wave mode propagating along the stiffener-bond-plate region and radiating energy in the aluminium plate, at 100 kHz. The grey zone indicates the stiffened region.*

the horizontal displacement u_1, similarly to the shear horizontal (SH0) mode in the plate. The eigenvalue for this mode is $k = 82.625 - 0.0222i/m$, from which the corresponding phase velocity is: $C_{ph} = 3041.8$ m/s and the attenuation is: $\alpha = 0.193$ dB/m. Since the phase velocity of this mode is higher than the A0 mode of the 3mm-thick plate but slower than the SH0 mode (3130 m/s) and the S0 mode (5428.7 m/s) at this frequency, it is only able to radiate the A0 mode in the side plate, at an angle of 19.99°. Fig. 6.8(c) shows a guided mode, which is dominated by the horizontal displace u_1 at the top of the stiffener and in the region of the plate its mode shape is similar to the bending mode (A0). The eigenvalue for this mode is $k = 325.744 - 0.0021i/m$, from which the corresponding phase velocity is: $C_{ph} = 771.58$ m/s and the attenuation is: $\alpha = 0.018$ dB/m. Since the phase velocity of this mode is slower than all the guided modes in a 3mm-thick plate at this frequency, no radiating modes are able to be launched, thus this mode is considered

to be a non-leaky mode. The small attenuation of this mode is believed to come from the adhesive which has a complex elastic modulus.

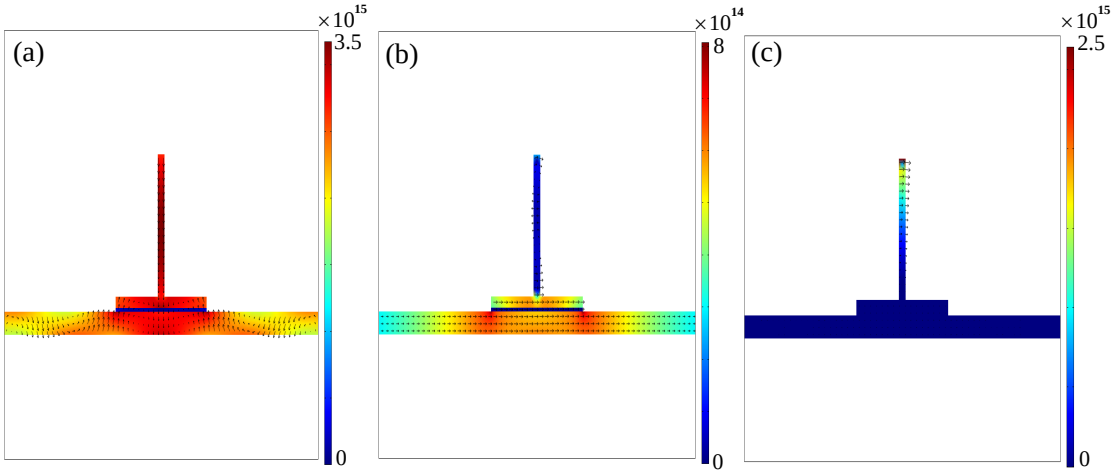

Figure 6.8: *The energy flow snapshot for the three feature guided modes at 40 kHz, with arrows indicating displacements of the cross-section.*

The reason for the energy trapping around the stiffener can be explained by modally investigating a separate model of the stiffened region, containing the stiffener, the adhesive layer and part of the plate with the same width as the stiffener (shown in Fig. 6.9), and comparing with the plate modes. The SAFE method was carried out to study the dispersion curves and the mode shapes of the geometry. Similarly as discussed in Chapter 4 and in Sec. 6.1.3, it should follow two conditions for a mode in the stiffened area to be trapped: the mode shape of the guided mode in the stiffened geometry should be similar to a plate mode, and its phase velocity should be slower than the corresponding plate mode.

Fig. 6.9 shows the phase velocity dispersion curves of the central geometry (including stiffener, adhesive and part of the plate) at frequencies from 10 kHz to 70 kHz. Eight guided modes have been found in this frequency region and are labeled mode 1 to 8 in the figure. There are only three fundamental guided modes: S0, SH0 and A0, in a 3mm-thick plate at this frequency region, which are also shown in the figure. At 40 kHz, six modes are discovered, three of which are able to be trapped, and they are examined in Fig. 6.10. The snapshots of the axial energy flow in the cross-section are shown in the left column, and in the right column there presents

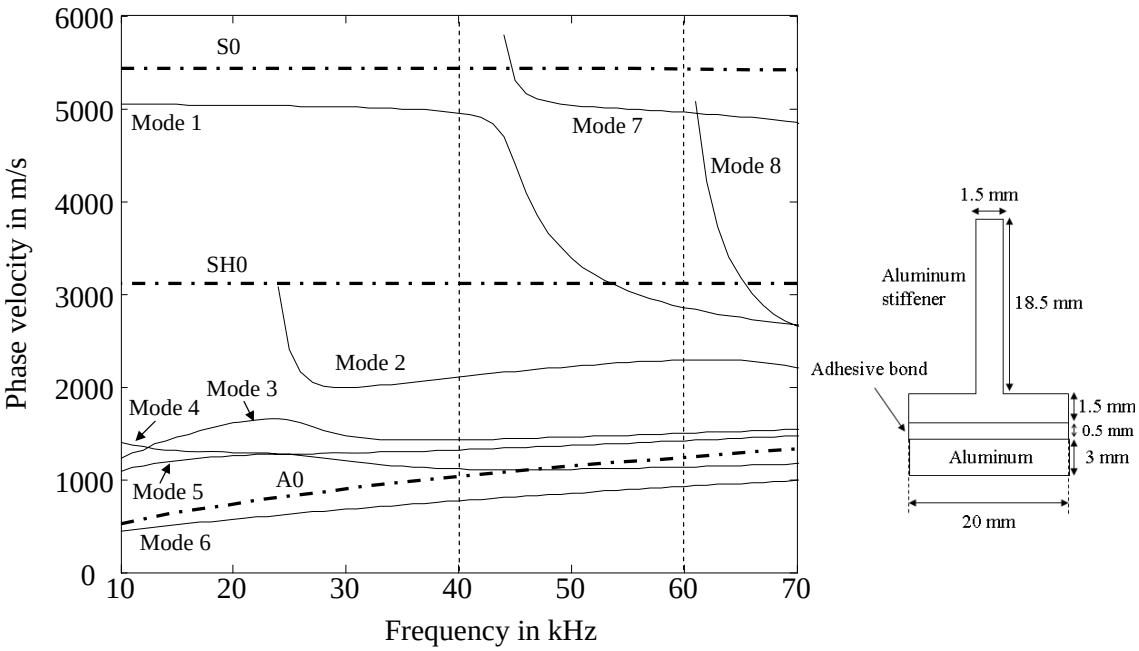

Figure 6.9: *Phase velocity dispersion curves of the central geometry with the aluminium stiffener, adhesive and aluminium plate with the same width as the stiffener, from 10 kHz to 70 kHz, are shown in solid lines. Phase velocity dispersion curves of a 3-mm thick aluminium plate are shown in dash-dot lines.*

the corresponding mode shape of the displacement on the border of the plate along the thickness of the plate. It can be seen that mode 1 is dominated by the axial displacement u_3 which is similar to the S0 mode in the plate. The phase velocity of this mode is 4957.1 m/s at 40 kHz , which is slower than the S0 mode (5437 m/s). Mode 2 is dominated by the horizontal displacement u_1, similar to the SH0 mode in the plate, and the phase velocity (2107.6 m/s) is slower than the SH0 mode(3130 m/s). Mode 6 is dominated by the horizontal displace u_1 at the top of the stiffener, but in the plate region it is dominated by the vertical displacement u_2, which is similar to the A0 mode in the plate, with phase velocity (770.1 m/s) slower than the A0 mode (1045 m/s). There are three other modes of the central structure existing at 40 kHz, whose mode shapes are all dominated by the vertical displacement u_2. However the phase velocities of mode 3, 4 and 5 are 1427.3 m/s, 1115.3 m/s and 1321.3 m/s respectively, which are all higher than the phase velocity of the A0 mode as they are shown in Fig. 6.9, thus none of these three modes are able to form a

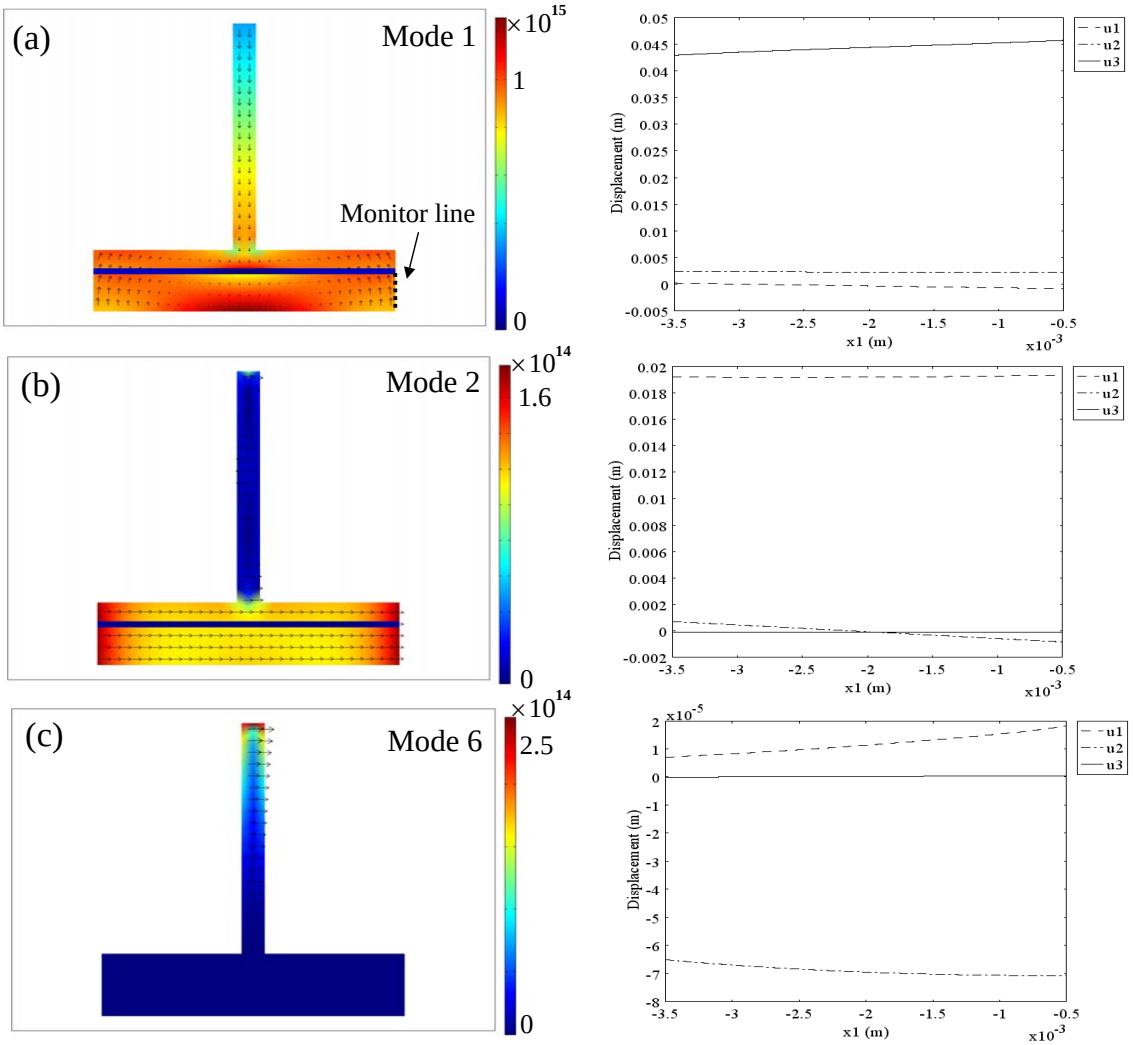

Figure 6.10: *Energy flow snapshots for the three guided modes which can form the feature guided modes at 40 kHz, with their displacement mode shapes on the border of the plate along the thickness presented in the right column.*

trapped mode.

The phase velocities of the guided modes in the central structure change with the frequency as shown in Fig. 6.9, and so do their mode shapes. More feature guided modes in the whole structure appear as the frequency increases. For example, Fig. 6.11 shows the energy flow snapshots of the four feature guided modes at 60 kHz. Comparing the mode shapes with Fig. 6.8, it can be seen that a new mode (shown in (c)) appears. It comes from mode 4 shown in Fig. 6.9, and its mode shape of displacement along the border is presented in Fig. 6.12(a) which suggests a

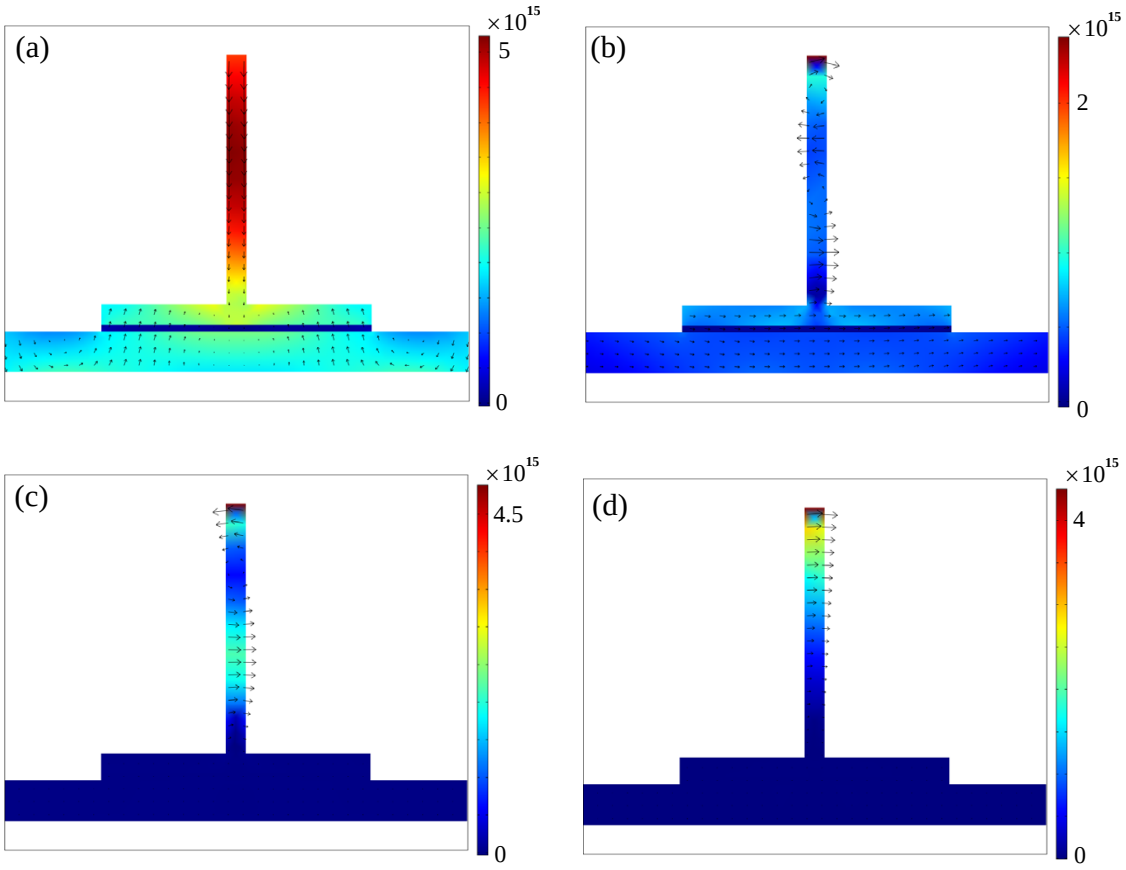

Figure 6.11: *Energy flow snapshot for the four feature guided modes at 60 kHz, with arrows indicating displacements of the cross-section.*

domination of the vertical displacement u_2. Fig. 6.9 shows that the phase velocity of mode 4 becomes slower than the A0 mode while frequency is higher than 50 kHz. Therefore this mode is able to form a trapped mode at 60 kHz. Another phenomenon is that the mode shape of mode 1 changes at 60 kHz, which is shown in Fig. 6.12(b). Its mode shape becomes dominated by vertical displacement u_2 at 60 kHz, and thus loses similarity to the S0 mode in the plate at this frequency, therefore it can no longer form a trapped mode. On the other hand, a new mode 7 appears at 60 kHz shown in the dispersion curves in Fig. 6.9. Its mode shape of displacement shown in Fig. 6.12(c) suggests a domination of the axial displacement u_3, which is similar to the S0 mode in the plate at this frequency. The phase velocity of the mode is 4958.3 m/s at 60 kHz and is slower than the S0 mode (5435 m/s), therefore this mode is able to be trapped, and the snapshot of this trapped mode is shown in Fig. 6.11 (a).

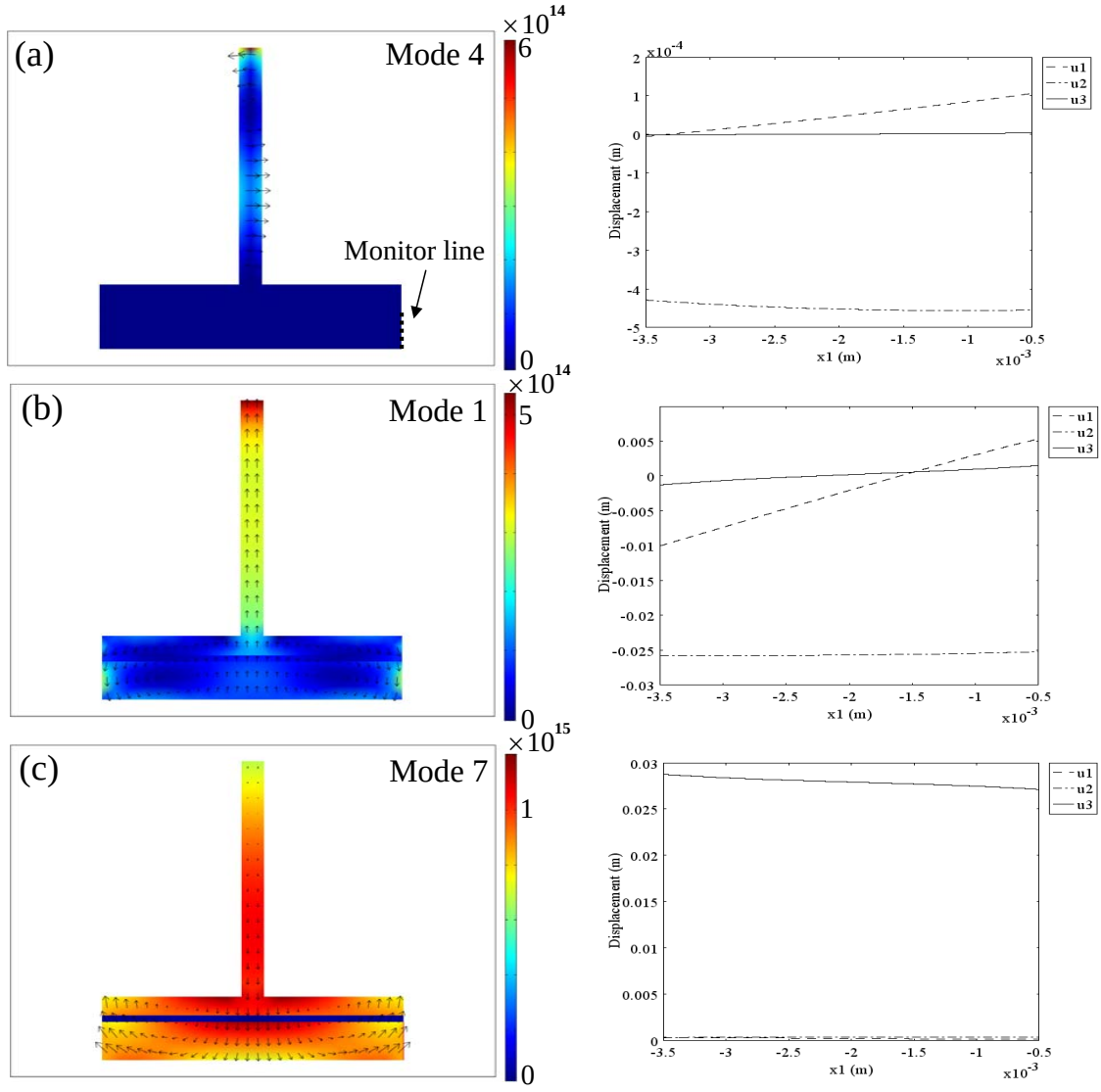

Figure 6.12: *The energy flow snapshot for mode 4, 1 and 7 in the central structure including the stiffener at 60 kHz, and their displacement mode shapes along the thickness of the plate are presented in the right column.*

6.3 Interconnected Heat Exchanger Tube (Tube plate)

6.3.1 Introduction

Guided wave inspection of pipelines has been very successful over the years, and commercial products have already been developed in industry [10, 11]. However

when the geometry is not strictly pipes, but interconnected heat exchanger tubes, the application of the guided wave technique remains challenging, as the wave properties of the guided modes on these geometries are unknown.

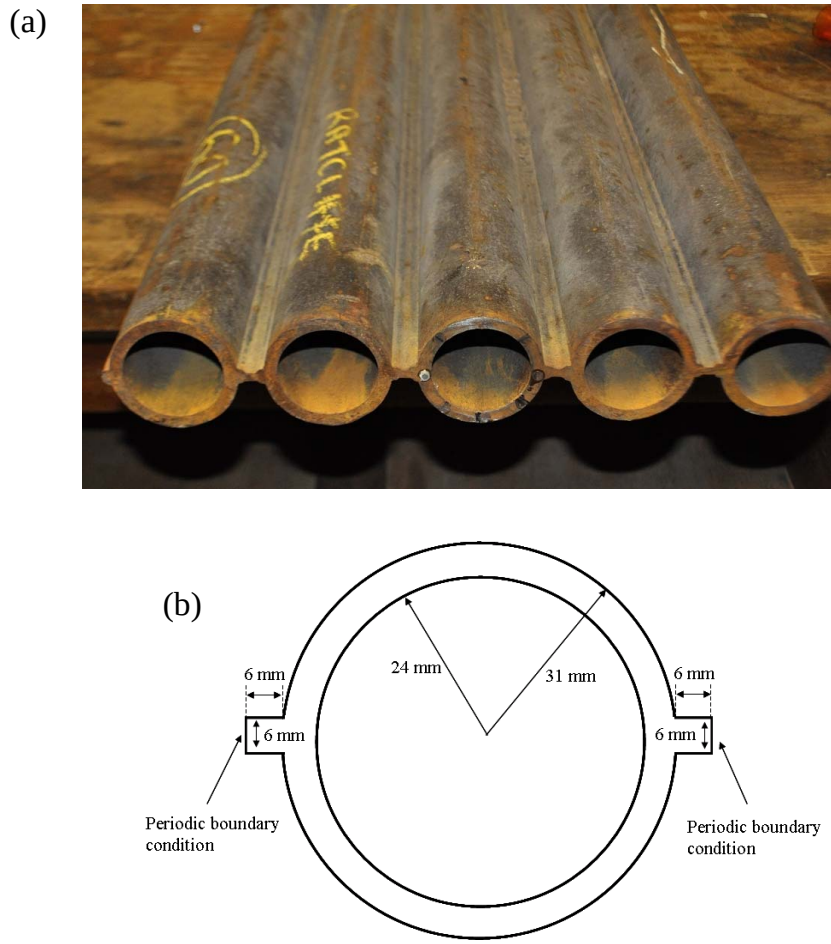

Figure 6.13: *(a) Picture of a heat exchange tube plate and (b) 2D cross-section of 1 period of the geometry.*

Fig. 6.13(a) shows a picture of one type of interconnected heat exchanger tubes which contains periodically structured pipes and plates, which is known as a tube plate. It will be useful to know if the existing guided wave techniques can be applied to inspect for defects located on the pipes in these geometries. Moreover, it will also be interesting to investigate if it is possible to inspect the connections between pipes and plates, as there is particular concern to detect defects at these locations.

The geometric data for one element of the structure is indicated in Fig. 6.13(b).

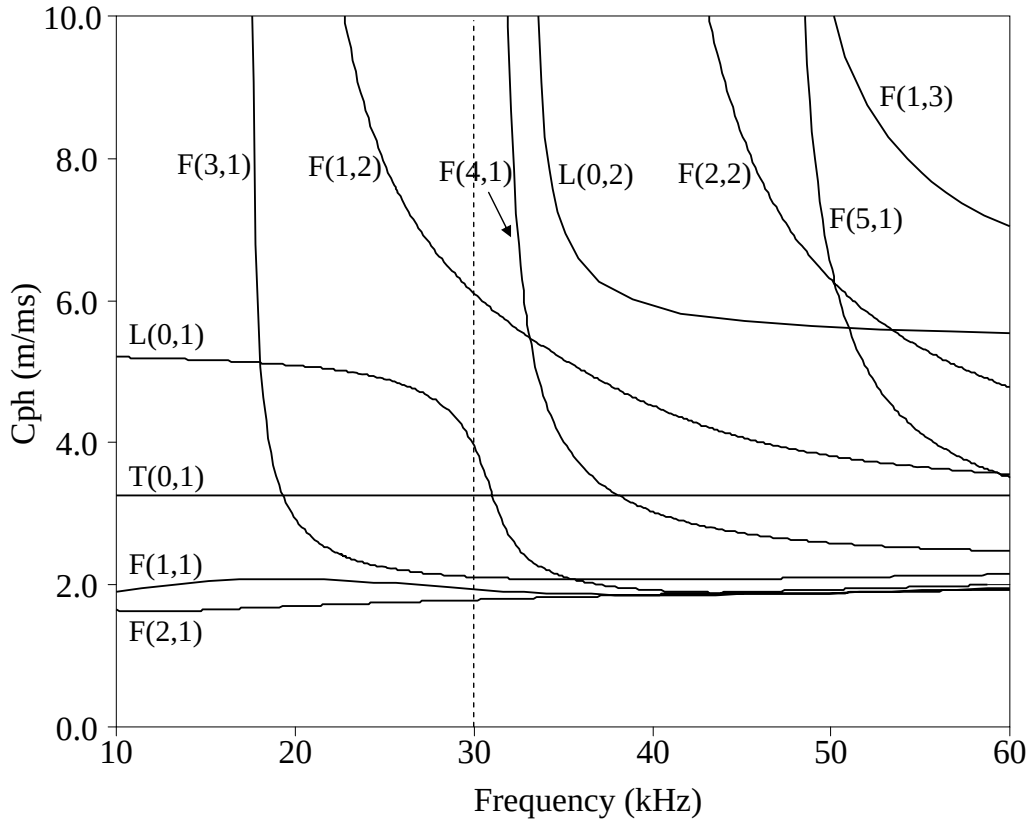

Figure 6.14: *Phase velocity dispersion curves of 7 mm thick steel pipe with 24 mm inner radius.*

The pipes are 7 mm thick with inner radius of 24 mm, and the plates are 6 mm thick located in the middle of the pipes. The dispersion curves of the pipe can be calculated by DISPERSE [9], and they are shown in Fig. 6.14. From the figure it can be seen that there are many modes existing in the pipes between 10 kHz and 60 kHz, which are all labeled according to the criteria given by Silk and Bainton [35].

6.3.2 SAFE modelling and discussion

The SAFE method has been developed by Predoi *et al* [48] to describe periodic geometries by introducing periodic boundary conditions in the modelling, which is a particular case of Neumann boundary conditions, and validated by experiments on a periodically grooved plate. The periodic boundary condition forces the elements on a pair of boundaries of the structure to have identical variables, thus representing

continuity of displacement and stress between the two edges. In this section, it is applied on the outer borders of the plate on one element of the tube plate shown in Fig. 6.13(b), which suggests that the tube and plates are periodically placed. The geometry was meshed by 530 triangular elements of first order. These elements are automatically generated by the software used, and the number of degrees of freedom is 7212. Since there was no damping in the system, the real eigen solutions corresponded to the propagation modes were picked up; while the complex eigen solutions corresponded to the evanescent modes were unwanted.

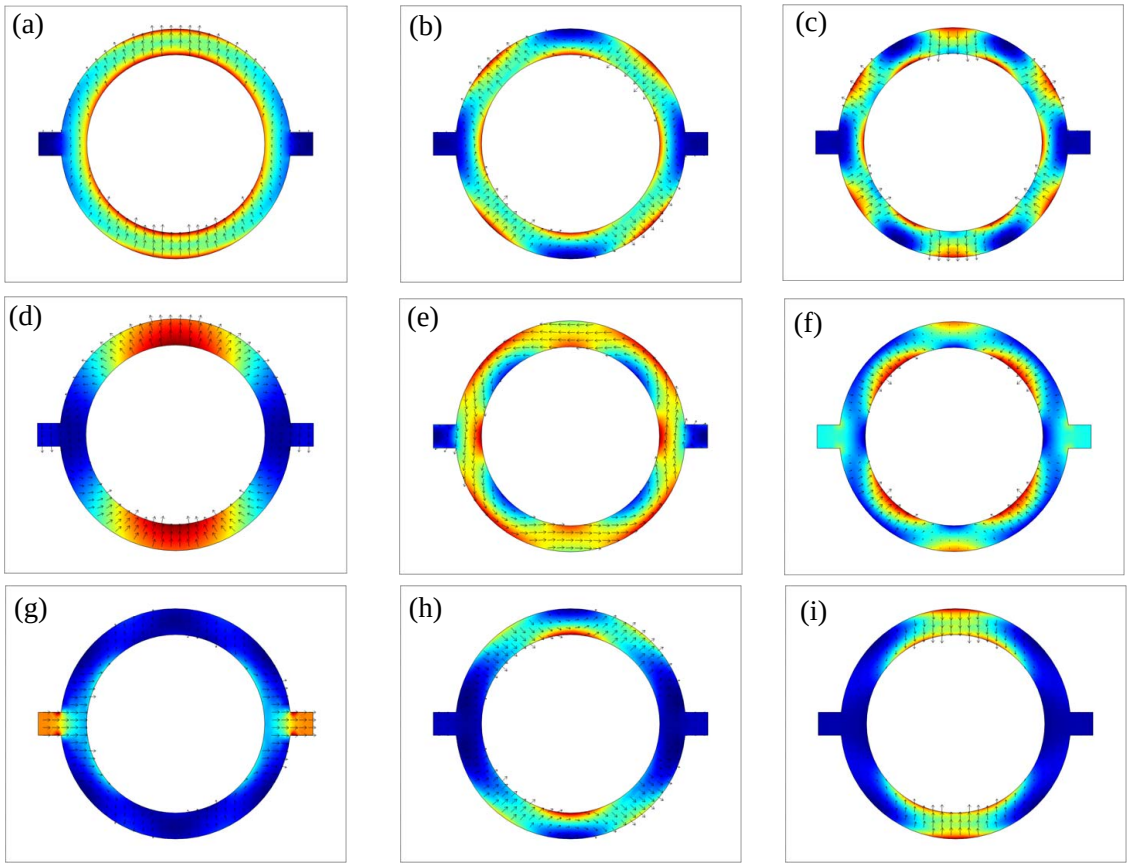

Figure 6.15: *The energy flow snapshot for all the guided modes in the heat exchanger tube at 30 kHz, with arrows indicating displacements of the cross-section.*

As the geometry is still dominated by the pipe, it can be expected that some guided modes are similar to the pipe modes. For example, nine propagation modes were discovered at 30 kHz, six of which have similar mode shapes to the pipe modes. The energy flow snapshots of these modes are plotted in Fig. 6.15, with arrows

indicating the displacement of the cross-section. Fig. 6.15(a) shows a mode with eigen solution of 99.44/m, from which the corresponding phase velocity is 1895.6 m/s. It can be seen that there is a one-wave cycle of variation of displacement around the circumference, which is similar to the F(1,1) mode in the pipe. The eigen solution shown in Fig. 6.15(b) is 106.263/m, from which the corresponding phase velocity is 1773.9 m/s. It can be seen that there are two wave cycles of variation of displacement around the circumference, which is similar to the F(1,2) mode in the pipe. Fig. 6.15(c) shows a similar mode to the F(1,3) mode in the pipe, as there are three wave cycles of variation of displacement around the circumference. The eigen solution of this mode is 89.851 /m and the phase velocity is 2097.9 m/s. Fig. 6.15(d) shows a mode with eigen solution of 32.406/m, from which the corresponding phase velocity is 5816.6 m/s. This mode also has one wave cycle of variation of displacement around the circumference, but with higher phase velocity, thus is similar to the F(2,1) mode of the pipe. Fig. 6.15(e) shows a guided mode which is dominated by the circumferential displacements, similar to the T(0,1) mode in the pipe, although it is not strictly axially symmetric due to the presence of the plate. The eigen solution of this mode is 54.983 /m and the phase velocity is 3428.3 m/s. Fig. 6.15(f) shows a similar mode to the L(0,1) mode in the pipe, with the mode shape dominated by the axial displacement although not symmetrically distributed. The eigen solution of this mode is 44.741/m and the phase velocity is 4213.1 m/s. Fig. 6.15(g) shows a very interesting mode with phase velocity of 2479.8 m/s. The energy of this mode is concentrated in the plate area, thus it may have the potential to inspect the connections between the pipe and the plate where there is particular concern to find defects. Fig. 6.15(h) and (i) present another two new modes which do not have corresponding modes in the pipe, with phase velocity of 1957.9 m/s and 1978.3 m/s, respectively.

Fig. 6.16 shows the phase velocity dispersion curves of the heat exchanger tube plate for frequency from 10 kHz to 60 kHz, some high order modes are omitted for simplicity. Modes in solid lines are labeled similarly as the pipe modes, but with the subscript q standing for "quasi", while "new" modes are plotted in dash-dot lines. Comparing with Fig. 6.14, it can be seen the dispersion curves of the

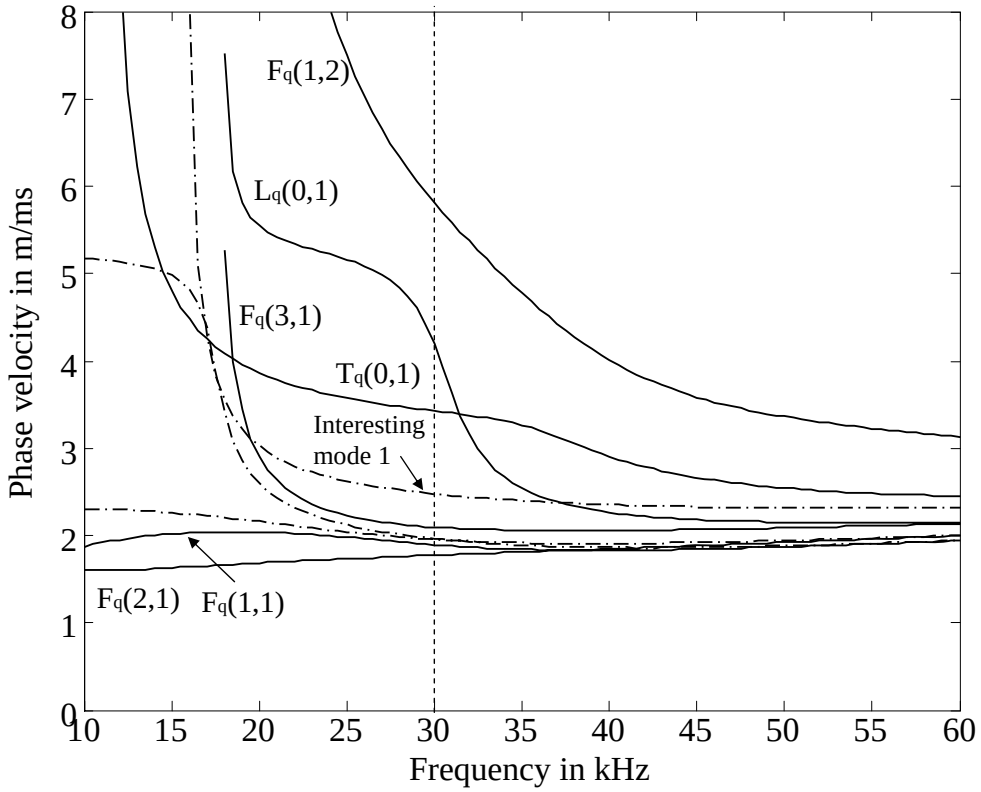

Figure 6.16: *Phase velocity dispersion curves of the heat exchanger tube from 10 kHz to 60 kHz, without showing higher order modes.*

heat exchanger tube plate are similar to those of a simple pipe, for example at 30 kHz phase velocities of quasi modes (shown in Fig. 6.16) are close to those of their corresponding pipe modes (shown in Fig. 6.14). However there also exist differences. Except for the appearance of some new modes which has been discussed previously, both the $L_q(0,1)$ mode and the $T_q(0,1)$ mode have cut off frequencies. This is because the side plates constraint the axial and the circumferential motions of the longitudinal and the torsional mode respectively, thus below certain frequency it is not possible for them to propagate. Another discovery is that the new mode shown in Fig. 6.15(g) has very little dispersion above 30 kHz, which provides the potential of applying this mode to inspect the connections between the pipe and the plate for long distance, given that the energy is concentrated in this area.

6.4 Summary

In this chapter, guided modes on a lap joint, a stiffened plate and a interconnected heat exchanger tube plate are investigated. It can be concluded that feature guided waves exist in a wide range of geometries, provided that geometry can lower the phase velocity of the guided waves in the feature. The SAFE method can be applied as a generic tool to modally investigate guided waves propagating along waveguides with any arbitrary cross-section. The properties of the guided modes, such as mode shapes, velocity dispersion curves and leakage rate, can be predicted by the method. Therefore it is possible to suggest candidate modes to inspect for particular structures that are interesting for industry.

Chapter 7

Conclusions

7.1 Thesis Review

Ultrasonic guided waves have been widely applied in industry since they can be generated from a single transducer position and propagate for a long distance. Analytical theory for guided waves propagation on regular geometries such as plates or pipelines has been well established. In this thesis, the application has been extended to waveguides with irregular cross-sectional geometries, in particular for waveguides which are surrounded by a fluid or solid medium of infinite extent, causing possible leakage of the guided wave energy. Chapter 1 introduced the background and the motivation. The work in the thesis has been conducted in three parts: (a) the modelling development in Chapter 2, (b) ultrasonic dipstick application in Chapter 3 and (c) applications of feature guided waves in Chapters 4, 5 and 6.

In Chapter 2, the basic theory of bulk ultrasonic waves and guided waves propagation on regular geometries was firstly reviewed. The properties of guided waves, such as dispersion relations and mode shapes were examined on a single plate and also on a cylindrical bar immersed in a fluid. The Semi-Analytical Finite Element method was introduced to describe the guided wave properties on geometries with irregular cross-sectional shapes. Then the method was extended for a solid waveguide immersed in both perfect and viscous fluids and validated with existing analytical solutions.

Chapter 3 presented a guided wave technique to measure the density of a fluid by the models developed in chapter 2. Previous approximate theory describing the technique was also reviewed and analyzed for the reason of its inaccuracy. Experiments were carried out on a rectangular bar immersed in a range of fluids, and the results were compared to both theories.

Chapter 4 investigated waves which can propagate along a weld joining two plates and concentrate the energy in and around the weld. Properties of the weld guided modes were examined in this chapter by the modelling techniques developed in Chapter 2. The physical reasons for the trapping of the energy were also discussed. Experimental work was undertaken to validate the existence of the weld guided mode and the accuracy of the model.

Chapter 5 proceeded the work in Chapter 4 by investigating the interaction of the weld guided wave to different types of detects, in order to exploit the potential to use this wave as a screening tool to rapidly inspect long lengths of the weld. Both time step simulations and experiments were carried out to study the reflection behavior of different types of defects in terms of frequency, defect size, depth and location.

Chapter 6 presented finite element studies on some other geometries, in which similar feature guided waves were also discovered. Properties of discovered modes and potential applications of exploiting them for defect inspection were discussed.

7.2 Summary of Findings

7.2.1 Extension of Semi-Analytical Finite Element Method

Analytical methods to study guided wave propagation on regular geometries such plates or pipelines has been well documented in literature. For waveguides with irregular but constant cross-sectional shape, a Semi-Analytical Finite Element method can be applied to study the properties of guided waves propagating in the structure. This approach uses finite elements to represent the two dimensions of the cross-

section of the waveguide, plus a harmonic description for the axial dimension. The SAFE method has been investigated by previous researchers on perfect waveguides which do not leak energy.

In our work, the SAFE method has been extended to the problem of solid waveguides embedded or immersed in an infinite medium, in which case a guided wave may leak energy away from the waveguide when it propagates. The SAFE method in solids has been reviewed and then developed in fluids, including both non-viscous and viscous fluids. In order to model the infinite surrounding medium, an absorbing region has been applied which has the same mass density as the medium but with viscous damping of increasing rate with distance away from the waveguide. Therefore there will be no reflections from the outer border of the geometry by applying the absorbing region. Based on the development of the modelling, two applications have been carried out.

7.2.2 Dipstick for ultrasonic density measurements

The first application concerns density measurements in fluids. A torsional wave pulse is applied to propagate along a solid non-circular waveguide immersed in a fluid, which interacts at the boundary with the surrounding fluid. Thus some fluids will be trapped at the corners of the cross-section and this affects the propagation velocity of the torsional wave. Therefore by measuring the propagation speed of the torsional waves it is possible to inversely work out the density of the trapping fluid. A previous analytical model had been developed by others based on the calculation of the inertia of the surrounding medium, however the accuracy of that approach is compromised due to the complexity of the wave behavior in the non-circular cross-sectional shape.

In Chapter 3, the SAFE method was applied to describe a rectangular bar immersed in alcohol. At low frequency, four fundamental modes were discovered which were the longitudinal, torsional and two flexural modes. The torsional mode was picked up, and the dispersion curve was generated by repeating the SAFE method over a

range of frequencies. It was shown that this mode is non-attenuative and almost non-dispersive, thus it could be a good candidate mode for fluid density measurements.

An inverse model relating the group velocity of the torsional mode and the density of the surrounding fluid was established, which presented a linear relationship between them. Experiments were carried out on an aluminium rectangular bar immersed in fluids. The first experiment validated the group velocity dispersion curve of the rectangular bar immersed in alcohol, showing good agreement with the SAFE prediction. The second experiment verified the inverse model to predict the density of the fluid, which used fluids with densities varying from ($800kg/m^3$) to ($1100kg/m^3$). Compared to the approximate theory, the SAFE method predictions showed a significant improvement on the accuracy of the model.

With SAFE modelling, different geometries and material properties of the waveguide can be designed to optimize the sensitivity of the sensor. It was shown that with the same aspect ratio, the diamond shaped cross-section had better sensitivity than the elliptical shape and the rectangular shape, and thus could be a good candidate shape for the sensor. It was also presented that the solid bar with smaller density would be more sensitive to the fluid.

7.2.3 Feature guided waves

Study of the principle

The second application is regarding large area inspections with feature guided waves. It was a previous experimental finding of a compression wave whose energy was concentrated in and around the weld, and propagated along the weld, which had introduced this topic of research at the beginning. Three-dimensional time step FE simulation was carried out to study a simple geometry to illustrate the trapping phenomena, however it was very time consuming.

In Chapter 4, the SAFE method was applied to modally investigate the wave propagation along a weld. As a two-dimensional model, the calculation time was signif-

icantly reduced. The properties of the compression weld guided mode, which were found experimentally, were studied. It was shown that this mode has similar mode shapes and dispersion relations as the S0 mode in plates, but with energy concentrating more and more in the weld with the increasing of frequency. Moreover, at low frequency, the compression weld guided mode is a leaky mode which radiates SH0 waves into the side plates.

During the modal study, a new weld guided mode which has similar mode shapes as the SH0 mode in the plate, was discovered. Compared to the compression mode, this mode is non-leaky and little dispersive, thus it is very attractive for long distance inspections. While the frequency increases the energy of the shear mode also becomes more and more concentrated in the weld.

The energy trapping effect for the weld guided mode was discussed, concluding that the waves propagating in the weld should have similar mode shapes as the surrounding plate but should have smaller phase velocities.

A validation experiment had been carried out on an idealized geometry which trapped the energy in the same way as a real weld. The experimental results for the group velocity, attenuation and energy concentration of the shear mode all showed very good agreement with the SAFE predictions, which validated the existence of the shear mode and the accuracy of the modelling.

Investigation on applications

The interaction of the weld guided mode with different types of defects was studied in Chapter 5. It was demonstrated that the shear weld guided mode can be used as a screening tool to inspect defects for long distances of the weld, due to its low attenuation and minimally dispersive characteristics. The interaction of this wave with three types of defects located on the heat affected zone were studied both experimentally and in Finite Element simulations.

The reflection spectrum for cracks parallel to the edge of the weld showed simi-

larity to the case studied elsewhere of the SH0 wave interacting with cracks in a plate aligned in the propagation direction. However the amplitude of the reflection coefficient decreases as the frequency increases, because the energy becomes more concentrated in the center of the weld. Therefore the low frequency range is more interesting for practical applications. It has also been discovered that the shear weld guided mode is more sensitive to the defects located closer to the weld, and this can be explained by its mode shapes. Experimental results have shown good agreement in the shape of the reflection coefficient spectrum with the FE predictions, but with slightly higher amplitude, which was believed to be caused by the difference in the milled slits used in the experiments and zero-width cracks defined in the FE model.

For cracks normal to the edge of the weld, the reflected energy from the crack decreases with increasing frequency. There are substantial differences in the reflection coefficient between cracks of different lengths, however the difference decreases as the frequency increases. The curve of the reflection coefficient spectrum predicted by the FE simulation had similar shapes as the experimental measurement, however the amplitude of the curve disagreed. This was believed to be due to the variation of the shape of the weld cap, so that the mode shape of the shear weld guided mode was affected. Both FE and experiment showed that waves had better sensitivity at low frequency than at high frequency.

The reflection coefficient spectrum for flat-bottom holes has shown that at low frequency the reflection coefficient increases as the frequency increases. It reaches its maximum while the diameter of the hole is around a quarter of the wavelength, and decreases with the increasing of the frequency. Moreover the shear guided mode was tested to have better sensitivity to the depth of the hole at lower frequency than at higher frequency. The experimental results on the reflection coefficient spectrum of a hole with three different depths have shown the same shapes as the FE predictions.

Feature guided waves have also been discovered on other example geometries of lap joints, stiffened plates or interconnected heat exchanger tubing. It is possible to use the SAFE method as a generic tool to predict the wave properties of the feature guided modes, and thus to suggest suitable modes and frequencies for NDT

applications.

7.3 Future Work

In future, it should be possible to extend the dipstick technology in viscous fluid and establish inverse models to predict the viscosity as well as the density of the fluid, following the preliminary work described in Chapter 3. It will be challenging if both the velocity and viscosity of the fluid are unknown, as theoretically two equations will be required for unicity of the solution. One possible method is to measure the velocities of two different modes, i.e. the longitudinal mode and the torsional mode, and then do the inversion. An alternative solution is to measure two properties of one single guided mode, for example the velocity and the attenuation of the torsional mode. Therefore there will be two equations, each of which links to the density and viscosity in a different way.

In our research of the feature guiding phenomenon, the experimental plate was manufactured to be wide enough so that the reflection from the edge of the plate would not interfere with the inspection signals. However, the existence of the edge reflection signal (shown in Fig. 5.2) will cause a blind zone where it may overlap with reflections from defects. If the plate is narrow, or if there are some other features existing on the plate, the blind zone will become large due to multi wave reflections between the target feature and other features. Therefore in practice, it would be very interesting to absorb the guided waves in side plates, for example by placing an absorber on top of the plate as shown in Fig. 7.1. The absorber could be made of a viscoelastic medium such as rubber which has high damping properties. It should be contacted firmly to the plate, possibly with a coupling medium, so that the energy of the guided waves in the side plates will transmit into the absorber and then attenuate. Thus the reflection from the edge or other features of the plate will be significantly reduced. The length and the thickness of an efficient absorber could be calculated according to the choice of feature guided modes and operating frequencies.

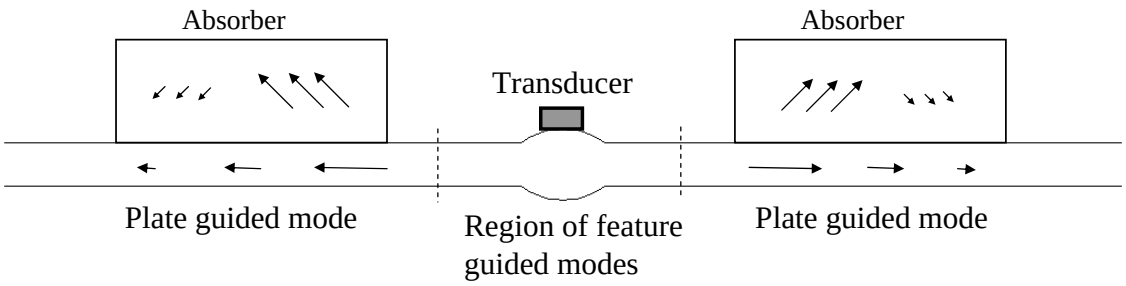

Figure 7.1: *Schematic of feature guided wave inspection with absorbers to attenuate guided waves in plates.*

In the modal study of the weld guided modes, we also found some high order weld-guided modes; however for simplicity only the two fundamental weld-guided modes were discussed since our interest is to reveal the principle of feature-guiding. These higher order modes might be interesting for NDE applications at higher working frequencies, if they are more sensitive to defects of specific interest. Therefore future work can be carried out to investigate the potential of using these higher order feature guided waves for inspection.

It is also important to perform experimental defect scattering studies of the weld guided modes on a number of different geometries. Although it is understood that the feature guiding phenomenon generally exists due to the geometry change in the welded part, it is necessary to evaluate the robustness of the technology of using weld guided modes as a screening tool to detect defects on long lengths of real welds. Especially when the weld cap is not uniform along the propagation direction, more coherent noise will be expected in the inspection.

This work was carried out within the research programme of the UK Research Centre in NDE (RCNDE). A meeting of interested industrial partners of the RCNDE has reviewed the outcome and members are identifying potential applications for exploiting the approach in industry. It will be useful to carry out further studies of feature guided waves on realistic geometries provided by the industrial partners, following the work in Chapter 6. Specific applications, such as evaluation of the bonding condition in lap joints or inspection for certain types of defects in the heat exchanger tubes, can be investigated upon request.

Appendix A

Laser Interferometric Measurement

This appendix discusses the theoretical background of laser interferometric velocity and displacement measurement. In a laser vibrometry measurement, a laser beam is focused on the tested structure whose moment causes the presence of the Doppler effect in the laser reflection. If the object can reflect the beam properly, it is possible to calculate its velocity and displacement. Since the laser has a very high frequency ($f = 4.74 \times 10^{14} Hz$ for the helium-neon), it is not possible to operate a direct demodulation. Instead an interferometer is used to mix the scattered light coherently with the reference beam. A schematic of a laser interferometric measurement is shown in Fig. A.1. The laser emits a spatially and temporally coherent source of light (all photons have same frequency, direction and phase), and the beam is split into reference and object beams. The scattered beam and the reference beam are recombined and received by a photo detector, which measures the intensity of the mixed light. The intensity varies with the phase difference $\Delta\Phi$ between the two beams according to the equation:

$$I(\Delta\Phi) = \frac{I_{max}}{2}(1 + cos\Delta\Phi). \tag{A.1}$$

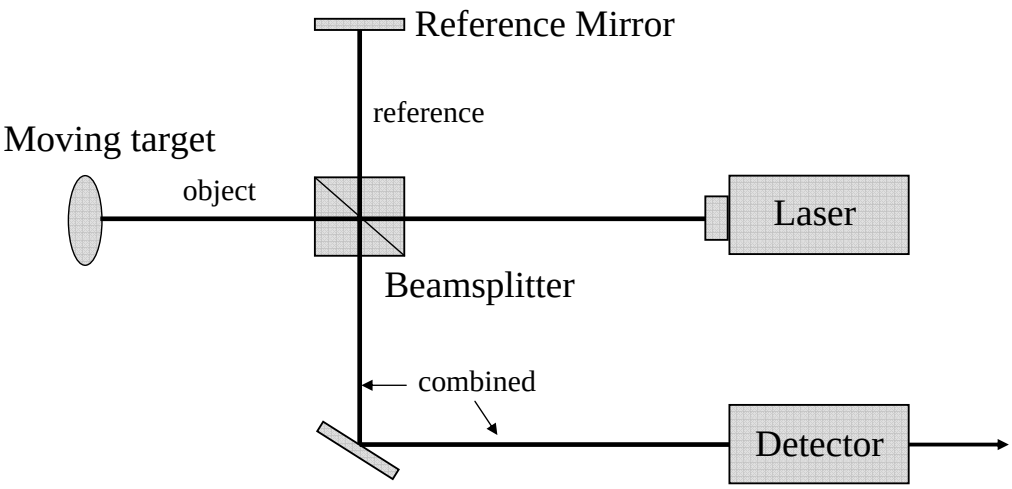

Figure A.1: *Schematic of a laser interferometer .*

The phase difference $\Delta\Phi$ is a function of the path difference ΔL between the two beams according to

$$\Delta\Phi = 2\pi \cdot \frac{\Delta L}{\lambda}, \tag{A.2}$$

where λ is the laser wavelength. When the object moves at a constant velocity V, the optical path difference ΔL becomes a function of the time $\Delta L = \Delta L(t)$. The interference fringe pattern moves on the detector and the displacement of the object can be determined by counting of the passing fringe pattern. The intensity at the detector changes sinusoidally. The frequency that is produced as a function of velocity is called the Doppler frequency shift f_D and is a function of the velocity component in the direction of the object beam according to

$$f_D = 2 \cdot \frac{|V|}{\lambda} \tag{A.3}$$

Fig. A.2 shows the schematic of using laser interferometers to measure the out-of-plane and in-plane vibration. If the laser beam is aligned perpendicular to the surface of the object, the out-of-plane vibration may be obtained from the above theory. For the measurement of in-plane vibration, two laser beams are aligned at a certain angle to the surface of the object. The in-plane displacement U_x can be expressed as $U_x = 2Ucos\theta$, where U is the displacement measured by one of the

beams. If θ is set to be 60° as we did in the experiment, the in-plane displacement $U_x = U$.

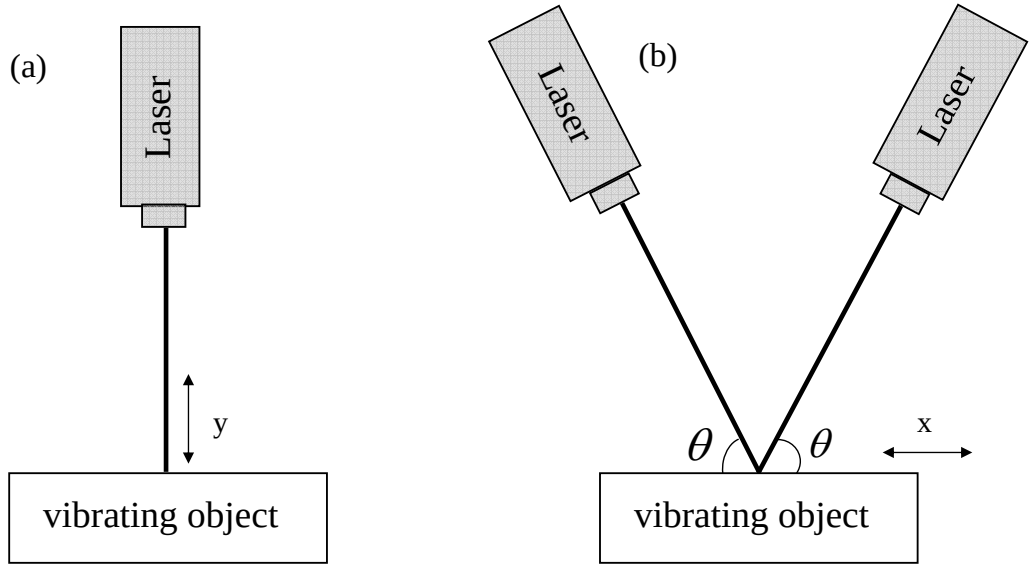

Figure A.2: *Schematic of the measurement of out-of-plane (a) and in-plane (b) vibration .*

References

[1] J. Krautkramer and H. Krautkramer. *Ultrasonic Testing of Materials. 3rd edition.* Springer-Verlag, 1983.

[2] L. W. Secmerr. *Fundamental of Ultrasonic Nondestructive Evaluation: A Modeling Approach.* Plenum, 1998.

[3] A. S. Birks, R. E. Green, and P. Mclntire. *Nondestructive testing handbook*, volume 7. second edition, Amercian Society of Nondestructive Testing, The United States of American, 1991.

[4] M. L. Mester. *Nondestructive testing handbook*, volume 4. Amercian Society of Nondestructive Testing, The United States of American, 1986.

[5] J. Blitz. *Electrical and Magnetic Methods of Nondestructive Testing.* Chapman and Hall, 1997.

[6] W.T. Thomson. Transmission of elastic waves through a stratified solid medium. *J. Appl. Phys.*, 21:89–93, 1950.

[7] M. J. S. Lowe. Matrix techniques for modelling ultrasonic waves in multilayered media. *IEEE Trans. Ultrason. Ferroelectr. Freq. Control*, 42:525–542, 1995.

[8] B. Hosten and M. Castaings. Surface impedance matrices to model the propagation in multilayered media. *Ultrasonics*, 41:501–507, 2003.

[9] B. N. Pavlakovic, M. J. S. Lowe, D. N. Alleyne, and P. Cawley. Disperse: A general purpose program for creating dispersion curves. In D. O. Thompson and

D. E. Chimenti, editors, *Review of Progress in Quantitative NDE*, volume 16, pages 185–192. Plenum Press, New York, 1997.

[10] D. N. Alleyne, M. J. S. Lowe, and P. Cawley. The reflection of guided waves from circumferential notches in pipes. *Journal of Applied Mechanics*, 65:635–641, 1998.

[11] D. N. Alleyne, B. Pavlakovic, M. J. S. Lowe, and P. Cawley. Rapid, long range inspection of chemical plant pipework using guided waves. *Insight*, 43:93–96,101, 2001.

[12] M. Sheard and A. McNulty. Field experience of using long-range ultrasonic testing. *Insight*, 43(2):79–83, 2001.

[13] P. J. Mudge. Field application of Teletest(R) long-range ultrasonic testing technique. *Insight*, 43:74–77, 2001.

[14] P. Wilcox. Omni-directional guided wave transducer arrays for the rapid inspection of large areas of plate structures. *IEEE Trans. Ultrason. Ferroelect. Freq. Contr.*, 50(6):699–709, 2003.

[15] L. Gavrić. Finite element computation of dispersion properties of thin-walled waveguides. *J. Sound. Vib.*, 173:113–124, 1994.

[16] L. Gavrić. Computation of propagative waves in free rail using a finite element technique. *J. Sound. Vib.*, 185:531–543, 1995.

[17] T. Hayashi, W. J. Song, and J. L. Rose. Guided wave dispersion curves for a bar with an arbitrary cross-section, a rod and rail example. *Ultrasonics*, 41:175–183, 2003.

[18] A. C Hladky-Hennion. Finite element analysis of the propagation of acoustic waves in waveguides. *J. Sound Vib.*, 194:119–136, 1996.

[19] T. Hayashi, C. Tamayama, and M. Murase. Wave structure analysis of guided waves in a bar with an arbitrary cross-section. *Ultrasonics*, 44:17–24, 2006.

[20] H. H. Bau. Torsional wave sensor - a theory. *Trans.ASME J. Appl. Mech.*, 53:846–848, 1986.

[21] J. P. Sargent. Corrosion detection in welds and heat affected zones using ultrasonic Lamb waves. *Insight*, 48:160–167, 2006.

[22] J. Postnova and R. V. Craster. Trapped modes in 3d topographically varying plates. *IMA Journal of Applied Mathematics*, Advance Access published March 18, 2008.

[23] N. Juluri, M. J. S. Lowe, and P. Cawley. The guiding of ultrasound by a welded joint in a plate. In D. O. Thompson and D. E. Chimenti, editors, *Review of Progress in Quantitative NDE*, volume 26, pages 1079–1086. American Institute of Physics, New York, 2007.

[24] K. F. Graff. *Wave motion in elastic solids*. Clarendon Press, Oxford, 1975.

[25] L. M. Brekhovskikh. *Waves in layered media*. Academic Press, New York, London, 1980.

[26] B. A. Auld. *Acoustic Fields and Waves in Solids*. Krieger Publishing Company, Malabar, Florida, 1990.

[27] J. L. Rose. *Ultrasonic Waves in Solid Media*. Cambridge University Press, Cambridge, UK, 1999.

[28] B. N. Pavlakovic and M. J. S. Lowe. A general purpose approach to calculating the longitudinal and flexural modes of multi-layered, embedded, transversely isotropic cylinders. In D.O. Thompson and D.E. Chimenti, editors, *Review of Progress in Quantitative NDE*, volume 18, pages 239–246. Plenum Press, New York, 1999.

[29] L. Knopoff. A matrix method for elastic wave problems. *Bull. Seism. Soc. Am.*, 54:431–438, 1964.

[30] H. Schmidt and F. B. Jensen. Efficient numerical solution technique for wave propagation in horizontally stratified environments. *Comput. Math. Appl.*, 11:699–715, 1985.

[31] P. Roux, B. Roman, and M. Fink. Time-reversal in an ultrasonic waveguide. *Applied Physics Letters*, 70:1811–1813, 1997.

[32] P. Wilcox, M. J. S. Lowe, and P. Cawley. A signal processing technique to remove the effect of dispersion from guided wave signals. In D. O. Thompson and D. E. Chimenti, editors, *Review of Progress in Quantitative NDE*, volume 20, pages 555–562. American Institute of Physics, New York, 2001.

[33] P. M. Morse and H. Feshbach. *Methods of theoretical physics*. McGraw-Hill Book Company, New York, London, 1953.

[34] A. H. Nayfeh. *Wave propagation in layered anisotropic media with application to composites*. Elsevier, Amsterdam, 1995.

[35] M. G. Silk and K. F. Bainton. The propagation in metal tubing of ultrasonic wave modes equivalent to Lamb waves. *Ultrasonics*, 17(1):11–19, 1979.

[36] D. J. Mead. Wave propagation in continuous periodic structures: Research contributions from southampton, 1964¨c1995. *J. Sound. Vib.*, 160:495–524, 1996.

[37] D. J. Mead. A general theory of harmonic wave propagation inlinear periodic systems with multiple coupling. *J. Sound. Vib.*, 27:235–260, 1973.

[38] W. X Zhong and F. W. Williams. On the direct solution of wave propagation for repetitive structure. *J. Sound Vib.*, 181:485–501, 1995.

[39] L. Gry and C. Gontier. Dynamic modeling of railway track: A periodic model based on a generalized beam formulation. *J. Sound Vib.*, 199:531–558, 1997.

[40] B. R Mace, D. Duhamel, M. J. Brennan, and L Hinke. Finite element prediction of wave motion in structural waveguides. *J. Acoust. Soc. Am.*, 117:2835–2843, 2005.

[41] F. Treysséde. Numerical investigation of elastic modes of propagation in helical waveguides. *J. Acoust. Soc. Am.*, 121(6):3398–3408, 2007.

[42] P.E Lagasse. Dispersion of axially symmetric waves in empty and fluid-filled cylindrical shells. *Acustica*, 27:317–329, 1972.

[43] V. Damljanovic and R. L. Weaver. Propagating and evanescent elastic waves in cylindrical waveguides of arbitrary cross section. *J. Acoust. Soc. Am.*, 115:1572–1581, 2004.

[44] V. V. Volovoi, D. H. Hodges, V. L. Berdichevsky, and V. G Sutyrin. Dynamic dispersion curves for non-homogeneous, anisotropic beams with cross-section of arbitrary geometry. *J. Sound. Vib.*, 215:1101–1120, 1998.

[45] I. Bartoli, A. Marzani, F. L. Scalea, and E. Viola. Modeling wave propagation in damped waveguides of arbitrary cross-section. *J. Sound. Vib.*, 295:685–707, 2006.

[46] P. Wilcox, M. Evans, M. J. S. Lowe, and P. Cawley. Dispersion and excitability of guided acoustic waves in isotropic beams with arbitrary cross-section. In D. O. Thompson and D. E. Chimenti, editors, *Review of Progress in Quantitative NDE*, volume 21A, pages 203–210. American Institue of Physics, New York, 2002.

[47] D. Hitchings. FE77 user manual. Technical report, Imperial College, 1994.

[48] M. V. Predoi, M. Castaings, B. Hosten, and C. Bacon. Wave propagation along transversely periodic structures. *J. Acoust. Soc. Am.*, 121(4):1935–1944, 2007.

[49] COMSOL. *User's Guide and Introduction*. Version 3.3 by-COMSOL AB 2007, http://www.comsol.com/, most recently viewed 20th July 2008.

[50] M. Castaings and M. J. S. Lowe. Finite element model for waves guided along solid systems of arbitrary section coupled to infinite solid media. *J. Acoust. Soc. Am.*, 123(2):696–708, 2008.

[51] T.P. Pialucha. *The reflection coefficient from interface layers in NDT of adhesive joints*. PhD thesis, University of London, 1992.

[52] P. B. Nagy and A. H. Nayfeh. Viscosity-induced attenuation of longitudinal guided waves in fluid-loaded rods. *J. Acoust. Soc. Am.*, 100(3):1501–1508, 1996.

[53] A. H. Nayfeh and P. B. Nagy. Excess attenuation of leaky Lamb waves due to viscous fluid loading. *J. Acoust. Soc. Am.*, 101(5):2649–2658, 1997.

[54] A. Bernard, M. J. S. Lowe, and M. Deschamps. Guided waves energy velocity in absorbing and non-absorbing plates. *J. Acoust. Soc. Am.*, 110(1):186–196, 2001.

[55] M. J. S. Lowe and B. N. Pavlakovic. Disperse user manual, version 2.0.11d. Technical report, Imperial College, 2001.

[56] T. Vogt, M. J. S. Lowe, and P. Cawley. Measurement of the material properties of viscous liquids using ultrasonic guided waves. *IEEE Trans. Ultrason. Ferroelect. Freq. Contr.*, 51(6):737–747, 2004.

[57] F. B. Cegla, P. Cawley, and M. J. S. Lowe. Material property measurement using the quasi-Scholte mode-A waveguide sensor. *J. Acoust. Soc. Am.*, 117(3):1098–1107, 2005.

[58] J. O. Kim and H. H. Bau. On line, real-time densimeter - theory and optimization. *J. Acoust. Soc. Am.*, 85(1):432–439, 1989.

[59] L. C. Lynnworth. Slow torsional wave sensors. *Ultrasonic Symposium Proceedings, IEEE*, 77 CH:1344–ISU, 1977.

[60] C. L. Shepard, B. J. Burghard, M. A. Friesel, B. P. Hildebrand, Moua X., A. A. Diaz, and C. W. Enderlin. Measurements of density and viscosity of one- and two-phase fluids with torsional waveguides. *IEEE Trans. Ultrason. Ferroelect. Freq. Contr.*, 46(3):536–548, 1999.

[61] C. C. J. Smit and E. D. Smith. The analysis and results of a continuous wave ultrasonic densitometer. *J. Acoust. Soc. Am.*, 104(3):1413–1417, 1998.

[62] A. C. Ugural and S. K. Fenster. *Advanced strength and applied elasticity.* Prentice-Hall Inc., Englewood Cliffs, NJ., 1995.

[63] *http://www.guided-ultrasonics.com.*

[64] P. Wilcox, B. Pavlakovic, M. Evans, K. Vine, P. Cawley, M. J. S. Lowe, and D. Alleyne. Long range inspection of rail using guided waves. In D. O. Thompson and D. E. Chimenti, editors, *Review of Progress in Quantitative NDE*, volume 22A, pages 236–249. American Institue of Physics, New York, 2003.

[65] J. L. Rose, M. J. Avioli, and W. J. Song. Application and potential of guided wave rail inspection. *Insight*, 44(6):353–358, 2002.

[66] M. J. S. Lowe and O. Diligent. Low-frequency reflection characteristics of the S0 Lamb wave from a rectangular notch in a plate. *J. Acoust. Soc. Am.*, 111(1):64–74, 2002.

[67] B. C. Lee and W. J. Staszewski. Modelling of Lamb waves for damage detection in metallic structures: Part I. Wave propagation. *Smart Mater. Struct.*, 12(5):804–814, 2003.

[68] P. Wilcox, M. J. S. Lowe, and P. Cawley. Omnidirectional guided wave inspection of large metallic plate structures using an emat array. *IEEE Trans. Ultrason. Ferroelect. Freq. Contr.*, 52(4):653–665, 2005.

[69] J. C. Huber. Getting down to the basis of fiber-optic transmission. *R&D Magazine*, pages 115–118, 1994.

[70] N. Juluri. *Inspection of complex structures using guided waves.* PhD thesis, University of London, 2008.

[71] ABAQUS. *Analysis User's Manual.* Version 6.5, http://www.simulia.com/, 2004.

[72] Y. Ozaki, H. Sumatini, T. Tomoda, and M. Tanaka. A new system for real-time synthetic aperture ultrasonic imaging. *IEEE Trans. Ultrason. Ferroelectr. Freq. Control*, 35:828–838, 1988.

[73] P. Wilcox. Modelling the excitation of Lamb and SH waves by point and line sources. In D. O. Thompson and D. E. Chimenti, editors, *Review of Progress in Quantitative NDE*, volume 23, pages 206–213. American Institue of Physics, New York, 2004.

[74] D. N. Alleyne and P. Cawley. The interaction of Lamb waves with defects. *IEEE Trans. Ultrason. Ferroelectr. Freq. Control*, 39:381–397, 1992.

[75] M. J. S. Lowe, P. Cawley, J-Y. Kao, and O. Diligent. The low frequency reflection characteristics of the fundamental antisymmetric Lamb wave A0 from a rectangular notch in a plate. *J. Acoust. Soc. Am.*, 112(6):2612–2622, 2002.

[76] R. Rajagopal and M. J. S. Lowe. Short range scattering of the fundamental shear horizontal guided wave mode normally incident at a through-thickness crack in an isotropic plate. *J. Acoust. Soc. Am.*, 122:1527–1538, 2007.

[77] M. Ratassepp, M. J. S. Lowe, P. Cawley, and A. Klauson. Scattering of the fundamental shear horizontal guided wave mode in a plate when incident at a through crack aligned in the propagation direction of the mode. *J. Acoust. Soc. Am.*, 124(5):2873–2882, 2008.

[78] R. Rajagopal and M. J. S. Lowe. Scattering of the fundamental shear horizontal guided wave by a part-thickness crack in an isotropic plate. *J. Acoust. Soc. Am.*, 124(5):2895–2904, 2008.

[79] O. Diligent and M. Lowe. Reflections of the S0 Lamb mode from a flat bottom circular hole. *J. Acoust. Soc. Am.*, 118:2869–2879, 2005.

[80] N. McPherson. *from BVT Surface Fleet Ltd.* Glasgow, UK, private communication in July 2009.

[81] A. Demma, P. Cawley, M. Lowe, and A. G Roosenbrand. The reflection of fundamental torsional mode from cracks and notches in pipes. *J. Acoust. Soc. Am.*, 114(3):611–625, 2003.

[82] M. Drozdz, M. J. S. Lowe, E. Skelton, and R. Craster. Modeling bulk and guided wave progaptaion in unbounded elastic media using absorbing layers in commercial Finite Element packages. In D. O. Thompson and D. E. Chimenti, editors, *Review of Progress in Quantitative NDE*, volume 26, pages 87–94. American Institute of Physics, New York, 2007.

[83] P. Fromme and M. B. Sayir. Measurement of the scattering of a Lamb wave by a through hole in a plate. *J. Acoust. Soc. Am.*, 111:1165–1170, 2002.

[84] J. Ma and P. Cawley. Low-frequency pulse echo reflection of the fundamental shear horizontal mode from part-thickness elliptical defects in plates. *submitted to the J. Acoust. Soc. Am.*, 2010.

[85] O. Diligent, T. Grahn, A. Boström, P. Cawley, and M. Lowe. The low-frequency reflection and scattering of the s_0 Lamb mode from a circular through-thickness hole in a plate: Finite element, analytical and experimental studies. *J. Acoust. Soc. Am.*, 112(6):2589–2601, 2002.

[86] R. Rajagopal and M. J. S. Lowe. Angular influence on the scattering of fundamental shear horizontal guided waves by a through-thickness crack in an isotropic plate. *J. Acoust. Soc. Am.*, 124(4):2021–2030, 2008.

[87] M. J. S. Lowe, R. E. Challis, and C. W. Chan. The transmission of Lamb waves across adhesively bonded lap joints. *J. Acoust. Soc. Am.*, 107(3):1333–1345, 2000.

List of Publications

Z. Fan, M. J. S. Lowe, M. Castaings and C. Bacon. Torsional waves propagation along a waveguide of arbitrary cross section immersed in a perfect fluid. *Journal of the Acoustic Society of America,* 124(4):2002-2010, 2008.

Z. Fan, M. J. S. Lowe, M. Castaings and C. Bacon. Prediction of the propagation and leakage of torsional waves in a waveguide of arbitrary cross-section immersed in a fluid. in D. Thompson and D. Chimenti, editors, *Review of Progress in Quantitative NDE,* 27: 1567-1574, 2008.

Z. Fan, M. J. S. Lowe. Elastic waves guided by a welded joint in a plate. *Proceedings of Royal Society A,* 465:2053-2068, 2009

Z. Fan, M. J. S. Lowe. Propagation of feature guided waves in a plate with a welded joint. in D. Thompson and D. Chimenti, editors, *Review of Progress in Quantitative NDE,* 28: 185-192, 2009.

F. Cegla, **Z. Fan**, M. J. S. Lowe. Ultrasonic density measurements. *McGraw-Hill Yearbook of Science Technology,* 2010.